Order Number 1346436

# Development and mechanical properties of structural materials from lunar simulants by thermal liquefaction

Girdner, Kirstin Kay, M.S.

The University of Arizona, 1991

U·M·I
300 N. Zeeb Rd.
Ann Arbor, MI 48106

# DEVELOPMENT AND MECHANICAL PROPERTIES OF STRUCTURAL MATERIALS FROM LUNAR SIMULANTS BY THERMAL LIQUEFACTION

by

Kirstin Kay Girdner

---

A Thesis Submitted to the Faculty of the

DEPARTMENT OF CIVIL ENGINEERING AND
ENGINEERING MECHANICS

In Partial Fulfillment of the Requirements
For the Degree of

MASTER OF SCIENCE
WITH A MAJOR IN CIVIL ENGINEERING

In the Graduate College

THE UNIVERSITY OF ARIZONA

1991

STATEMENT BY AUTHOR

This thesis has been submitted in partial fulfillment of requirements for an advanced degree at The University of Arizona and is deposited in the University Library to be made available to borrowers under rules of the Library.

Brief quotations from this thesis are allowable without special permission, provided that accurate acknowledgement of source is made. Requests for permission for extended quotation from or reproduction of this manuscript in whole or in part may be granted by the head of the major department or the Dean of the Graduate College when in his or her judgement the proposed use of the material is in the interests of scholarship. In all other instances, however, permission must be obtained from the author.

SIGNED: 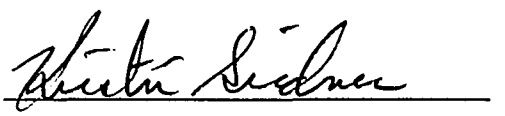

APPROVAL BY THESIS DIRECTOR

This thesis has been approved on the date shown below:

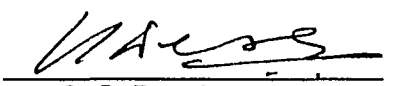

C. S. Desai
Regents' Professor
Department of Civil Engineering
and Engineering Mechanics

10/29/91
Date

ACKNOWLEDGEMENTS

The author would like to express gratitute and appreciation to the following people who have been of help over the course of the project. I wish first to thank Dr. C.S. Desai for his direction and advice during the entire course of this project. Committee members Drs. Sonia Armaleh and Hamid Saadatmanesh are highly appreciated for their time and suggestions contributing to the final written product. I am also indebted to Carl Peters, Peter Boyle and Tom Demma whose help in aspects of fabrication, laboratory use and repair and general advice were extremely valuable. For his help in running experiments and preparing samples, Robert Rasmussen was irreplacable. Finally, fellow graduate students Tom, Janos, Ali and Mohan were extremely helpful by sharing their laboratory and other research experiences with me.

This research was funded in part by Grant No. 347184 from the NASA Space Engineering Research Center, University of Arizona, Tucson, Arizona.

# TABLE OF CONTENTS

## TABLE OF CONTENTS (Continued)

# LIST OF FIGURES

## LIST OF FIGURES (CONTINUED)

page

## LIST OF TABLES

## ABSTRACT

Plans for development of human colonies on the Moon, Mars or other planets will require the investigation of new structural materials. In order to foster self-sufficiency and to make the colonies economically feasible, materials must be developed from locally available resources when possible. In this investigation a material made from a lunar soil simulant has been developed and tested for its mechanical properties. The simulant was mixed with varying percentages of aluminum, stainless steel and carbon steel fibers and heated to 1100°C to form a solid material. Beam shaped samples were cut from these specimens for bending tests. From the intact portions of the tested beams, samples for compression testing were cut and tested. Analysis of the results includes bending strength, compressive strength, and investigation of elastic moduli. The material was found to have significant strength in bending and compression. Results indicate the presence of fibers significantly changes the behavior of the material.

# CHAPTER 1
# INTRODUCTION

In the near future, the human race will surely expand its habitat to include outposts on the Moon, Mars and other planets. The establishment of such colonies will require much transport of resources to these locations, the cost of ferrying mass from earth is extremely prohibitive. The current goal of space research is to limit the amount of materiel to be initially transported from earth and to foster colony self sufficiency by developing processes to use locally available resources, wherever possible. Even the transport of mass between other planetary bodies, such as the Moon, asteroids, Mars or an orbiting space station, is many times less costly than from earth. The ability of engineers and scientists to develop and test methods now for converting resources readily available in space to the materials of the infrastructure of future civilizations will determine the success of the colonization of space.

For the beginnings of an outpost on the lunar surface, the most abundant and easily attainable resource is the soil or regolith, of the Moon. Current research investigates methods of extracting oxygen, metals and glasses from the soil. Another focus of research is the use of the regolith for structural materials. This project concentrates on the development of a material to be made on the moon of locally derived resources, although such a process could be relevant elsewhere, including the Earth or Mars. The applications of a material on the lunar surface are varied, including roads, excavation supports, shelters, human habitation, and radiation shielding. Each of these uses requires different mechanical response from the material, some, such as

radiation shielding which can be accomplished simply by compacted fill, are not so demanding; others, such as the construction of an environment for human habitation require far greater strength and reliability.

The purpose of this research is to develop structural materials made from a simulated lunar regolith with fibers or other additives and investigate their mechanical properties. The material is similar to a ceramic, in that it is formed by heating a lunar soil simulant, nearly to melting, forming a rock-like substance. The imperfect and unrefined material has been called an intermediate ceramic composite (ICC), Desai, (1990). Fibers, in this case aluminum, carbon steel and stainless steel, are added in order to increase the strength of the material and to modify its mechanical properties. The variables having an effect on the material are the temperature to which they are subjected and the percentage of fibers added. The tests performed are beam bending and uniaxial compression, from these, the bending strength and compressive strengths can be determined, as well as the modulus of elasticity and stress-strain response of the materials.

Such a material has many benefits to space colonization. As the material is formed at high temperatures, solar power, readily available on the lunar surface, could easily provide most of the necessary energy for large scale production. Alternatively, other forms of energy such as microwaves and electricity produced from nuclear generators are often discussed. It is versatile, a partial list of potential shapes includes blocks, beams, columns, slabs, domes, roads, and pipes. With some refinement, the material can also be useful for machine parts, or other applications requiring high strength and durability. The

full investigation of the material, its formation, properties and applications plays a prominent role in the future role of space exploration and development.

# CHAPTER 2
# LITERATURE REVIEW

## 2.1 Lunar Construction Considerations

One point made clear in the literature on construction on the lunar surface is that it will be vastly different from that on the earth. Building on the earth has been developed over thousands of years of trial and error methods, and only over the last few hundred years has it been greatly influenced by science. Engineers and scientists will have to be certain that the initial building procedures used on the moon will be successful; there will be no margin for failure due to time, safety and material constraints. The following paragraphs detail the major considerations of construction on the moon.

### 2.1.1 Gravity

The gravity level on the moon is 1/6 that of earth. As a result a structural member would be able to support 6 times the mass on the moon that it would on the earth.

### 2.1.2 Atmosphere

The moon's virtual lack of atmosphere causes several problems. High levels of solar radiation not safe for long term human exposure, blanket the surface of the moon. It has been calculated that 2.4m of lunar regolith could protect human habitats, reducing the radiation to safe and acceptable levels, Guerra, (1988). The lack of atmosphere requires any structure in which people are to work and live without specialized protective equipment to be pressurized to nearly one atmosphere or 14.7 psi (100 kPa). This very large internal force is the dominant load that habitable structures must be designed to withstand. It

is also crucial that the material and design of such structures do not allow for catastrophic failure, Toups, (1990). The final effect of the lack of atmosphere on structures on the surface is that they are subject to the extreme range of temperatures. Temperatures measured on the moon range between 111°C and -171°C, Schmitt, (1988). Any material used must be able to first, not degrade under such extreme temperatures, and second, not be subject to significant expansion causing the build up of internal stresses within this range.

### 2.1.3 Automation

Due to the aforementioned harsh characteristics present on the surface, the use of automation becomes as important for safety as it is for time constraints. Most of the human labor must be done in low risk IntraVehicular Activity (IVA), where crew members are not exposed to life threatening risks, Toups, (1990). Any construction to be done as ExtraVehicular Activity (EVA), must be minimized to prolong life expectancy of those living on the lunar surface, Toups, (1990). Materials and procedures developed for lunar construction must be sensitive to this requirement.

### 2.1.4 Energy

The energy needs of a colony on the moon must be minimized. The most readily available source of energy is solar energy. A material that is to be manufactured using mostly thermal power,and minimizing all energy requirements, would have the least impact on other activities drawing large amounts of power.

## 2.2 Sintering of Lunar Simulants

Many proposed methods of developing construction materials on the moon from the lunar regolith focus on the sintering of the soil into a solid matrix. Sintering is the process in which a granular material is heated and held at temperature below its melting point. Viscous flow on the grain surfaces forms necks between particles, bonding them together. In general, the resulting material is porous and brittle. Variables which can decrease the porosity and thereby enhance the mechanical properties of the material include higher temperature, longer sintering times, smaller material grain sizes and applied external pressure during sintering. Processing a material under heat and pressure is also referred to as hot pressing.

### 2.2.1 Sintering as Applied to Lunar Breccias

Early experimentation of sintering as applied to lunar soils is described by Simonds (1973), in an attempt to explain the formation of lunar breccias under low stress conditions and heat produced by meteorite impacts. The range of temperatures at which a cohesive solid was produced under no applied stress is 800°C to 1000°C. Under hot pressing, a densely welded material can be produced at 600°C, when held at temperature for one week. These experiments were conducted on a powdered glass with composition approximating that of the returned Apollo 14 breccias.

### 2.2.2 Hot Pressing for Construction Materials

In later discussion by Simonds (1988), the hot pressing of lunar regolith for construction materials and the resulting useful by-products is further investigated. He proposes that a small solar powered test plant producing sintered products could provide 31 kg of hydrogen ($H_2$) and 187 kg of oxygen

($O_2$) per month. It is conceded that structural design from such sintered materials is limited by the available tensile and flexural strengths and ductility.

### 2.2.3 Sintering using Microwave Radiation

The sintering of regolith has been widely discussed but there is little published on actual test results on these materials. Research by Meek et al (1988) focused on the production and testing of simulants sintered using microwave radiation, a process that would be faster than thermal sintering but does not take advantage of the abundance of solar energy available on the lunar surface.

Samples of three different lunar simulants, approximating the compositions of returned soils from Apollos 11, 15 and 16, were processed and tested. The cylindrical pellets (0.9 cm diameter and 2 cm long) were cold pressed to 50,000 psi (350 MPa), then sintered at 2.45 gigaHerz of microwave energy frequency. The peak temperature reached within a sample was a function of the length of the microwave process. Sintering times ranged from 5 minutes to reach a temperature of 1000°C, to 45 min. to reach 1204°C.

### 2.2.4 Mechanical Properties of Sintered Soils

The mechanical and physical properties determined by testing the samples included compressive strength, Young's modulus, percent strain to failure, thermal shock, hardness and density. Thermal shock, an important property for ceramics when a large range of temperature is expected, as it is on the lunar surface, is measured in the following manner: a sample is heated and held for 15 minutes at a specific temperature then quenched in boiling water, after which a compression test is performed. This is done at successively higher temperatures. For a sample whose strength suddenly drops in

comparison to that of one that has not been shocked, the temperature it was subjected to is called the ΔTf.

Test results from this research are shown in Table 2.1. The variation of mechanical properties, although showing a general trend of increasing strength and density with higher sintering temperature, also shows a large variation of strength within a specific process temperature range. This can be seen in Figure 2.1. It is suggested this may be due to variations in electric field intensity affecting the uniformity of temperature reached within the sample.

Inspection of the change in sample length under compression to failure, also in Table 1, shows several ultimate strain values between twenty and forty percent. This is extremely high for a sintered and therefore brittle material. There is no discussion of these results in their paper.

## 2.3 Casting of Lunar Simulants

It is generally acknowledged that with greater energy expenditure, the lunar regolith or basaltic rock could be melted and cast in order to form a glass-ceramic with greater mechanical properties than sintered materials. The process of basalt casting is described by Kopecky and Voldan (1965) where, in their native Czeckoslovakia, manufacture of basaltic pipes, tiles and other industrial products began in 1950.

A maximum temperature of 1350°C is required to fully melt the crushed basaltic rock, which is poured at 1200°C. After casting into sand or metallic molds, the pieces solidify at 900°C to 1000°C and must be cooled from 800°C to nearly room temperature over a period of 24 hours. The long cool down period is necessary to promote crystallization and release internal stresses, which often cause bursting if no preventative action is taken. The following

Table 1

Test Results of Sintered Simulants

from Meek et al (1988)

| SAMPLE | TEMPERATURE °C | DENSITY g/cc | COMPRESSIVE STRENGTH psi | YOUNG'S MODULUS E, psi | ΔL/L | ΔTf °C |
|---|---|---|---|---|---|---|
| 1 A11 | 1000.00 | 1.99 | 4003 | 34532 | 0.1160 | |
| 2 A11 | 1000.00 | 2.14 | 6918 | 61697 | 0.1050 | |
| 3 A11 | 1024.00 | 1.84 | 2509 | 10877 | 0.2130 | |
| 4 A11 | 1024.00 | 1.73 | 2611 | 30689 | 0.0851 | |
| 5 A11 | 1038.00 | 2.31 | 15649 | 82712 | 0.1890 | |
| 6 A11 | 1038.00 | 2.30 | 7716 | 30413 | 0.2570 | 400.0 |
| 7 A11 | 1038.00 | 2.27 | 3060 | 55315 | 0.0552 | 300.0 |
| 8 A11 | 1038.00 | 2.34 | 3713 | 165033 | 0.0225 | 200.0 |
| 9 A11 | 1038.00 | 2.19 | 3394 | 81015 | 0.0419 | 200.0 |
| 10 A11 | 1038.00 | 2.06 | 12415 | 41015 | 0.3070 | |
| 11 A11 | 1038.00 | 1.98 | 5468 | 21508 | 0.2550 | 200.0 |
| 12 A11 | 1038.00 | 1.96 | 7266 | 69616 | 0.1050 | 100.0 |
| 1 A15 | 1177.00 | 1.80 | 3524 | 60232 | 0.0586 | |
| 2 A15 | 1177.00 | 2.25 | 8078 | 95373 | 0.0851 | |
| 3 A15 | 1187.00 | 2.01 | 21639 | 169050 | 0.1280 | |
| 1 A16 | 1175.00 | 2.16 | 9398 | 408093 | 0.0230 | |
| 2 A16 | 1175.00 | 1.94 | 3843 | 167034 | 0.0230 | 200.0 |
| 3 A16 | 1175.00 | 2.15 | 2393 | 199043 | 0.0120 | 200.0 |
| 4 A16 | 1204.00 | 2.55 | 44656 | 112067 | 0.4000 | 300.0 |
| 5 A16 | 1204.00 | 2.55 | 20725 | 170080 | 0.1210 | |

1 psi = 6.895 kPa

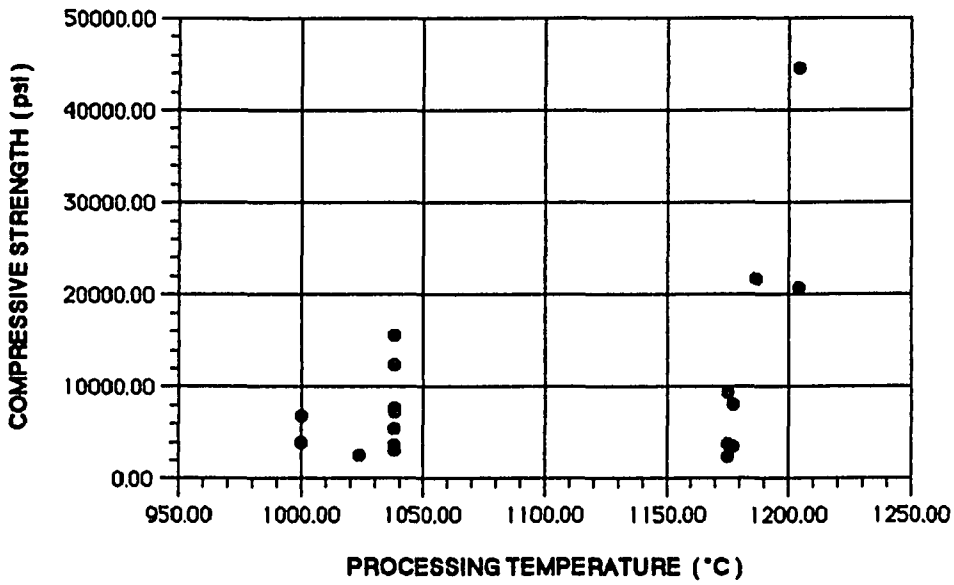


1 psi = 6.895 kPa

Fig. 2.1 Compressive Strength of Sintered Simulants
from Meek et al (1988)

range of values for mechanical properties of cast basalt was reported by the authors:

| | |
|---|---|
| Compressive strength | 57,000 to 71,500 psi (399 to 501 MPa) |
| Tensile strength | 3550 to 5000 psi (25 to 35 MPa) |
| Bending strength | 5500 to 6500 psi (39 to 46 MPa) |
| Thermal expansion | 78 x $10^{-7}$ /°C |

In terms of thermal resistance, the less complex pieces such as tiles or pipes fared well, as an instantaneous change in temperature of up to 100°C caused no damage. Other advantages of these products include high resistance to abrasion, moisture, weathering and chemical agents.

### 2.3.1 Lunar Facilities from Cast Basalts

The design and production of lunar facilities constructed of cast basalt is discussed separately by Binder et al, (1990) and Capps and Wise (1990). Binder et al have analyzed a two story structure conceptualized by Dalton and Hohman, (1972) that would provide living and work space for eight people. The facility would actually consist of two separate vessels, one inside the other, effectively reducing the pressure differential on the walls. The interior space air pressure must be 1 atmosphere for habitation (14.7 psi, 103 kPa), the air space between the two vessels would be 0.5 atm (7.4 psi, 51.5 kPa), and outside pressure is of course 0 atm.

The authors theorize that such a facility can be built as a combination of six basic structural elements, each with a thickness of 7 cm (2.8 in). The authors do not state what design values for the properties of the cast basalt or safety factors they used for this analysis.

As a method of joining the individual structural shapes, the authors propose that superheated basalt be poured into spaces between the in-place abutted slabs. This action would remelt the basalt along the edges, then resolidify the old and new basalt into a seamless monolithic structure. The lack of expansion joints or gaps between sections could allow the buildup of destructive internal stresses from minute expansions or contractions.

Capps and Wise suggest another way of joining pieces that would allow for small movements. They propose a slender steel strip with a dog bone shaped cross section to be inserted into precast slots that would behave like a sealing gasket when the structure was internally pressurized. Despite its brittleness, Capps and Wise recommend the use of cast basalt for lunar construction and maintain that its major drawback is transportation of the equipment necessary to begin processing.

## 2.4 Fibers for Composites from Lunar Soils

In order to increase the properties such as flexural and tensile strengths and ductility of materials made from the regolith, it may be advantageous to add fiber reinforcements. These fibers can be made of metal or glass, and can be produced either from resources on the moon or imported from earth, the latter in the initial stages of colonization.

### 2.4.1 Basalt Fibers for Polymer Composites

The production and use of fibers drawn from basalt is discussed by Subramanian, et al, (1977). In this study the fibers were tested as reinforcements in polymer composites. Fibers can be drawn from basalt within the temperature range of 1175°C to 1375°C. In their testing of the fibers, they

found that the tensile strength of fibers drawn within the range of 1250°C to 1375°C increases linearly and is greater than that of fibers drawn at lower temperatures. Fibers drawn at the lower temperatures showed crystalline inclusions which were suspected to create weak spots allowing for crack initiation and premature failure.

The tensile strength of the fibers drawn between 1250°C and 1325°C ranged from 330,000 psi (2.3 GPa) to 432,000 psi (2.9 GPa). The authors tested several basalt rocks of slightly varying chemical composition, so the above range given is not strictly a function of processing temperature.

Also tested were fibers drawn at 1360°C from E-glass marbles. These fibers were prepared and tested in the same manner as the basalt fibers and were found to have an average tensile strength of 365,000 psi (2.5 GPa), versus the commercially manufactured fiber strength of 500,000 psi (3.4 GPa). For this reason the authors determine that under optimum processing and testing conditions, the strength of the basaltic fibers could approach that of commercially available E-glass.

### 2.4.4 Fibers from Lunar Materials

Ho and Sobon (1979) have conceptually designed a system to produce a more refined fiberglass made of lunar materials either on the lunar surface or in space. For every kilogram of lunar soil, 590 g of fiberglass can be produced in this design. In the proposed processing system, the mass initially transported from earth would be approximately $110 \times 10^3$ kg (120 tons). In one year, it is estimated the plant could process raw material of 90 times its own mass,

producing $5.84 \times 10^6$ kg of fiberglass. The plant uses solar energy as the source of power to melt and process the soil.

Goldsworthy (1985) gives a more comprehensive study of the production, uses and economics of fiber composites for structural materials to be produced on the moon. He maintains that the cost of producing metals and their alloys on the moon would not be competitive with regard to the cost of transportation from earth. He proposes that for a structural material produced in space the most efficient would be a glass/glass composite with both matrix and fibers originating in the lunar soil.

Prime candidates for glass fibers include basalt, feldspar, present in surficial materials and rock outcroppings, and basalt/feldspar blend. Goldsworthy notes that a feldspar enriched with 36% $SiO_2$ would closely match the composition of S-glass, the fiberglass with the highest mechanical properties commercially available. The composition of S-glass is 65% $SiO_2$, 25% $Al_2O_3$, and 10% MgO. The enriched feldspar would substitute calcium oxide (CaO) for magnesium oxide (MgO), a substitution he claims would have no significant effect on the properties of the glass, and minor amounts of iron oxide (FeO), sodium oxide ($Na_2O$) and potassium oxide ($K_2O$). As a composite matrix material he suggests a low-melt glass with a melting point of 585°C such as one composed of 1 part lead oxide (PbO), 0.1 part alumina ($Al_2O_3$) and 1.5 parts silicon dioxide ($SiO_2$).

The use of metal fibers as reinforcements has been briefly mentioned in several articles, but not discussed in detail. The properties of conventional metals are widely known and their availability in the soil is recognized although the derivation of them from the regolith may require more processing and

energy usage than glass fibers. Another source of metals, however, is asteroids, where their presence is often in purer forms. Harnessing and mining of asteroids is another possibility in the scheme of resource development in space. Metals have an advantage over glass in that they exhibit more ductile behavior and are therefore less susceptible to catastrophic failure.

## 2.5 Summary

Current literature in the field of lunar derived materials for construction or other purposes points to the use of the regolith as the most efficient and available source. It is also apparent that the methods of developing such materials and potential composites are widely discussed but not widely pursued and tested. The full development of such a material, including investigation of the effect of various fibers and a full range of mechanical testing, is necessary to continue development of materials for use in space.

# CHAPTER 3
# SCOPE OF RESEARCH

## 3.1 Liquefaction

The process forming the material produced in this research is referred to as liquefaction, Desai, (1990). Here liquefaction is defined as the creation of a composite material from a lunar simulant and fibers or other admixtures, where it is heated, held and perhaps cycled somewhere below the powder melting point, but not necessarily sintered. The fibers present may melt before the soil or not at all, and similarly, the soil may liquify before fibers or not at all, but the resulting material is a solid matrix, drawn and held together by the heated or melted fibers and the zones of influence containing heated or liquefied soil simulant.

## 3.2 Fibers for the Composite Material

Appropriate and available fibers were investigated, chosen and obtained to be mixed with the lunar soil simulant for liquefaction. The fibers obtained were aluminum, carbon steel and stainless steel. The produced material could be classified as an intermediate ceramic composite, (ICC), Desai, (1990), because it is a fiber reinforced material, but not as perfect as a high tech ceramic, yet not as crude as a brick.

## 3.3 Molds for the Liquefaction Process

Materials for and designs of molds were investigated to develop a mold that could withstand the high temperatures involved, not react with the soil and

fibers, and release the samples upon completion of heating. For these experiments, a titanium cradle holding graphite sheets was used. During the investigation it has been determined that this mold is not adequate for temperatures above 1100°C or those involving long heating cycles, hence, the original scope of study of temperature effects on the mechanical properties of the samples was curtailed. Castable refractories and suface coatings have been investigated for future work. Up to this point, the castable refractory has not been proved satisfactory for this purpose, but shows promise with some modifications. For subsequent work a combination of the refractory with graphite and/or boron-nitride coating may be feasible.

### 3.4 Sample Preparation

Samples were made by placing the lunar soil simulant either by itself or mixed with given percentages of fibers in the mold. The filled mold was transferred to the furnace, and heated under a programmed temperature cycle. After cooling, the samples of approximate dimensions 10" x 1" x 2.5" (25 x 2.5 x 6.25 cm) were cut, and ground to beam shapes for testing.

### 3.5 Bending Test Device

A small scale bending test device was designed and built according to ASTM standard C78-84. The device is a four point bending apparatus with a nine inch unsupported span and fixed loading blocks at the third points, three inches from either end. It was designed to be used on a Geotest unconfined compresison test frame under manual operation. Measurements of strain and displacement were to be made using strain gages and dial gages.

### 3.6 Bending Tests

Beam specimens were tested using the beam bending device built for this research. Measurements taken were load and displacement in all tests and strains at four locations for about half of the tests. The samples were tested to failure, and all but two included one or more unloading cycles. The results were analyzed to determine the ultimate bending strength, modulus of elasticity and stress-strain behavior.

### 3.7 Compression Tests

Compression tests were performed on specimens cut from the beams after bending tests. The testing apparatus used was an MTS frame under manual operation and data collection. Specimens were loaded to failure during which the axial deformation and load applied were measured. The results were analyzed to determine the ultimate compressive strength, modulus of elasticity and stress-strain behavior. The moduli were compared with those calculated from the bending tests.

# CHAPTER 4
# ESSENTIALS OF SAMPLE PREPARATION

## 4.1 The Lunar Soil Simulant

The lunar soil simulant, called Arizona Lunar Simulant or ALS, used in this research was conceived by Desai and was prepared under a previous research study involving its compaction and triaxial testing; these results are described in Allen (1990), and Desai, Saadatmanesh and Allen, (1991). Every effort was made to match the properties of this soil with that of the lunar soils. It was, however, not feasible to formulate agglutinates for inclusion into the soil. Agglutinates are the small spherical glassy fragments produced by meteor impacts on the lunar surface. One simulant commercially available, the Minnesota Lunar Simulant, or MLS, does contain artificial agglutinates. A quantitiy of MLS was obtained and several preliminary samples have been prepared from it; however, testing of these samples is not included in this research.

### 4.1.1 Physical properties of the simulants

The ALS is produced from crushed and ground basalt rock obtained from the Pomona Flow near Hanford, WA. A grain size distribution curve of the simulant in comparison to that of soil samples returned from the moon is shown in Fig. 4.1. The specific gravity of the simulant is 2.86 as determined by Allen, (1990).

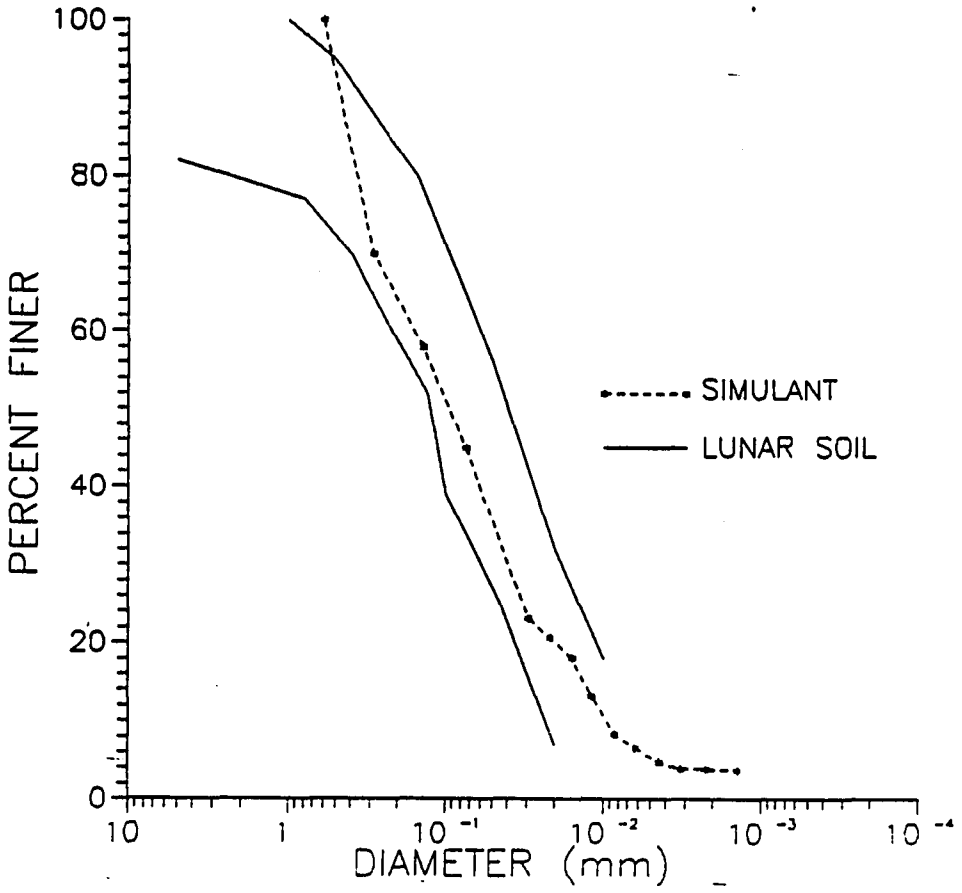


Fig. 4.1 Grain Size Distribution of Actual and Simulated Lunar soils from Allen (1990)

This particular basalt was chosen because its composition approximates that of the maria soils. Table 2 shows the chemical composition of the simulant and its comparison to that of the lunar soils and the MLS. Most simulants attempt to match the characteristics of the maria as it is a good assumption that any development on the moon will likely initiate in the lowlands. The maria soils and the MLS have a higher concentration of titanium dioxide ($TiO_{2)}$, this is important for much of the lunar colonization research as it is a key ingredient in the process currently being investigated to extract oxygen from the regolith. However, that deficiency, along with other minor differences between the compositions, was considered to be adequate for the purposes of developing structural materials at this stage in the research.

### 4.1.2 Liquefaction of the simulants

Initial heating experiments with the ALS showed that its range of liquefaction begins at about 1050 °C. Eleven hundred °C was chosen as the optimal temperature at which the bulk of the samples prepared for this research would be formed. Several invesitigatory experiments with the MLS showed that its range of liquefaction is slightly higher, and solid samples exhibiting the same strength could not be formed until 1150°C. A sample produced from MLS at 1100°C crumbled when scratched with a fingernail. Samples of the MLS also showed more susceptibility to oxidation and less production of bubble forming gases in the solid matrix. A photgraph showing the contrasting matrices of the two samples is shown in figure 4.2.

Table 2

Chemical Composition (% by weight)

| | SIMULANTS | | LUNAR SOILS* | |
|---|---|---|---|---|
| COMPOUND | ALS** | MLS*** | MARIA | HIGHLANDS |
| $SiO_2$ | 48.0 - 50.0 | 43.86 | 45.4 | 45.5 |
| $Al_2O_3$ | 13.5 - 16.0 | 13.68 | 14.9 | 24.0 |
| $TiO_2$ | 1.6 - 3.2 | 6.32 | 3.9 | 0.6 |
| FeO | 7.0 -12.5 | 13.4 | 14.1 | 5.9 |
| MnO | 0.2 -0.25 | 0.198 | -- | -- |
| MgO | 4.3 - 6.5 | 6.68 | 9.2 | 7.5 |
| CaO | 8.3 - 10.3 | 10.13 | 11.8 | 15.9 |
| $Na_2O$ | 2.7 - 3.0 | 2.12 | 0.6 | 0.6 |
| $K_2O$ | 0.5 - 1.5 | 0.281 | -- | -- |
| $Fe_2O_3$ | 1.9 - 4.6 | 2.6 | -- | -- |
| $P_2O_5$ | -- | 0.2 | -- | -- |
| $CO_2$ | -- | 0.0015 | -- | -- |

* (Taylor, 1975)
** (Fuenkajorn and Daemen, 1986)
*** (Weiblein and Gordon, 1988)

Fig. 4.2 Photograph showing ALS (top) and MLS (bottom) Matrices

## 4.2 Fibers

Three metal fibers were chosen for investigation in this research; aluminum, carbon steel and stainless steel. Aluminum was chosen due to the fact that its melting point of 660°C is below that of the range of melting of the lunar simulant. These fibers were cut from a length of aluminum wire. Carbon steel and stainless steel fibers were donated by Ribtec Corp. where they are produced for use as reinforcements in concrete and refractory materials respectively. A comparison of the shapes and sizes of the fibers is shown in Fig 4.3. Although neither of the steel fibers would approach their melting points in this study (1426°C for carbon steel and approximately 1450°C for stainless steel), it was expected that the liquefaction of the soil would provide a bond to the fibers, adding strength to the material.

The choice of these fibers was based mainly on their availability and familiarity. Fiberglass was considered, as it may be the simplest fiber to produce on the lunar surface, but not obtained and incorporated into this research. This project is considered to be preliminary research from which procedures and concepts can be learned and developed.

## 4.3 Molds

By far, the most challenging and frustrating part of this investigation was designing and fabricating a mold to contain the simulant during the heating process.

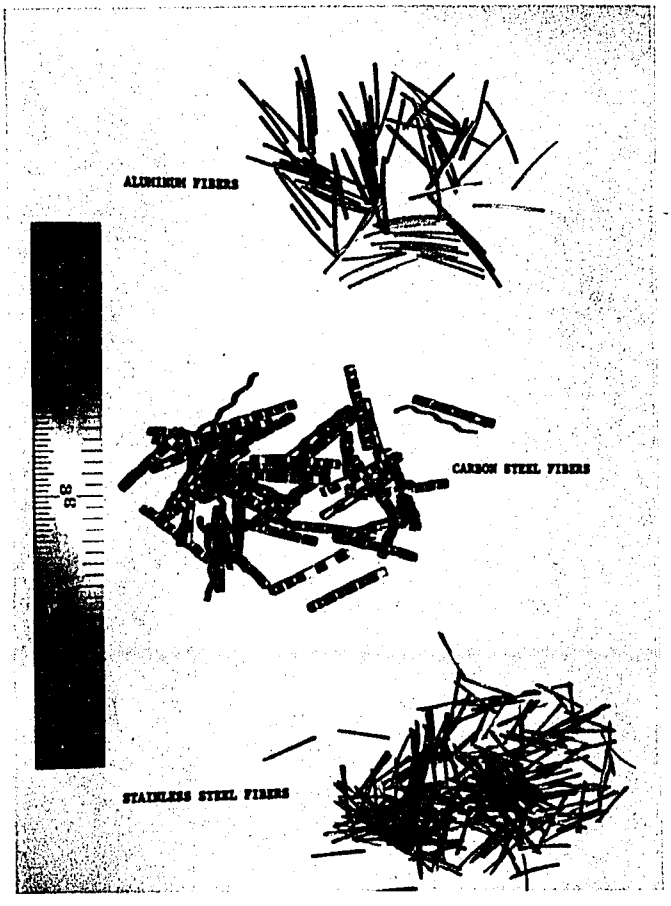


Fig. 4.3 Comparison of Fibers

### 4.3.1 The Graphite Titanium Cradle

Initially, various metals were investigated and titanium was chosen for its high melting point of 1668°C and reasonable cost when compared with metals of higher melting points such as molybdenum and platinum. It was quickly determined that due to its brittleness, the degree of difficulty in machining, rapid oxidation and plastic behavior at temperatures well below its melting point, it would need to be replaced or combined with another material to make a useful mold.

Graphite was suggested as a material possessing a high melting point, low cost and ease of use for this application. A titanium cradle was then built to hold sheets of graphite to contain the simulant and its fibers, as displayed in Fig. 4.4. The graphite noticeably decomposed under argon, nitrogen and air environments, but not rapidly enough to fail during the standard heating process. This mold was adequate to produce all samples produced for this research. It was deemed prudent not to use this mold for either longer cycles of heating or temperatures higher than 1100°C.

### 4.3.2 The Castable Refractory

A mold made from a castable refractory, called Super 32, was also developed but not used for the production of samples tested as part of this research. Best results were obtained when inside this trough shaped mold, graphite sheets painted with a water based solution of boron nitride were installed along the walls, this device is shown in Figure 4.5. When the graphite was not incorporated into this mold, the soil under heat treatment became viscous, welding itself to the sides of the mold. There was also more evidence

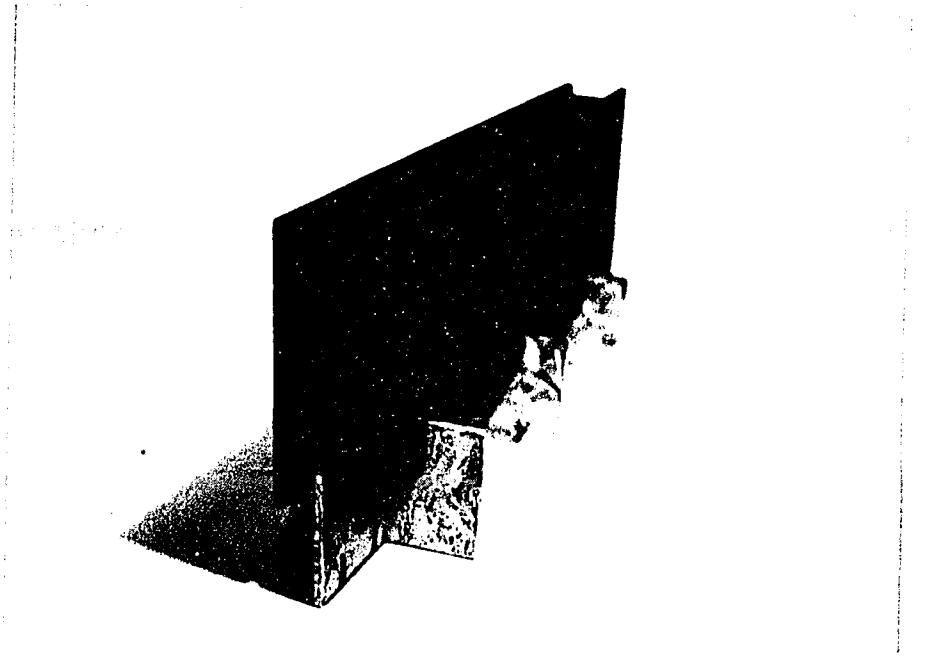

Fig 4.4 Photograph of Titanium - Graphite Mold

of oxidation in this sample than those produced in the graphite mold.

### 4.3.3 Effects of Carbon

It has been assumed from these observations and for the purposes of this research, that both the soil and the graphite will readily oxidize under air environment. However, when both are present, the carbon in the graphite oxidizes more readily, acting as an oxygen sink, effectively creating an inert environment for the soil. For this reason, coke granules, placed in refractory dishes inside the furnace, were also incorporated into the most recent sample preparations.

Several of the final material samples are currently being investigated for any form of carbon contamination that may inadvertantly be occuring with the soil during this process. If these results prove these samples have been produced carbon free, the refractory mold combined with graphite and boron nitride coating, heated in the presence of coke will likely be the mold and process used for continuing research.

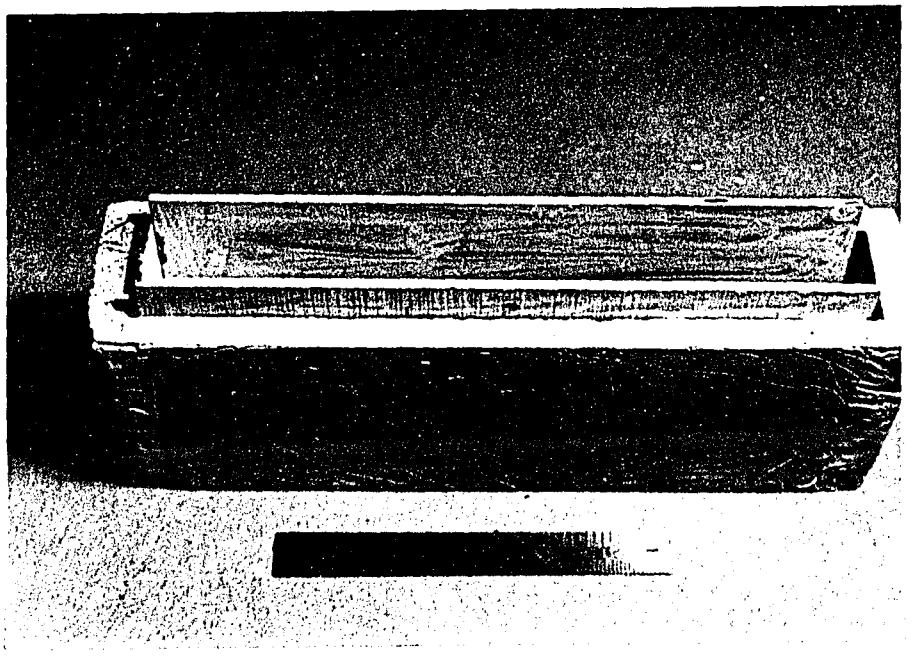

Fig. 4.5 Photograph of Castable Refractory Mold

# CHAPTER 5
# EQUIPMENT

## 5.1 The Furnace

The furnace obtained and used for sample preparation is a Lindberg model 51644. It has a maximum temperature capacity of 1700°C, and interior dimensions 10 x 11 x 14 inches (25 x 28 x 35 cm). It is heated using molybdenum alloy elements.

The programmable Eurotherm 818 controller allows the operator to choose any cycle involving the increase, decrease and maintenance of temperature. There are certain physical limits. because the mass of the furnace and its contents restrict the heating and cooling to some degree. Up to 8 steps can be programmed into the controller. Each step consists of three commands; ramp, level and dwell. The ramp controls the rate of heating or cooling in °C/minute, the lowest of which is one °C/min. The furnace cannot maintain a rapid rate of heating (10°C/min) when approaching or surpassing temperatures of 500°C. During the sample preparations it took about three hours for the furnace to achieve 1100°C, an average rate of six °C/min. The level command controls the temperature to which the furnace heats. The dwell determines how long in hours the furnace is to maintain the temperature level. After it has completed its dwell, the furnace approaches its next temperature level, higher or lower, at the rate specified by the next ramp.

Most of the specimens produced and tested in this research were heated under the program shown graphically in Fig 5.1(a). The resulting cycle of time

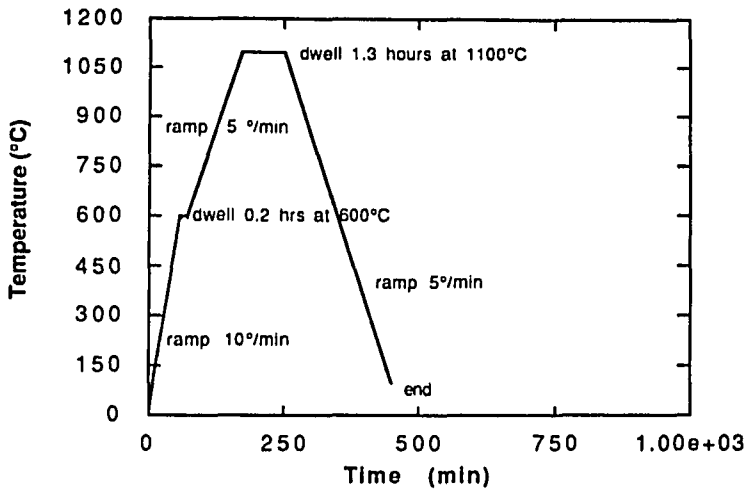


(a) Programmed Temperature Cycle

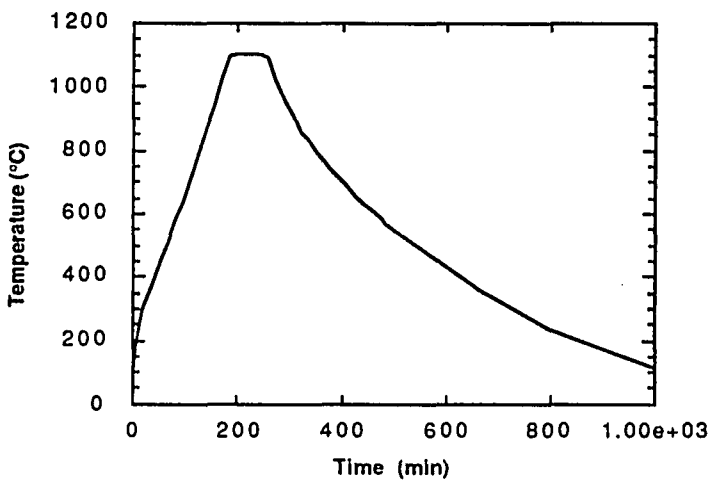


(b) Actual Temperature Cycle

Fig. 5.1 Temperature vs Time Cycle of Sample Preparation

and temperature which the specimens actually experienced is shown in Fig. 5.1(b).

## 5.2 The Beam Bending Test Device

A device was built in order to test the relatively small sized beams produced of this material. A four point loading device was chosen so that the failure of the beam would occur strictly from bending moment, assuming the beam failed within the middle third. ASTM standard C78-84 was used as a reference in design of this device, a photograph of which is shown in Fig. 5.2. A drawing used to fabricate the device is included in Appendix A. Individual components of the device are constructed of aluminum, brass and steel.

One of each of the end supports and loading blocks is capable of rotating in the direction of the length of the beam. The other of each of the two, positioned oppositely to each other, is capable of pivoting around a steel ball. This design concurs with the ASTM standard and allows for rotation of the loading and support blocks in order to minimize effects of torsion on the beam.

Initially, deflections were measured by mounting a dial gage to track the movement of the top loading block. This setup measured deflections at the third points of the beam. Results from this were unsatisfactory, including the seating of the concave head and loading block and deflections of the block itself. Finally, a different system, as shown in the figure, was devised to measure only the deflection between the beam center and the base loading block. This apparatus proved satisfactory in most cases except that seating of the arm on the dial gage stem contributed to error in the initial loading. When greater care

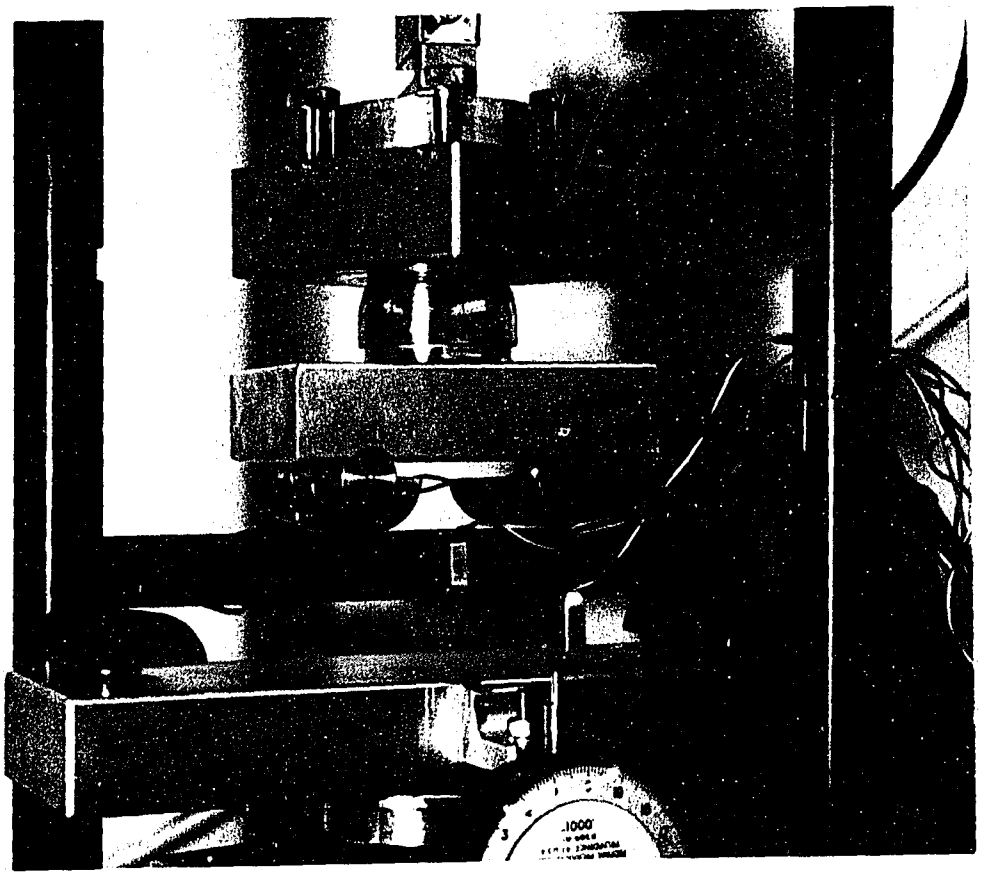

Fig. 5.2 Photograph of Beam Bending Device

was taken in the attachment of the arm and positioning of the dial gage, this effect was minimized, but it never disappeared.

# CHAPTER 6
# TEST RESULTS

## 6.1 BENDING TEST RESULTS

### 6.1.1 The Beam Samples

Bending tests were performed on 16 beam samples of approximate dimensions, 10 x 1 x 0.5 in. (25 x 2.5 x 1.25 cm). Of these, 13 were heat treated under the same conditions with respect to cycle length, temperature and atmosphere. The time-temperature relation of the preparation of these samples is shown in fig. 5.1(b). The furnace atmosphere was not purged with inert gases and the mold used was the previously discussed graphite - titanium cradle.

The other three samples were prepared under different environments. The furnace interior was purged with an inert gas during the heating cycle; two samples were purged with argon and one with nitrogen. They also experienced slightly shorter dwell times at the maximum temperature of 1100°C.

Table 3 shows the sample designation numbers, their fiber composition by weight, the bending strength at failure, the percent fibers by volume, and the density of the material matrix. Bending strength, $f'_b$, was computed from the peak load, $P_{max}$, the beam span, l, the beam width, b, and height, h, using:

$$f'b = \frac{P_{max}\, l}{b\, h^2} \qquad 6.1$$

The fiber volume fraction and density of the material matrix were calculated by weighing the prepared sample and calculating its volume from its rectangular dimensions. The fibers had been added to the mix before heating

Table 3

Beam Bending Test and Sample Data

| SAMPLE | FIBER - PERCENT BY WEIGHT | BENDING STRENGTH psi | MATRIX DENSITY g/cc | % FIBER BY VOLUME |
|---|---|---|---|---|
| 1A | NONE | 1300.4 | 2.38 | 0 |
| 1B | NONE | 1518.2 | 2.48 | 0 |
| 2 | NONE | 2620.7 | 2.43 | 0 |
| 4A | AL - 7.5 | 2249.8 | 2.58 | 7.19 |
| 4B | AL - 7.5 | 2872 | 2.61 | 7.27 |
| 5A | CS - 15 | 1567.9 | 2.01 | 4.31 |
| 5B | CS - 15 | 1075.9 | 2.18 | 4.65 |
| 7A | AL - 15 | 2553.3 | 2.39 | 13.5 |
| 7B | AL - 15 | 2661.5 | 2.36 | 13.3 |
| 8B | SS - 15 | 4278.8 | 2.2 | 4.54 |
| 8C | SS - 15 | 3207.1 | 2.46 | 5.04 |
| 9 | NONE | 1272.8 | 2.44 | 0 |
| 10 | AL - 10 | 597.4 | 1.82 | 6.95 |
| 11 | SS - 7.5 | 1953.2 | 2.39 | 2.32 |
| 12A | CS - 7.5 | 1599 | 2.39 | 2.39 |
| 12B | CS - 7.5 | 1958.1 | 2.41 | 2.42 |
| 18A | NONE | 1672.1 | 2.44 | 0 |
| 18B | NONE | 1616.1 | 2.53 | 0 |

Al - aluminum
SS - stainless steel
CS - carbon steel

1 psi = 6.895 kPa

as a percentage of total weight; this known weight corresponding to the percentage was subtracted from the final sample weight. As the density and weight of the fibers are known, the fiber volume in a sample, the matrix material volume and density can be calculated.

### 6.1.2 Samples Containing Aluminum

Figure 6.1 shows the ultimate bending strength results for the 14 specimens which were prepared under similar conditions. Samples for which the results are not shown are 1A, 1B, and 2, which were prepared under purged environments, and 10 which will be discussed later. It is apparent that the inclusion of aluminum fibers greatly increases the bending strength of this material. One reason for this is illustrated in the photgraphs of typical aluminum fiber samples, Figure 6.2. The fibers, with their relatively low melting point, diffuse and permeate into the surrounding soil before the soil has reached its fusing point. This often creates a hollow space where the fiber originally was, and a strong, dense zone where the aluminum and soil have bonded together around it. The close proximity of fibers before melting appear to cause these zones to overlap, creating a matrix of influenced zones.

Sample 10, not shown in Fig 6.1, also contains aluminum, but the difference in the shape and size of the additive has the opposite effect on the material. In this case 10% aluminum shavings, of particle size passing a No. 30 sieve, were added to the soil; the resulting material was brittle and crumbly and showed the lowest strength of all beams tested. It is possible that the small and irregularly shaped pieces of aluminum oxidized more readily due

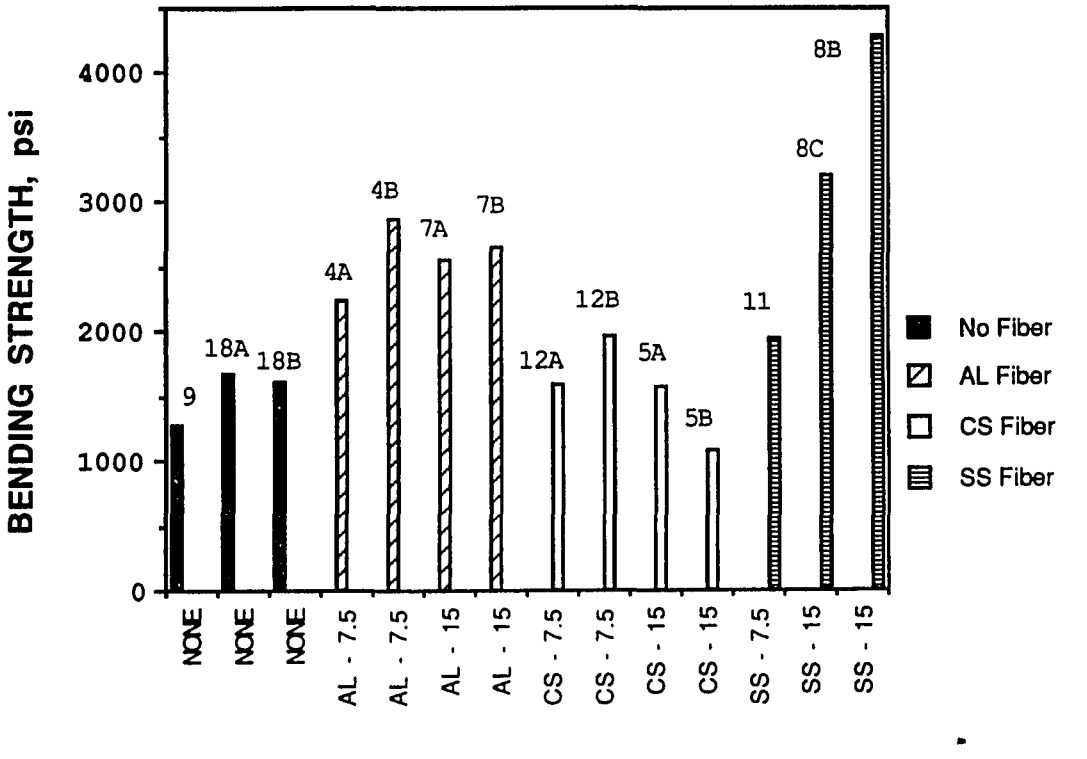


1 psi = 6.895 kPa

Fig. 6.1 Beam Bending Strengths

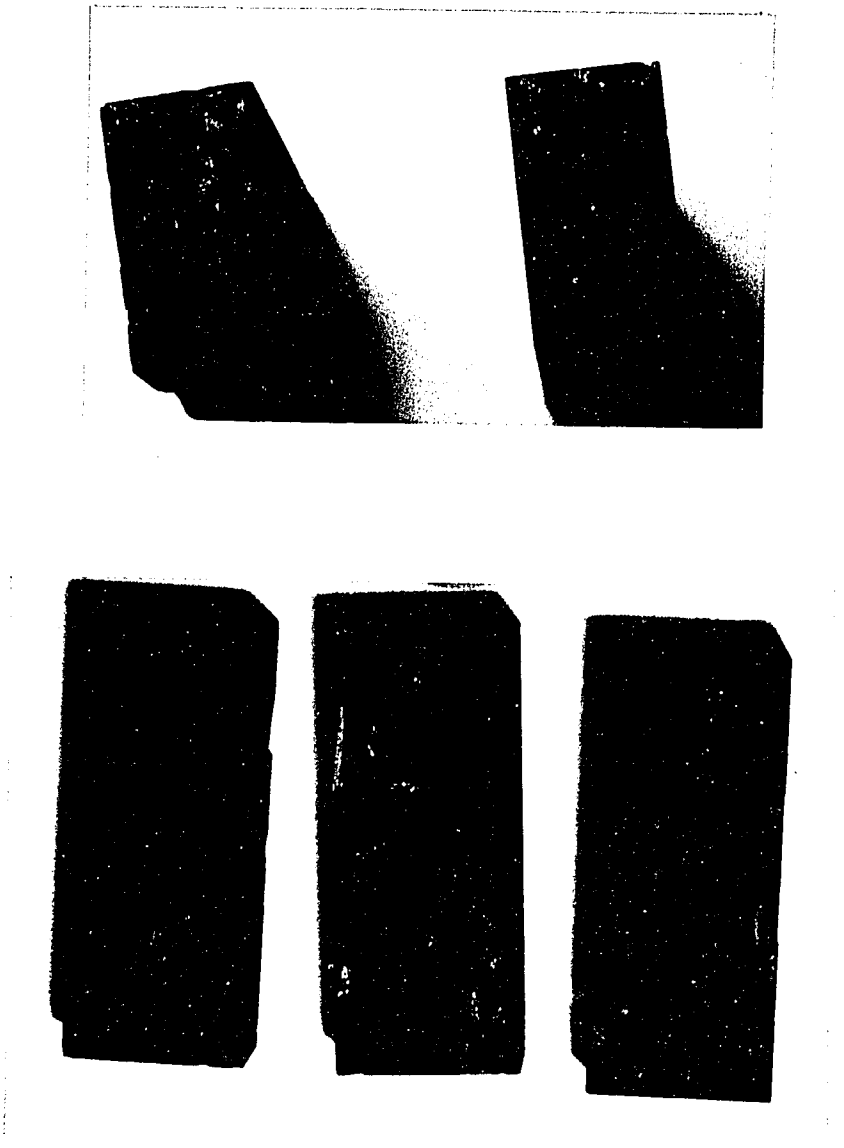

Fig. 6.2 Photographs of Samples with Aluminum Fibers

to the greater surface area per particle in contact with the atmosphere and surrounding soil. Whatever the exact cause, it is clear that the addition of small sized particles of aluminum has a detrimental effect on the strength of the "liquefied" material, whereas aluminum fibers generally have a strengthening effect.

### 6.1.3 Samples Containing Carbon Steel Fibers

The addition of carbon steel (CS) fibers had only a marginally positive effect on the bending strength of the beams. In one instance, a beam containing 15% CS fibers showed a drastic reduction in strength. Comparing the matrix densities of the four beams containing CS fibers shows that for the beams with higher proportion of fibers, the density and strength were lower. There are several probable explanations for this. The size of the carbon steel fibers, one inch long (2.5 cm), is relatively large compared to that of the beam, one half inch wide and one inch high (1.25 and 2.5 cm). Because the size of the mold is equal to or larger than the fiber length, random orientations of the fibers are still possible, however, the scale of sample to fiber is not ideal.

The effect of the larger, flatter fibers is to trap gas bubbles formed during the heating process, creating more hollow spaces and a more porous and non-homogenous material than that made with the other fibers. A photograph of a sample containing the carbon steel fibers is shown in figure 6.3. The large hollow pockets naturally transfer higher stresses in the continuous portions of a cross section.

Another possible explanantion of the larger and more frequent bubble formation in these samples is that the oxidation of the iron creates more gases

than the other fibers. The study of the gases which are forming the bubbles, and their source is important to understanding the creation and behavior of this material. It is, however, outside the scope of this project.

Regardless of their source, these trapped bubbles serve to weaken the material reinforced with the carbon steel fibers. This is not to say they should not be considered as a potential ingredient in developing building materials. It is likely that if production of the material were to include stirring or vibration, the bubbles and their detrimental effects would decrease.

### 6.1.4 Samples Containing Stainless Steel Fibers

Samples containing stainless steel fibers showed the greatest increase in bending strength of all samples, however, this increase was not as consistent or as close in magnitude as other samples, with strengths ranging from 1953 to 4278 psi (13.6 to 29.5 MPa). The stainless steel fibers were more evenly distributed within the samples than the carbon steel fibers, as shown in fig 6.4. Here again it is thought that the material would benefit from some sort of processing during liquefaction.

### 6.1.5 Bending Test Results Comparisons

Figure 6.5 shows the relation between ultimate bending strength and the density of the material matrix. Although it can be inferred that the specimens showing higher strength tend to have higher density, a specific relationship is not predictable at this time.

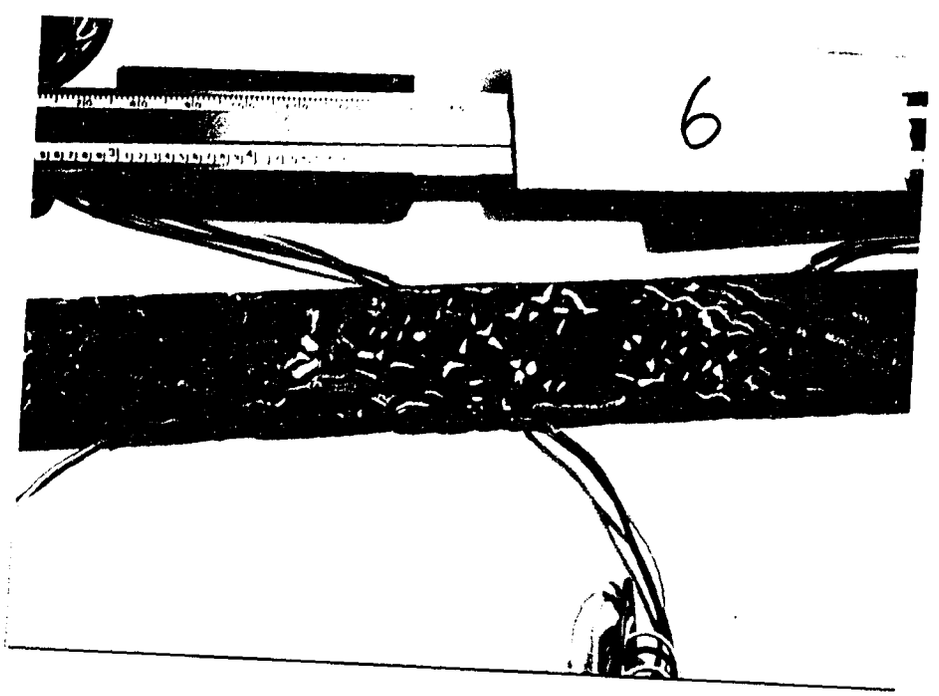


Fig. 6.3 Photograph of Sample with Carbon Steel Fibers

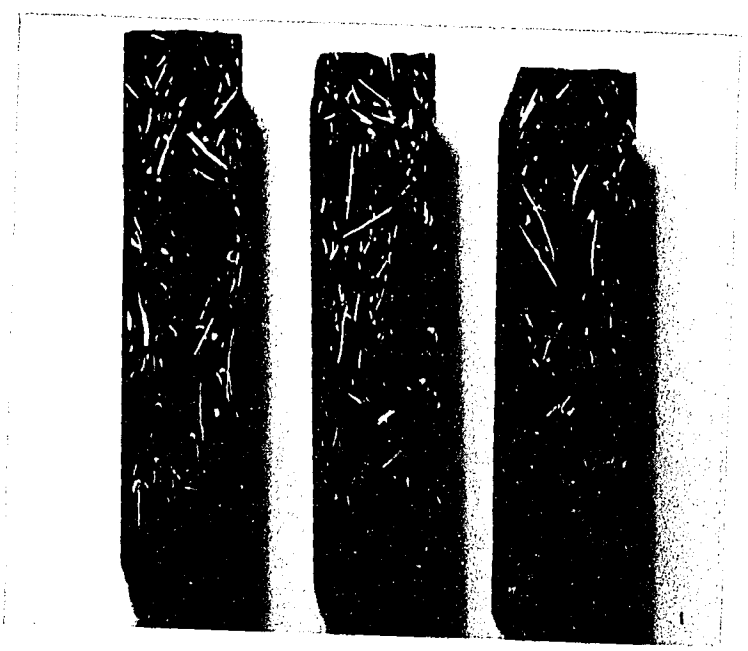

Fig. 6.4 Photograph of Samples with Stainless Steel Fibers

Bending tests on approximately half of the samples included measurements from strain gages attached to the beams. Stress-strain and load displacement curves for all of these tests are given in the appendix. The four gages were located at the center and the quarter points on the top and bottom of the sample as shown in Fig. 6.6. The deflection of the beam at the third point or at the center was also recorded in all tests. The stress at the center of each gage was calculated using the relationship between moment, distance to the neutral axis (the center) and moment of inertia. The following equations were used to calculate the stresses at the center point gages and quarter point gages, respectively.

$$\sigma_{1,3} = \frac{P\ l}{b\ h^2} \qquad 6.2$$

$$\sigma_{2,4} = \frac{3\ P\ l}{4\ b\ h^2} \qquad 6.3$$

Where P is the total applied load, l is the span of the beam and b and h are the width and height of the beam respectively.

From the stress-strain curves, the modulus of elasticity was computed in the following manner. Linear regression analysis was performed on each set of points to determine the best fit line, the slope of this line is the modulus. The following sets of stress-strain points were analyzed; the origin to 50% for the bending strength, its slope is the initial modulus, and each series of unloading points, from the peak to zero, this slope is taken as the elastic modulus. These series of points were analyzed from both compression and tension data.

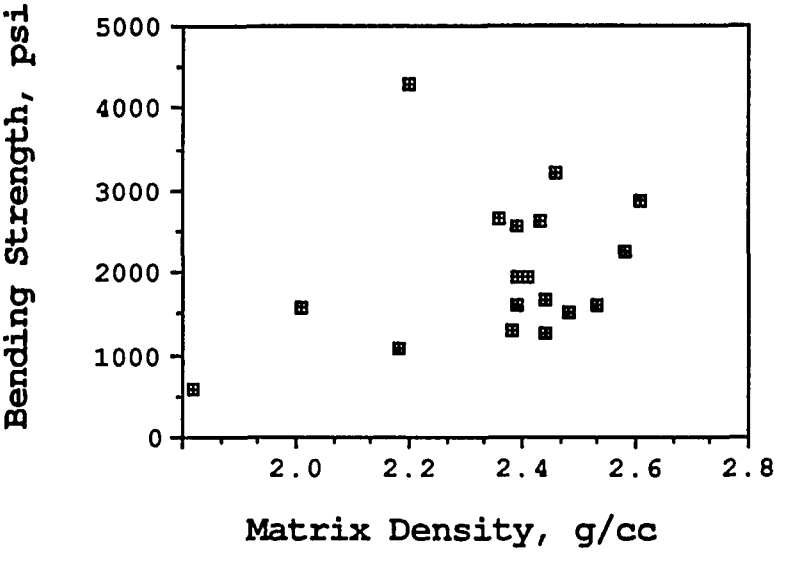


1 psi = 6.895 kPa

Fig. 6.5 Bending Strength vs. Matrix Density

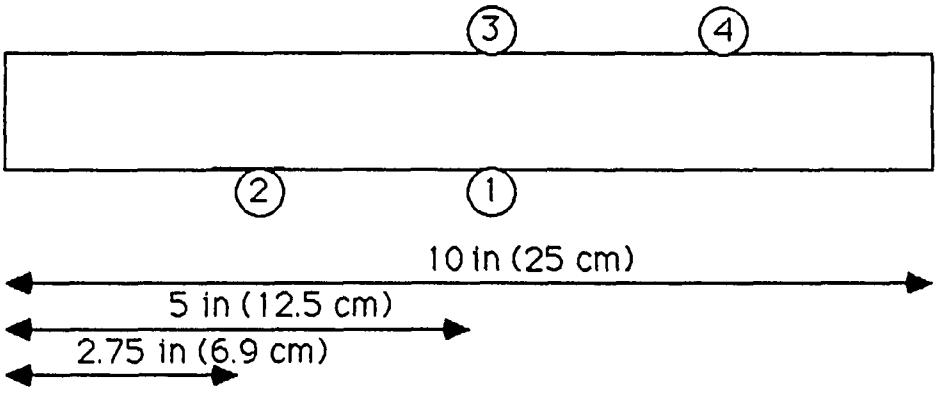


Fig. 6.6 Strain Gage Locations

Figure 6.7 shows plots of all the test data for a typical beam, No. 11 containing 7.5% by weight of stainless steel fibers. The plots show four stress-strain curves, Fig. 6.7 (a), (b), (c), (d), and one load-displacement curve, Fig 6.7 (e); the test included two unloading and reloading cycles.

The load-displacement curve shows consistent results after the displacement of about 0.01 inch (0.025 cm). The flat portion of displacement to about 0.01inch (0.025 cm) is most likely due to some initial looseness in the loading device and the initial seating of the load. This is common to all results when measurements were taken only at the third points of the beams. Measurements were subsequently taken at the center points and this effect was reduced but did not disappear altogether. The jump in displacement at the first unloading point in each cycle is common to all tests on this material, and also to a test of an aluminum beam performed using the same apparatus. The reason for this jump, when changing direction of the loading ram, is not clear but it is apparently a fault of the testing machine. If one looks beyond these aspects of the test results, which may have been affected by experimental deficiencies, a modulus can be determined from the later steep loading and reloading portions, which is apparently consistent. This modulus is determined using the relationship shown in Eq. 6.5 below for deflection at the center, $\partial$, where a is the distance from the end of the beam to the symmetrical loading points, and l is the span of the beam.

$$E = \frac{P\,a}{48\,\partial\,I}\,(3l^2 - 4a^2) \qquad 6.5$$

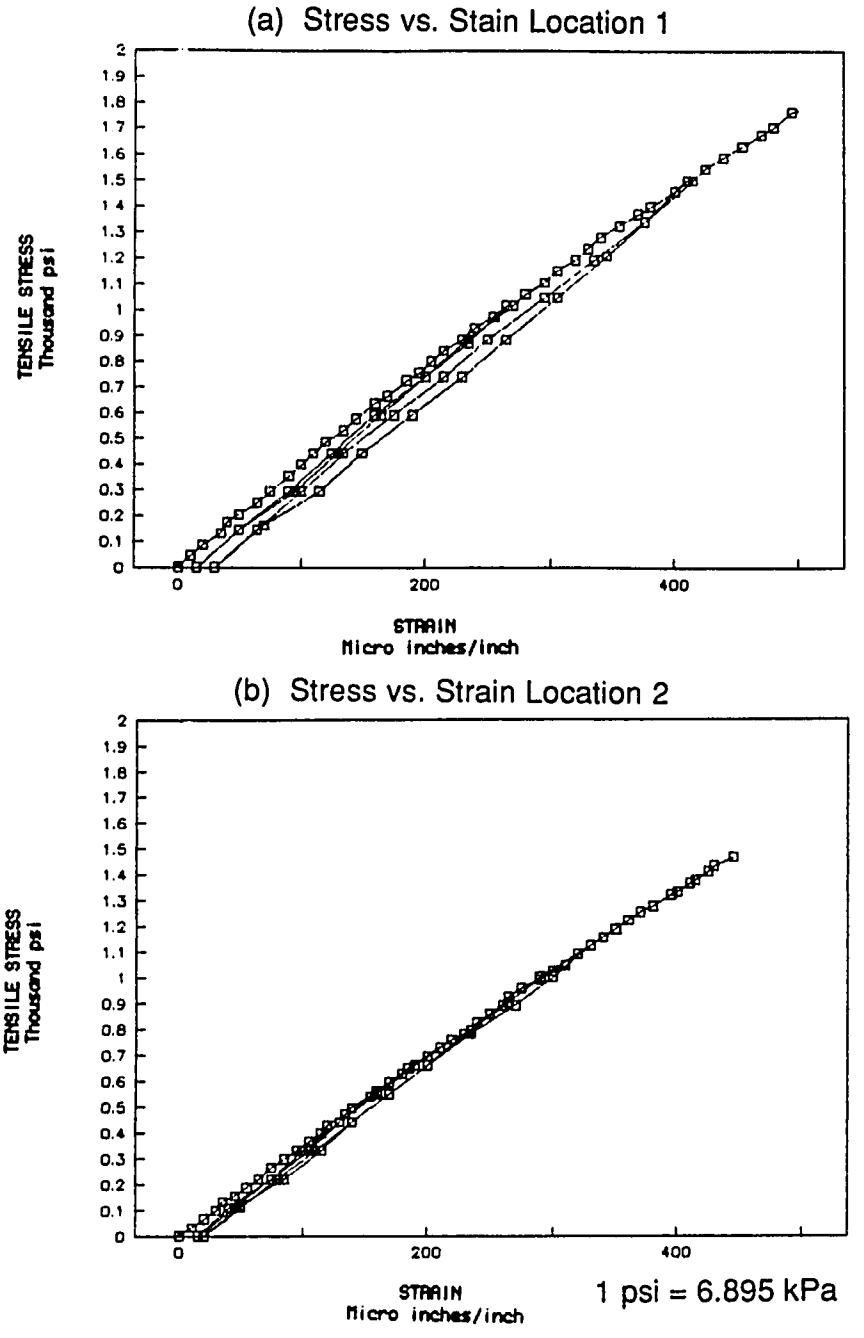


Fig. 6.7 Bending Test Results for Sample 11

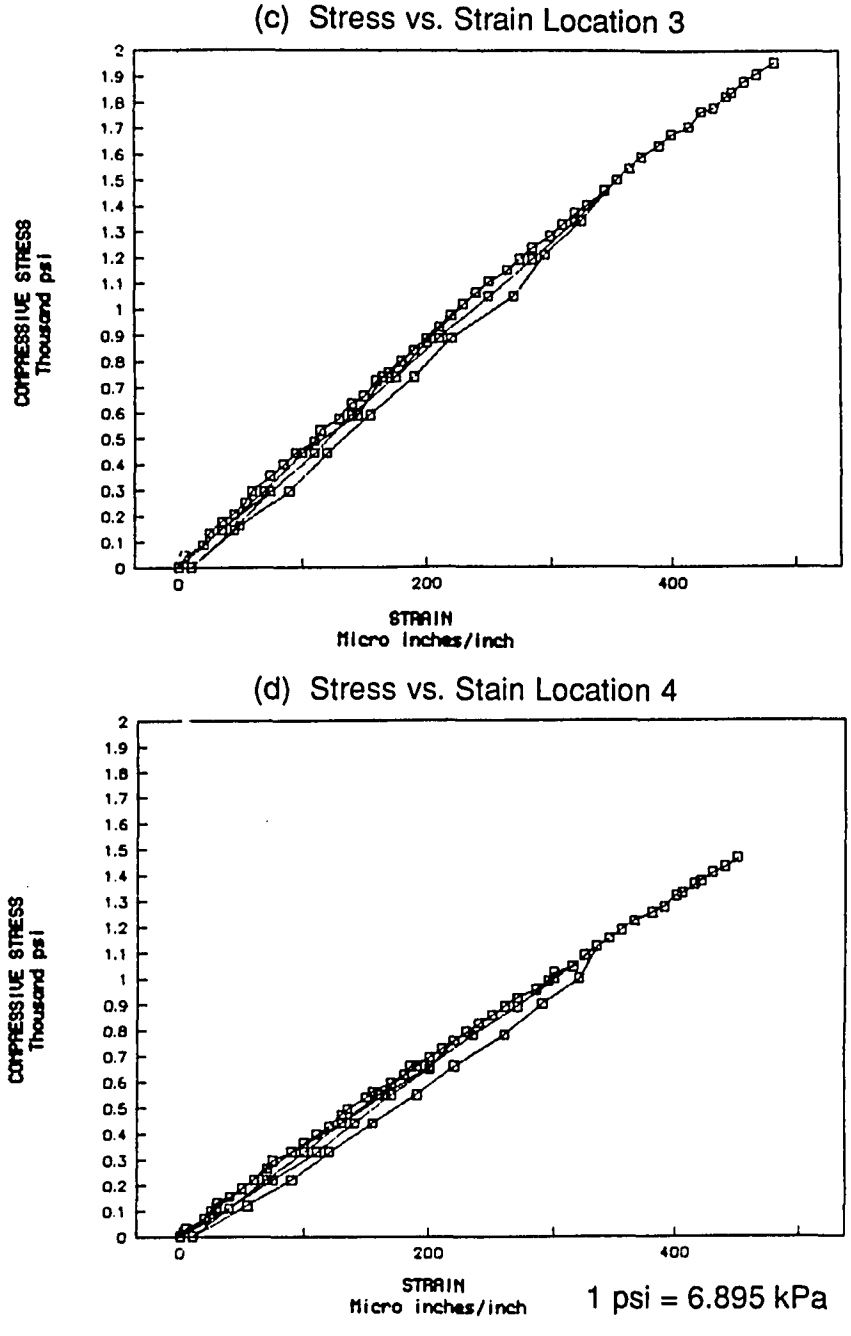


Fig. 6.7 Bending Test Results for Sample 11

(e) Load vs Displacement at Center

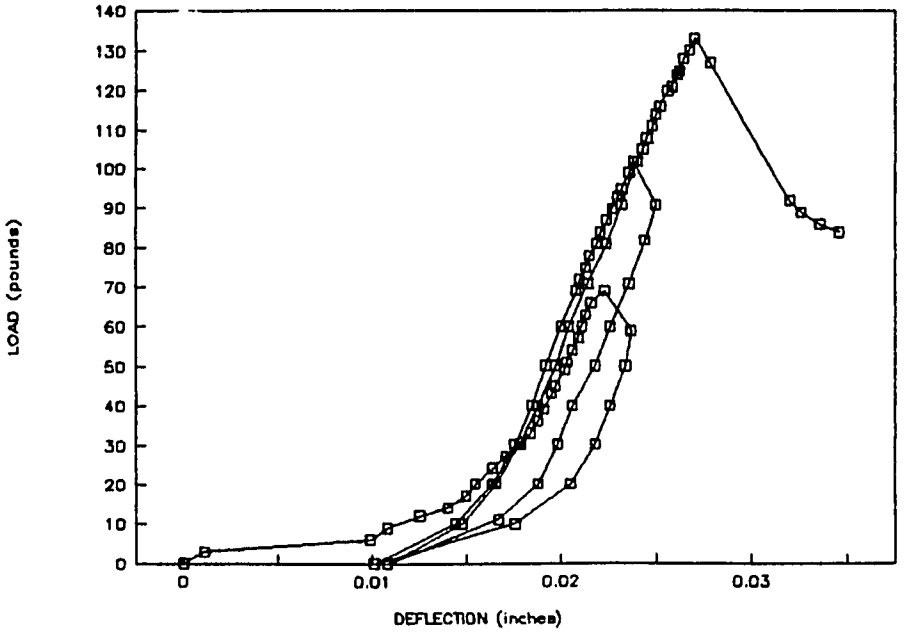


Fig. 6.7 Bending Test Results for Sample 11

Of interest in the load-displacement curve in Fig. 6.7 (e) is the fact that after the failure, the beam withstood considerable residual load, approximately two-thirds of the peak load. This post failure section of the curve is not shown in the stress-strain curves as the failure occured in a crack near the center of the beam and the strains in other portions were subsequently released, and accurate measurements were not possible. The stainless steel fibers in the beam bonded well into the basaltic material, and did not fully pull out upon failure of the matrix. This behavior was observed in all beams containing fibers of carbon or stainless steel. Long after the matrix had failed, the beams continued to carry no less than one-third and up to two-thirds of the peak load under continued applied displacement. This shows that significant bonding is provided via liquefaction of the simulant and a metal fiber of melting point higher than process temperature. Although the fiber does not approach its melting point, the heated and partially molten soil forms bonds on the surface of the soil-fiber interface creating a matrix of significant strength, which is able to withstand post failure loading.

Comparisons of stress-strain curves for beams with and without carbon steel fibers are shown in Figures 6.8 and 6.9. Fig. 6.8 shows the curves for the two locations under tension on the bottom of beam 18A which contained no fibers. Fig. 6.9 shows the curves from the same two locations for beam 12B containing 7.5% of carbon steel fibers. The beam containing carbon steel fibers exhibits nonlinear behavior becoming more obvious when approaching failure; this is not apparent in the beam without fibers, although most test results display some non linear behavior from the outset.

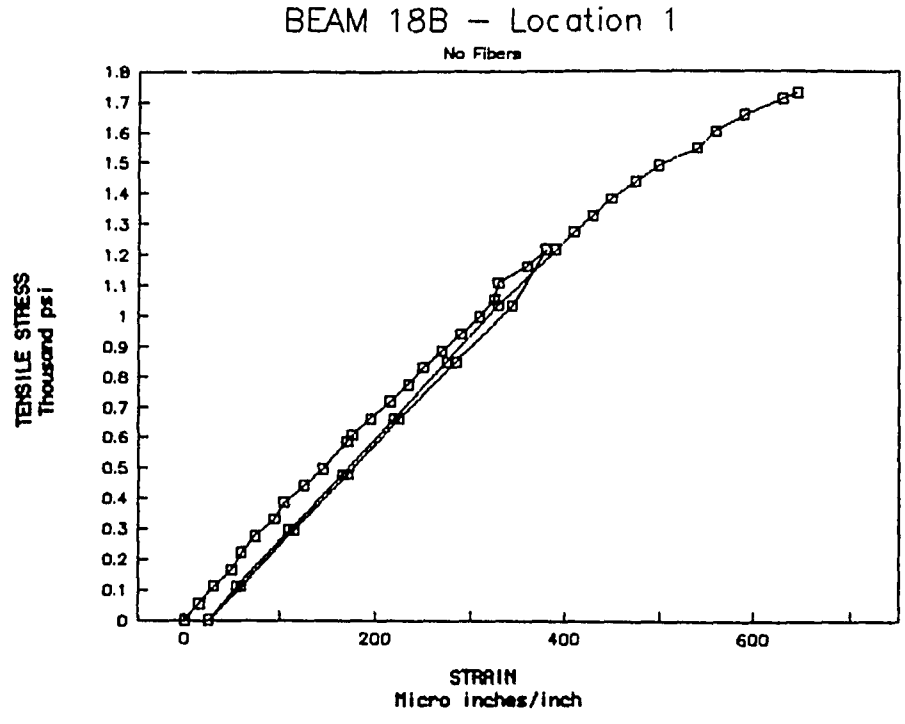


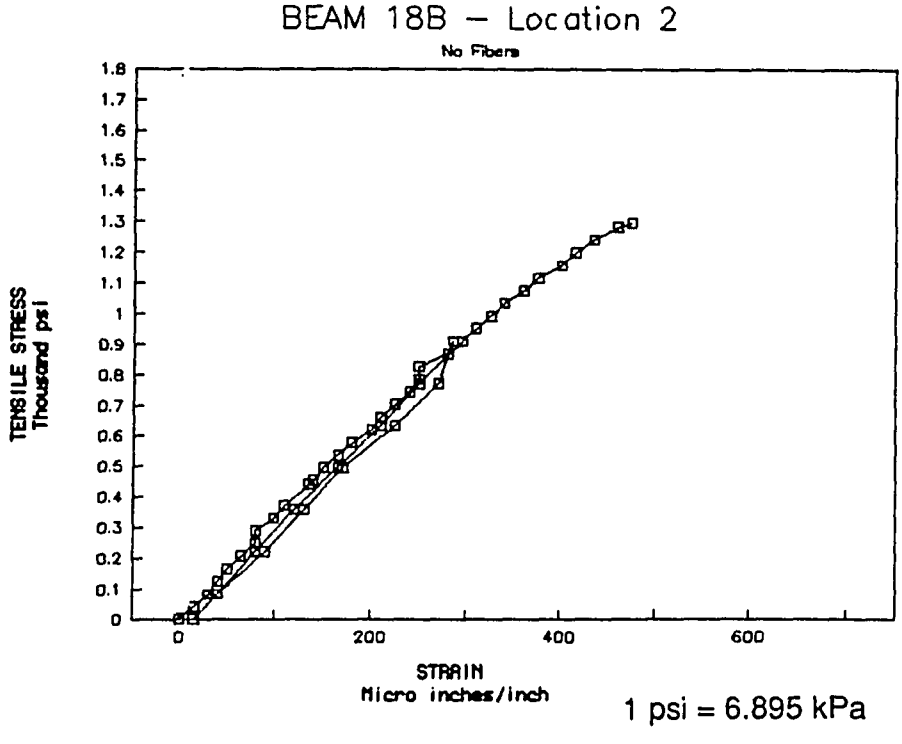


Fig. 6.8 Tensile Stress vs. Strain for Sample 18B in Bending

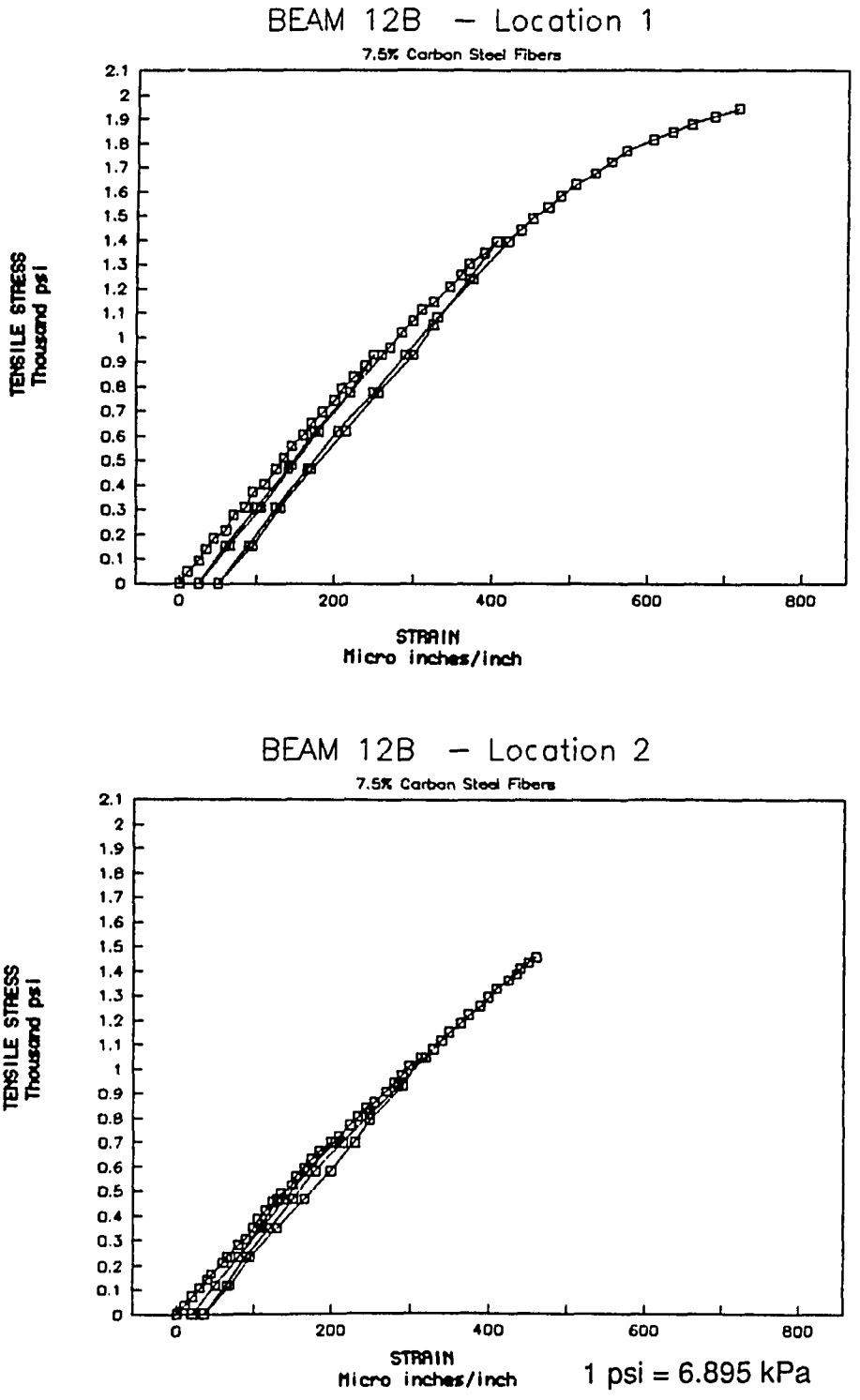


Fig. 6.9 Tensile Stress vs. Strain for Sample 12B in Bending

Figure 6.10 shows the stress-strain curves of beam 12B at the same locations as Fig. 6.9 but on the top of the beam that is under compression. The behavior of the material is obviously different in tension and compression. The strains in compression show essentially no permanent deformations, which are exhibited in the tensile behavior. The modulus from the loading and unloading curves is higher in compression than that in tension. This difference in compressive and tensile behavior was common to most of the beams.

## 6.2 Compression Test Results

Compression tests were conducted on samples cut from intact portions of the beams tested for bending, ASTM standard C116-89 was used as a reference for this procedure. Not all samples were the exact same size, but an attempt was made to conserve the l/r ratio, these dimensions and ratios are shown in Table 4 along with the results of compression testing. All tests were conducted using the MTS testing machine under manual operation.

Figure 6.11 shows the results from 17 compression tests. Graphs from all tests are located in Appendix C. The uniaxial compressive strength, $f'_c$, was calculated by dividing the peak or failure load by the sample surface area. The samples containing no fibers or aluminum fibers showed the highest strengths which are quite similar in magnitude. The strengths of the samples containing steel fibers, carbon and stainless are lower. It is speculated that as the sample size is quite small, the fibers actually create relatively large discontinuities along which the matrix ruptures.

Strains were measured using the LVDT in the MTS frame and computed using small strain theory as $\Delta L/L$, where $\Delta L$ is equal to the observed axial

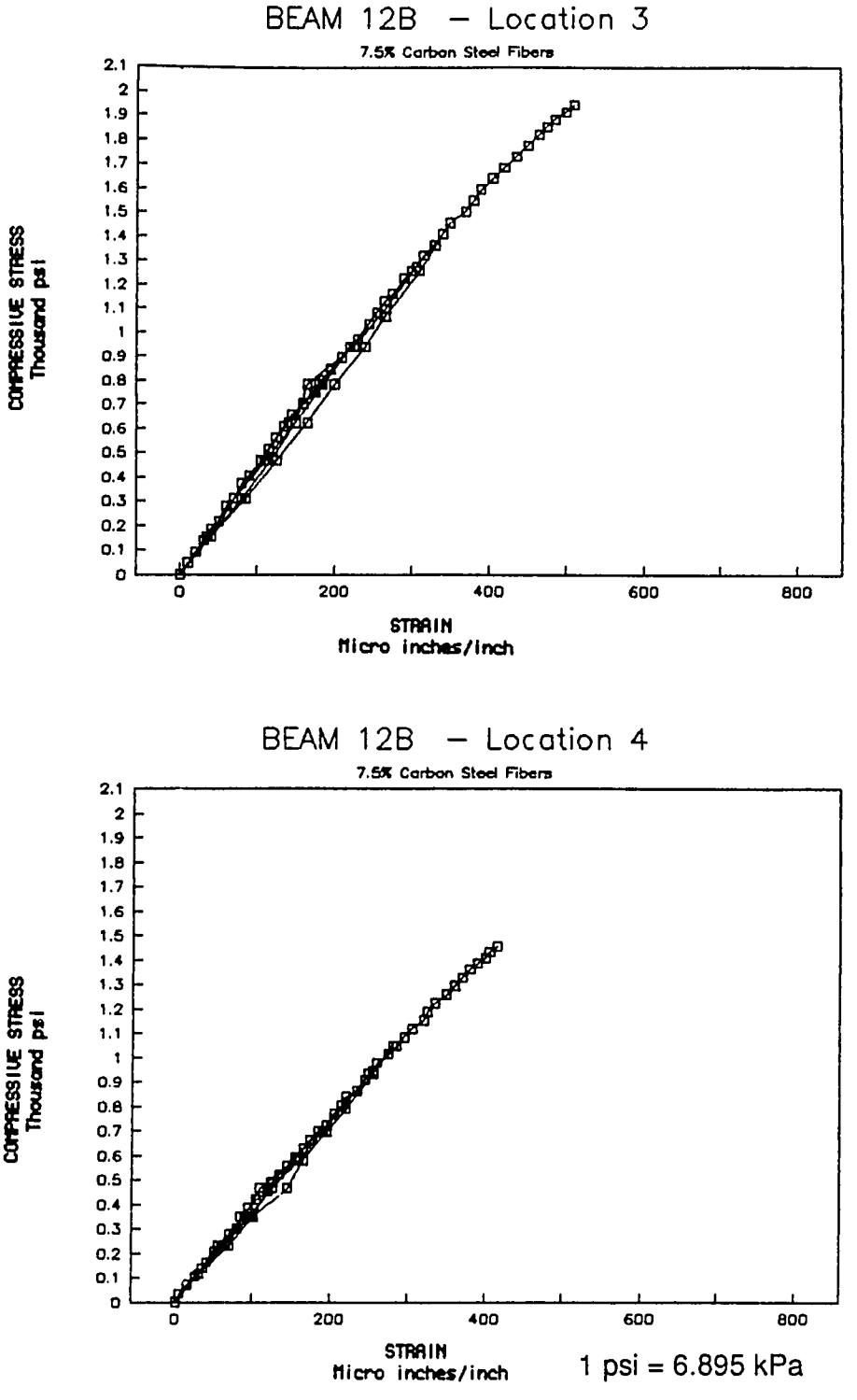


Fig. 6.10 Compressive Stress vs. Strain for Sample 12B in Bending

Table 4

Compression Test and Sample Data

| SAMPLE | FIBER % | MAX STRAIN | MAX STRESS psi | L/r | L in | y in | x in |
|---|---|---|---|---|---|---|---|
| 2 | NONE | 0.0125 | 17871.55 | 13.64 | 2.22 | 0.56 | 0.99 |
| 2 | NONE | 0.0162 | 19371.15 | 9.13 | 1.48 | 0.56 | 0.76 |
| 18B | NONE | 0.0181 | 26306.71 | 8.88 | 1.16 | 0.45 | 0.61 |
| 18B | NONE | 0.0183 | 24109.39 | 8.67 | 1.25 | 0.50 | 0.74 |
| 4A | 7.5 AL | 0.0166 | 23249.67 | 8.75 | 1.14 | 0.45 | 0.68 |
| 4A | 7.5 AL | 0.0240 | 29175.22 | 8.77 | 1.15 | 0.45 | 0.68 |
| 4B | 7.5 AL | 0.0125 | 18473.10 | 8.23 | 1.12 | 0.47 | 0.50 |
| 4B | 7.5 AL | 0.0164 | 23789.90 | 8.48 | 1.22 | 0.50 | 0.65 |
| 4B | 7.5 AL | 0.0147 | 18698.70 | 9.40 | 1.36 | 0.50 | 0.71 |
| 7B | 15 AL | 0.0183 | 23343.11 | 7.92 | 1.26 | 0.55 | 0.62 |
| 7B | 15 AL | 0.0159 | 25283.97 | 7.66 | 1.22 | 0.55 | 0.67 |
| 5A | 15 CS | 0.0135 | 10336.60 | 7.81 | 1.18 | 0.52 | 0.55 |
| 5A | 15 CS | 0.0109 | 8701.18 | 8.70 | 1.33 | 0.53 | 0.66 |
| 11 | 7.5 SS | 0.0167 | 20316.04 | 7.80 | 1.29 | 0.57 | 0.77 |
| 8C | 15 SS | 0.0129 | 11792.18 | 8.66 | 1.13 | 0.45 | 0.51 |
| 8C | 15 SS | 0.0182 | 25723.90 | 8.45 | 1.24 | 0.51 | 0.64 |
| 8C | 15 SS | 0.0137 | 18557.60 | 7.46 | 1.10 | 0.51 | 0.56 |

AL - aluminum
SS - stainless steel
CS - carbon steel

1 psi = 6.895 kPa

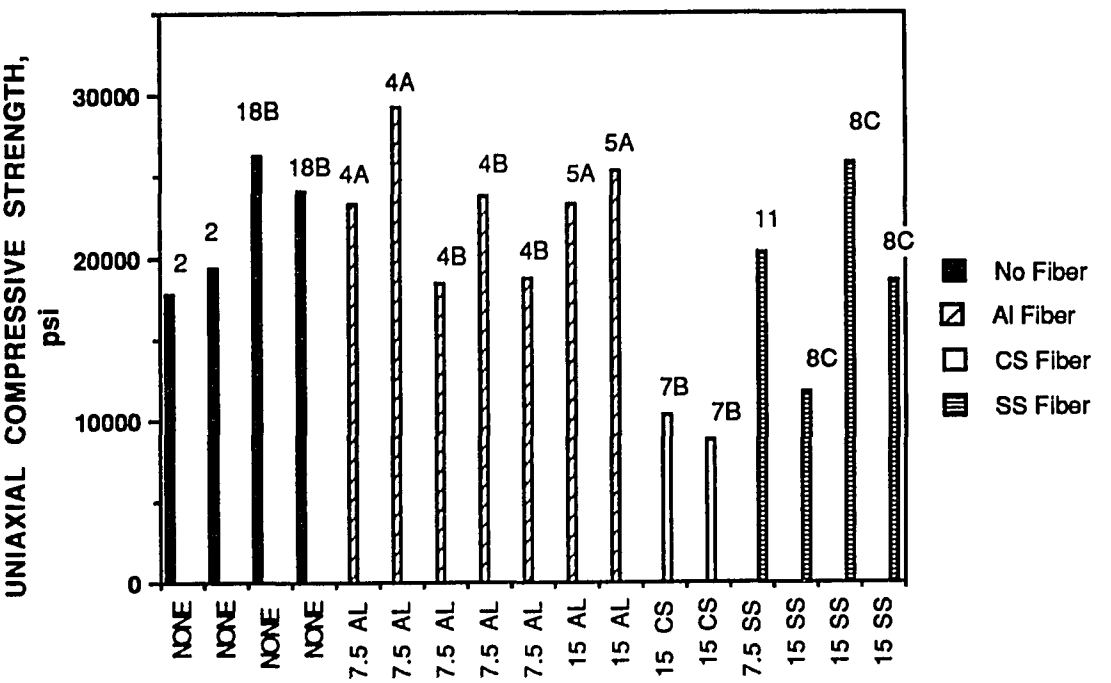


1 psi = 6.895 kPa

Fig. 6.11 Compression Test Results

displacement and L is the original specimen length. Figure 6.12 shows the relationship between ultimate strain, or strain computed at failure, and compressive stress.

Figure 6.13 shows an example of a stress-strain curve for the compression tests. From each of these curves a modulus was computed, using linear regression methods, from the points of stress and strain within the range of 0.2 $f'_c$ to 0.6 $f'_c$. It was impossible to gain information on the post failure behavior of these materials using the MTS device, because the hydraulic powered ram pulverized the sample at failure.

## 6.3 Comparison of Results. Moduli and Strengths.

The elastic or Young's modulus, E, from the bending and compression tests do not compare well. When the modulus from the compression test as calculated above is compared with the modulus from the initial loading curve of strain from the bending tests in compression, the modulus from the bending tests is consistently higher. The method of data collection from the bending tests should be considered more accurate, as the strains were directly measured over the locations directly beneath the1/2" gage, however the stresses were computed assuming uniform cross sections. Table 5 shows the moduli as computed from the bending tests in which strain gages were used.

Possible errors in collecting strain measurements in the compression testing include the following: 1) Computation of strains in the formerly described manner assumes the stress is uniformly distributed over the length of the sample, when in reality the stress may be nonuniform due to severe stress

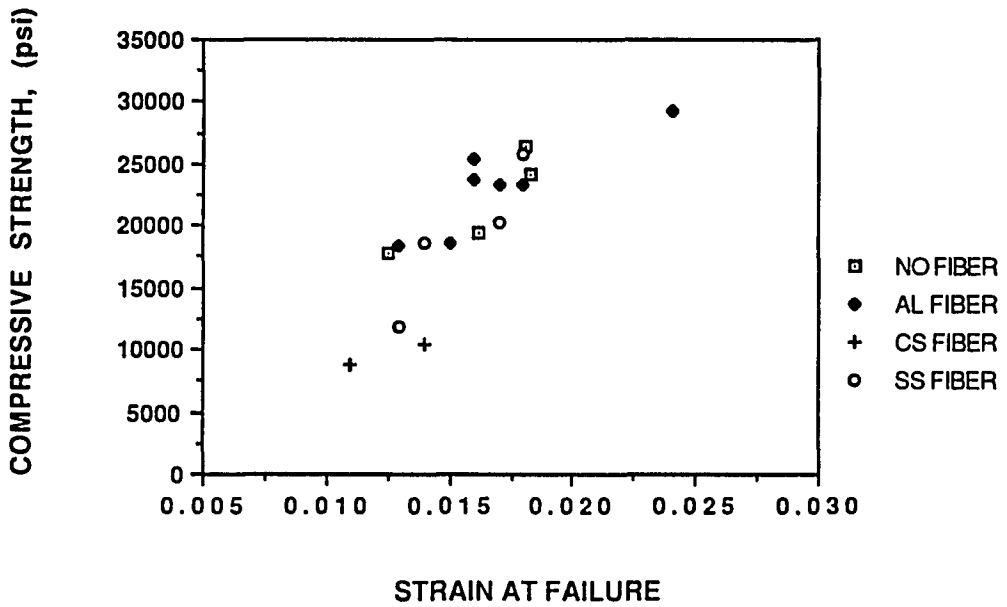


1 psi = 6.895 kPa

Fig. 6.12 Strength vs. Strain at Failure

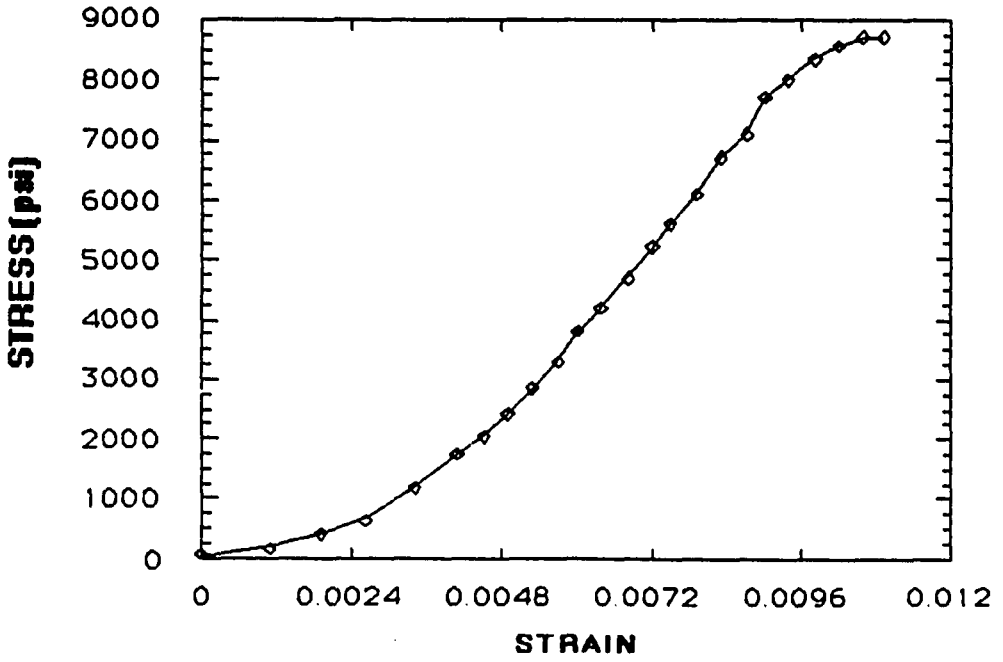


1 psi = 6.895 kPa

Fig. 6.13 Stress vs. Strain for Sample 5A - 2

concentration and damage in the top and bottom zones. 2) The fact that the portions tested in compression had already been subjected to some stress in the bending tests may have reduced the strength of the material and caused unreliable strain measurements. Every attempt was made, when cutting the sections to be tested, to use only the pieces from the ends of the beams, as these had been subjected to less stress. 3) End effects, from uneven stressing and friction on the surfaces may have cused this error in strain measurements as well as lowered strengths. One sample was tested using teflon squares placed between the ends and the machine plattens. This test showed extremely large strains up to the point where the teflon failed, after this point the teflon had no effect whatsoever. Subsequent samples were tested using a small film of graphite to lubricate the end surfaces, however, it is not clear if this was effective in reducing friction. Whatever the error causing lowered values of E may be, its value is consistent in all tests, hence, a comparison of moduli within the compression tests is possible.

A comparison of values of E from compression tests is shown in Figure 6.14. The value for E of samples containing no fibers is fairly consistent around $1.6 \times 10^6$ psi. For samples containing aluminum fibers this modulus increases to about $1.75 \times 10^6$. The modulus is significantly lower for samples containing carbon steel, implying that the inclusion of these fibers can cause reduction in stiffness of the specimens under compression. For stainless steel fiber samples the modulus is not as dramatically lower.

Figure 6.15 illustrates the comparison of moduli from compression and bending tests for a sample containing 15% carbon steel fibers. Note the moduli

Table 5

Moduli From Beam Bending Tests

| SAMPLE # | FIBER - % | INITIAL MODULUS COMPRESSION psi in 10^6 | INITIAL MODULUS TENSION psi in 10^6 | 1st UNLOADING MODULUS COMPRESSION psi in 10^6 | 1st UNLOADING MODULUS TENSION psi in 10^6 | 2nd UNLOADING MODULUS COMPRESSION psi in 10^6 | 2nd UNLOADING MODULUS TENSION psi in 10^6 |
|---|---|---|---|---|---|---|---|
| 18A | NONE | 3.50 | 3.08 | 3.48 | 3.21 | - | - |
| 18B | NONE | 4.63 | 3.27 | 4.69 | 3.33 | - | - |
| 4A | AL - 7.5 | 4.60 | 4.25 | 4.65 | 4.41 | - | - |
| 7A | AL - 15 | 7.20 | 6.10 | 8.44 | 5.80 | 7.78 | 6.58 |
| 12B | CS - 7.5 | 4.26 | 3.71 | 4.26 | 4.10 | 4.08 | 3.90 |
| 5A | CS - 15 | 3.46 | 2.65 | 3.37 | 2.74 | 3.10 | 2.71 |
| 8B | SS - 15 | 5.99 | 5.99 | 5.55 | 6.10 | 5.42 | 5.78 |
| 11 | SS - 7.5 | 4.33 | 3.81 | 4.01 | 4.38 | - | - |

1 psi = 6.895 kPa

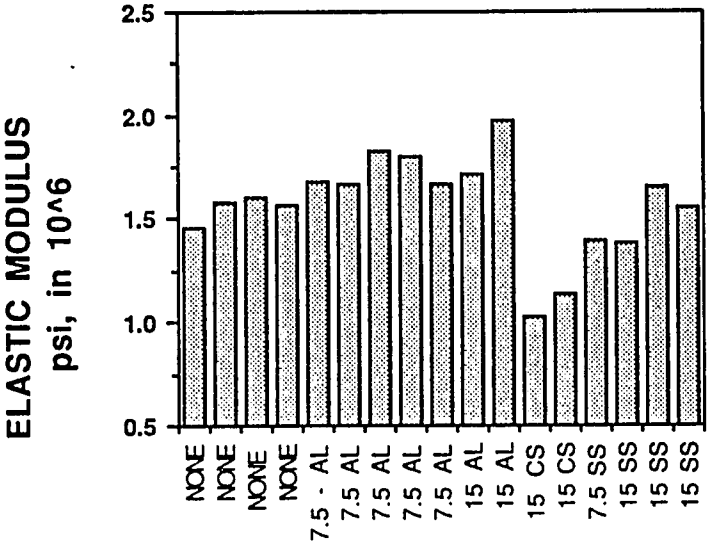


1 psi = 6.895 kPa

Fig. 6.14 Elastic Moduli from Compression Tests

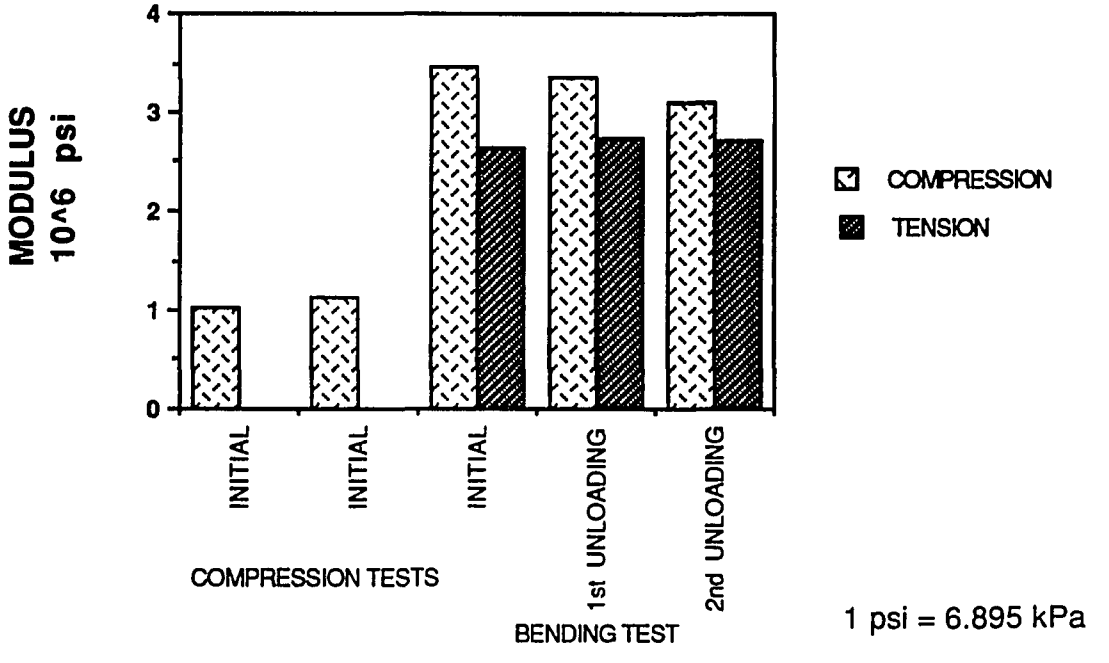


Fig. 6.15 Comparison of Moduli for Beam 5A with 15% Carbon Steel Fibers

from bending tests are about three times those from compression tests. Also of interest is that in the difference in moduli from the bending tests, the modulus in compression is significantly higher than that in tension, which decreases in successive unloading and reloading cycles indicating degradation. This may or may not be an experimental error; most materials exhibit the same modulus in compression as in tension.

This trend is observed in other test results also. Figure 6.16 shows the same trend in a sample containing 7.5% carbon steel fibers, and Fig. 6.17 shows this in a sample containing 7.5% Al fibers.

Figure 6.18 shows comparison of moduli from a sample containing no fibers. The average value in compression resulting from bending obtained from this test is $4.7 \times 10^6$ psi. This value compares favorably to the value of $4.96 \times 10^6$ psi reported for a basalt by Goodman (1989). It is also noted that values computed from all tests are in approximately the same range of the $3.0 \times 10^6$ psi commonly used for concrete. This comparison is reassuring, showing that the values obtained experimentally are reasonable for this type of material.

The values of compressive strength for samples with no fibers also compare closely with the values given earlier by Meek et al, (1988). Goodman, (1989), also gives 21,000 psi as the value of compressive strength for basalt. The compressive strength of standard concretes are much lower than the values obtained in this research. Ratios of bending strength to compressive strength are also around the 10% commonly used as a rule of thumb for concrete.

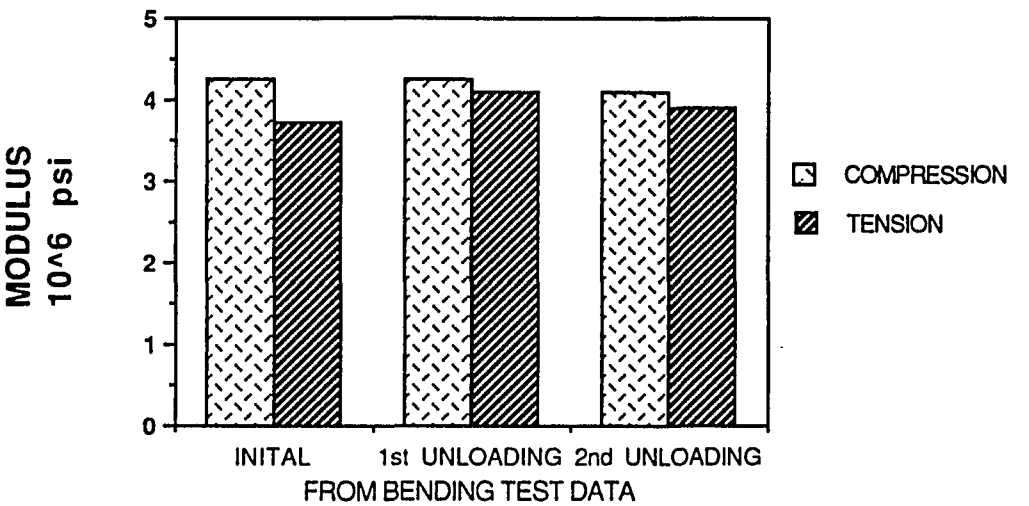


1 psi = 6.895 kPa

Fig. 6.16 Moduli From Bending Test of Sample 12B with 7.5% Carbon Steel Fibers

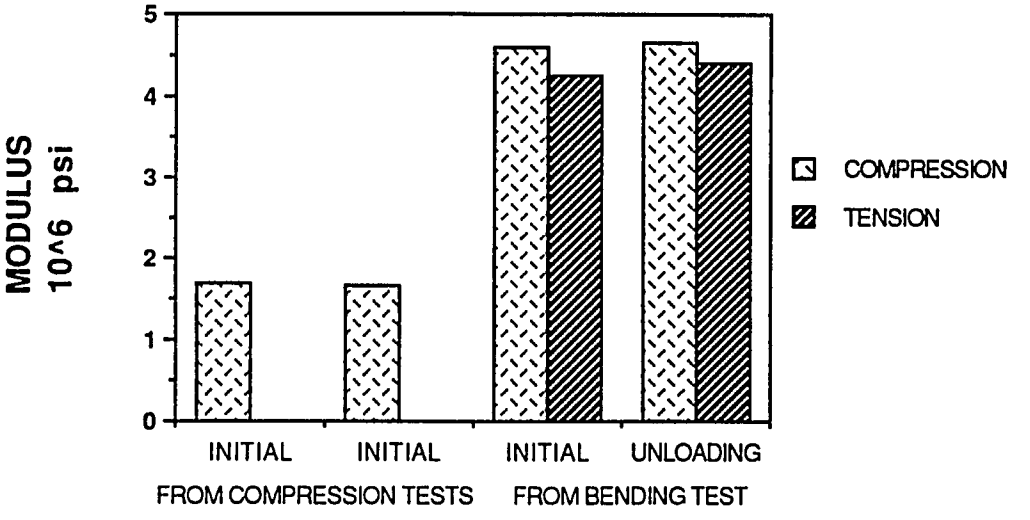


1 psi = 6.895 kPa

Fig. 6.17 Comparison of Moduli for Beam 4A with 7.5% Aluminum Fibers

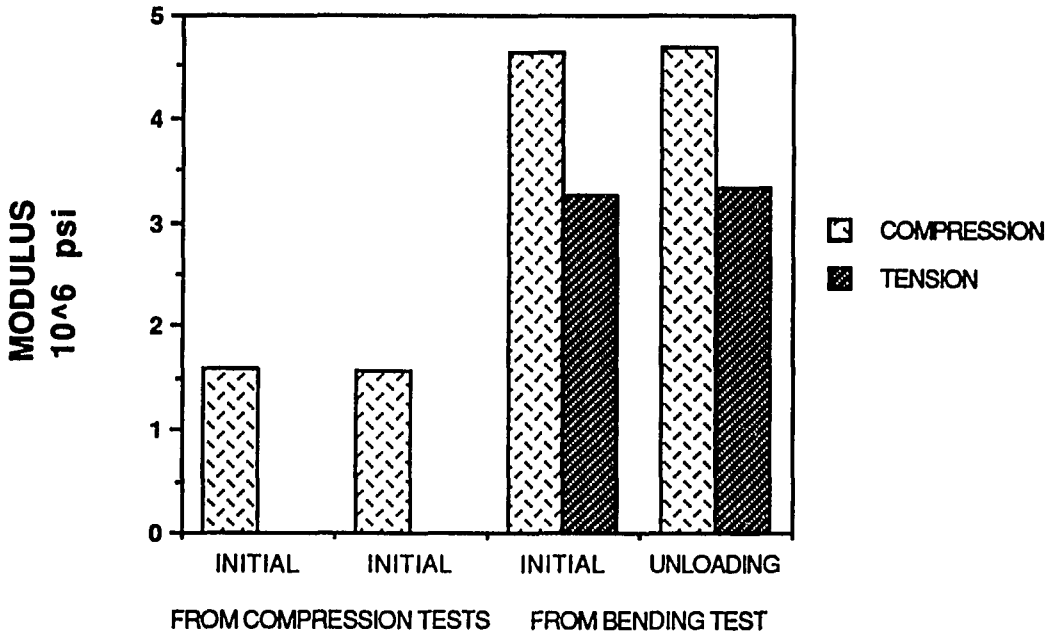


1 psi = 6.895 kPa

Fig. 6.18 Comparison of Moduli for Beam 18B with no Fibers

# CHAPTER 7
# CONCLUSIONS

## 7.1 Use of Liquefaction for Structural Materials

This research has shown that the liquefaction of a lunar simulant with fibers can yield a material of considerable strength and that the presence of fibers do modify the mechanical behavior of the material. Applications of a material with this strength would not be limited to construction on the lunar surface but can conceivably include production of tools and machine parts.

Among the fibers considered, the addition of aluminum fibers is seen to have great effect on the strength of the material but does little to enhance the elastic properties, effectively raising the modulus of elasticity and then failing in a brittle and sudden manner. The effect of liquefaction of the fibers, creating the influence zones of heated simulant, is evident. The addition of stainless steel fibers also has a strengthening effect in bending although not in compression and it modifies the elastic behavior of the material. The carbon steel fiber tended either to not affect or to weaken the strength of the material. It has a great influence on the elastic modulus, which it lowered. significantly. Both the carbon and stainless steel fibers affect the post failure behavior of the beams in a positive manner, as the complete fracture of the matrix is prevented and the fibers move, bend and continue to hold the beam together to resist load.

It is clear that the liquefaction of lunar simulants with fibers can provide a viable lunar material, capable of withstanding various loads; moreover, it can be easily produced by using solar energy.

## 7.2 Suggested Further Research

The research performed here is only the beginning of what needs to be investigated before any final conclusions can be made. It is necessary that beyond the development of the material, particular attention must be given to appropriate mechanical testing and the determination of mechanical properties necessary to design structural members on the moon. Further research to achieve the goal of materials for space made of locally derived resources includes the following.

### 7.2.1 Simulants

Similar preparation and testing to that included in this report can be performed with the Minnesota Lunar Simulant (MLS). The Arizona Lunar Simulant (ALS) is more than adequate for preliminary and subsequent work. However, due to its adoption as the optimal simulant, results from testing of samples made from the MLS would provide enhanced results and understanding.

### 7.2.2 Fibers

The use of other fibers and combinations of fibers should be investigated. Fiberglass, which can be produced from lunar soil simulants, should be incorporated into this research. It is suggested that the preparation and testing be done with samples that are made with various percentages of fiberglass, in the same manner these tests were conducted with metal fibers.

### 7.2.3 Temperature Cycling

Under the initial scope of this project, it was expected that thermal cycling of the material, above and below the range of liquefaction, would provide additional benefits. It was speculated that a prestressing effect may occur from

the cyclic expansion and contraction of fibers within the heated matrix. Such an investigation should be completed to determine if there are additional changes to the mechanical behavior from this form of heat treatment. For instance, the potential flaws and cracks at the (melted) fiber-soil interfaces, that may cause reduction in the (compressive) strength, may be reduced with such a procedure.

### 7.2.4 Vibration

This research discovered many effects which may be due to the porous nature of the matrix material. It is thought that if the porosity were to be reduced, the mechanical properties could be further affected. In order to increase the initial density and change the orientations of the fibers and particles to be heated, they could be systematically vibrated before melting. It may also be beneficial to vibrate the material during the liquefaction process. It is recommended that some form of vibration be investigated and the produced samples compared to those included in this reasearch.

### 7.2.5 Further Testing

As an initial investigation, rather simple testing was conducted on the specimens in this research. Although such testing is significant and can lead future researchers to better materials, it is in no way comprehensive mechanical testing. These materials, once the optimal combinations of fibers or additives and temperature have been determined, should be subjected to the full range of mechanical testing. This testing can include triaxial and multiaxial tests to develop models for stress-strain-strength behavior, and testing for tensile strength of the materials. Testing should also be done to determine the thermal expansion coefficients and long term degradation effects when subjected to

moon-like conditions. Final testing should incorporate scale model testing under vacuum or pressurized conditions, and investigation of the soil(regolith)-structure interaction effects on structures on the moon.

The results from detailed development and testing of structural materials can represent a significant contribution towards development of appropriate methodologies for construction of facilities on the moon and planets.

# APPENDIX A

## BEAM BENDING TEST DEVICE DRAWINGS

(APPENDIX A)

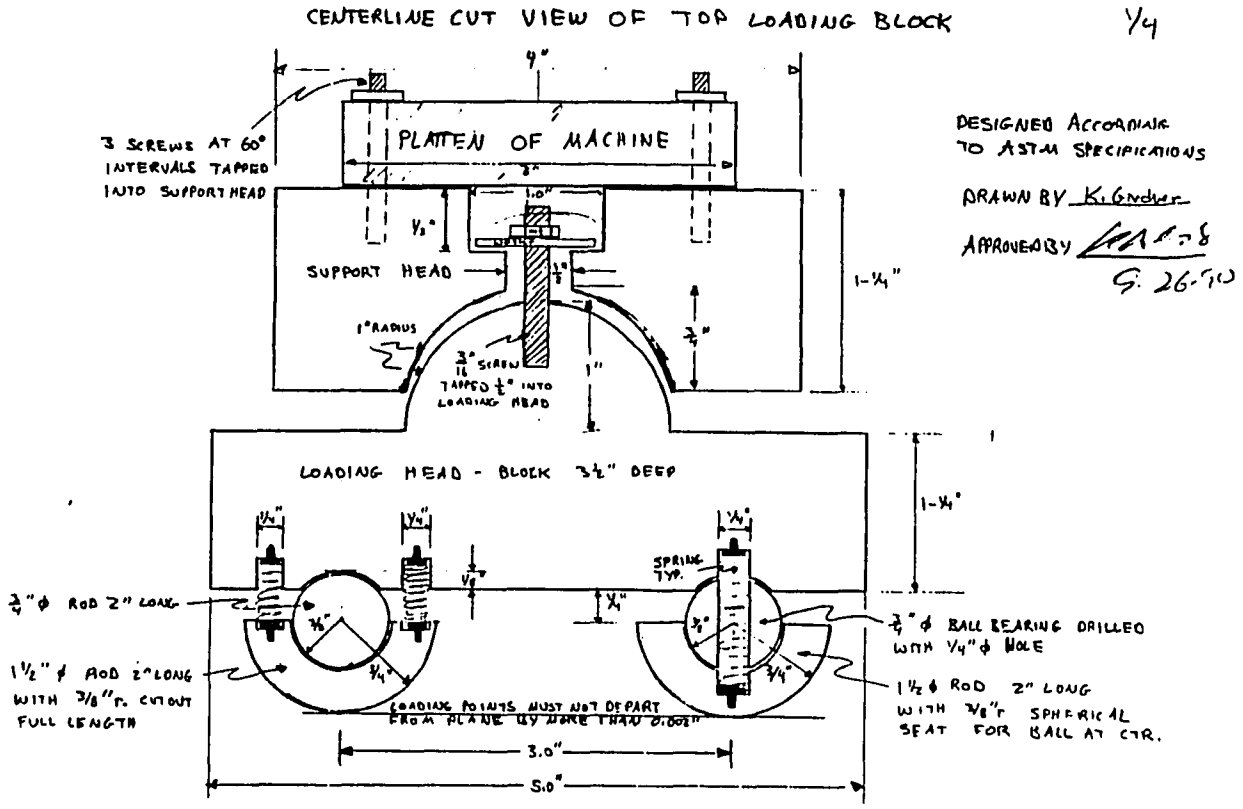
CENTERLINE CUT VIEW OF TOP LOADING BLOCK
PLATTEN OF MACHINE
3 SCREWS AT 60° INTERVALS TAPPED INTO SUPPORT HEAD
SUPPORT HEAD
1" RADIUS
LOADING HEAD - BLOCK 3½" DEEP
SPRING TYP.
¾" ϕ ROD 2" LONG
1½" ϕ ROD 2" LONG WITH ⅜" r. CUT OUT FULL LENGTH
¾" ϕ BALL BEARING DRILLED WITH ¼" ϕ HOLE
1½ ϕ ROD 2" LONG WITH ⅜" r SPHERICAL SEAT FOR BALL AT CTR.
LOADING POINTS MUST NOT DEPART FROM PLANE BY MORE THAN 0.002"
3.0"
5.0"
DESIGNED ACCORDING TO ASTM SPECIFICATIONS
DRAWN BY K. Gardner
APPROVED BY
G. 26-70

(APPENDIX A)

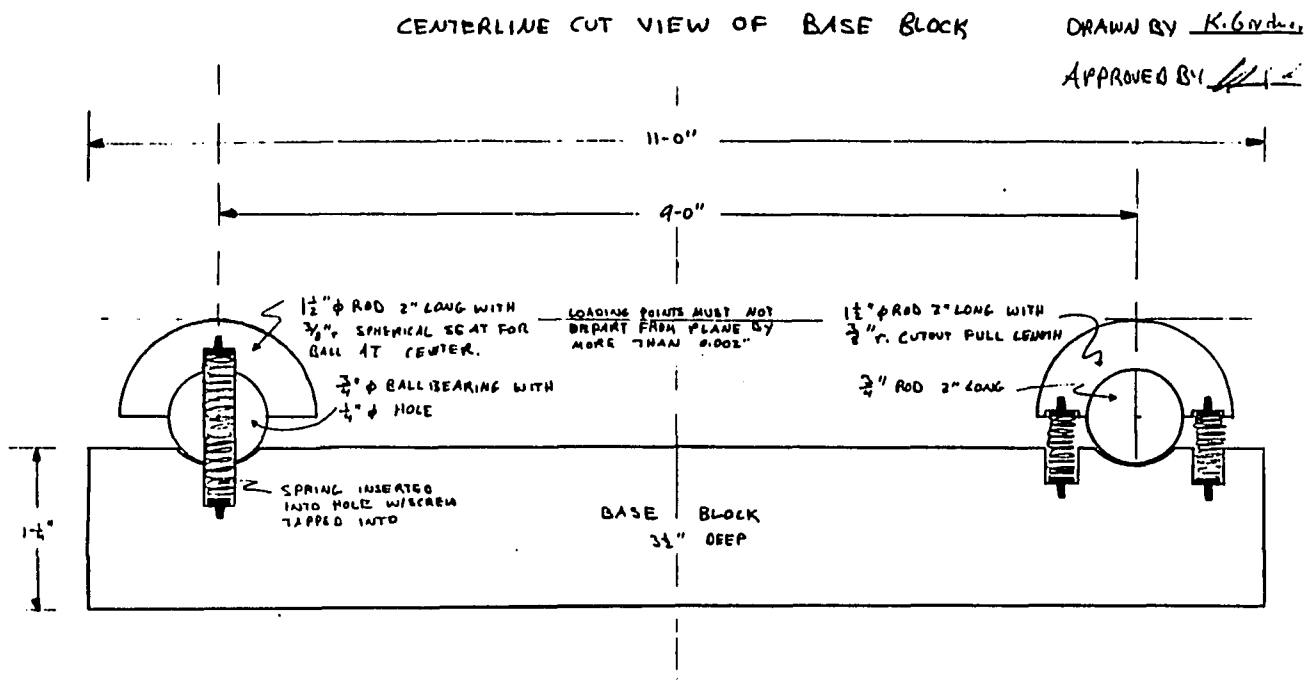
CENTERLINE CUT VIEW OF BASE BLOCK
DRAWN BY K. Gruber
APPROVED BY
11-0"
9-0"
1½"ϕ ROD 2" LONG WITH ⅜"r. SPHERICAL SEAT FOR BALL AT CENTER.
LOADING POINTS MUST NOT DEPART FROM PLANE BY MORE THAN 0.002"
1½"ϕ ROD 2" LONG WITH ¾" r. CUTOUT FULL LENGTH
¾"ϕ BALL BEARING WITH ¼"ϕ HOLE
¾" ROD 2" LONG
SPRING INSERTED INTO HOLE W/SCREW TAPPED INTO
BASE BLOCK 3½" DEEP
1½"

(APPENDIX A)

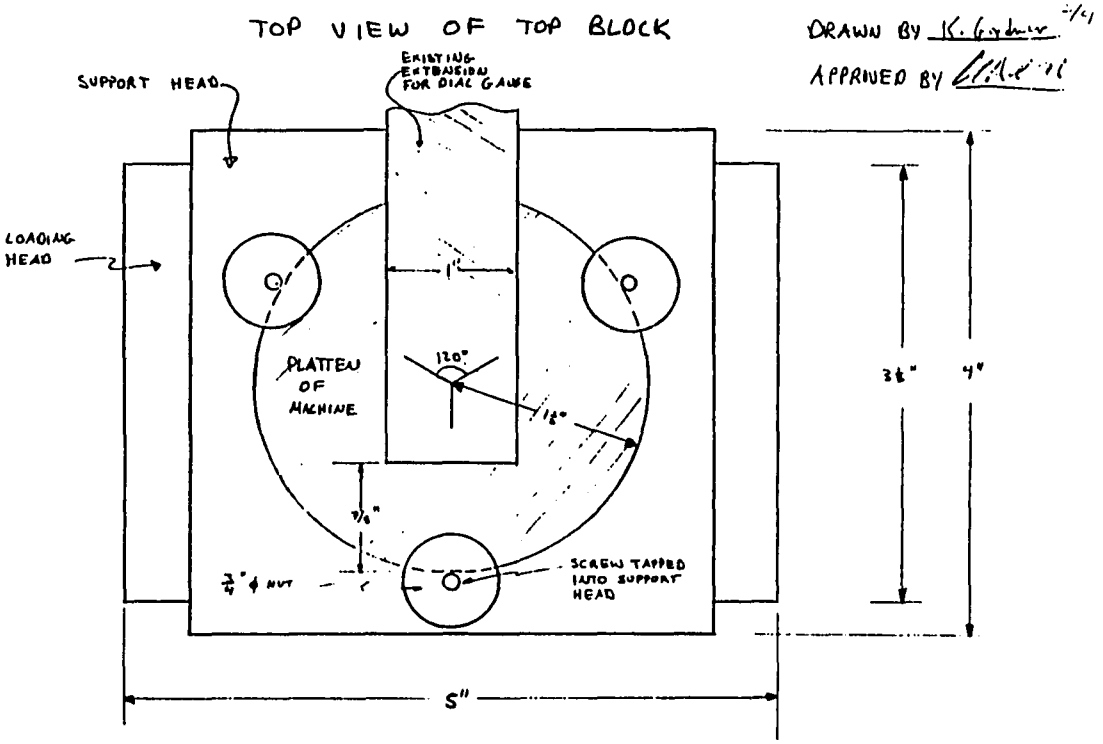
TOP VIEW OF TOP BLOCK
DRAWN BY K. Graham 7/91
APPROVED BY
SUPPORT HEAD
EXISTING EXTENSION FOR DIAL GAUGE
LOADING HEAD
PLATTEN OF MACHINE
120°
1"
1 1/8"
3/8"
3 1/2"
4"
3/4" ϕ HOLE
SCREW TAPPED INTO SUPPORT HEAD
5"

(APPENDIX A)

4/4

TOP VIEW OF BASE BLOCK

DRAWN BY K. Gruber

APPROVED BY

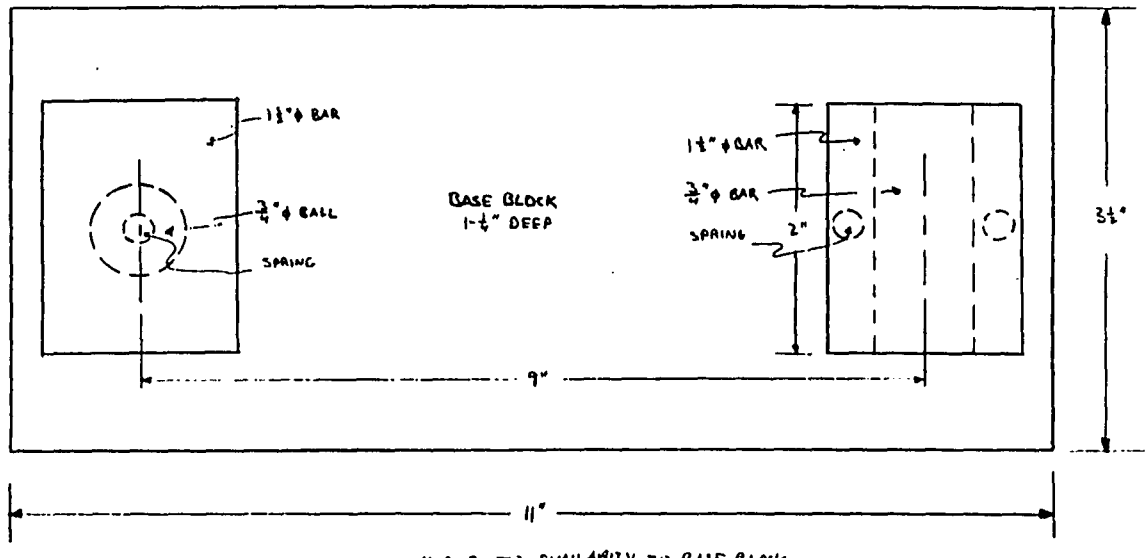


NOTES: VIEW OF LOADING HEAD NOT SHOWN DUE TO SIMILARITY TO BASE BLOCK
1-¼" RODS CAN BE REPLACED WITH 1-½"ϕ RODS
LOADING AND SUPPORT PIECES MUST ROTATE FREELY

# APPENDIX B

# BEAM BENDING TEST RESULTS

(APPENDIX B)

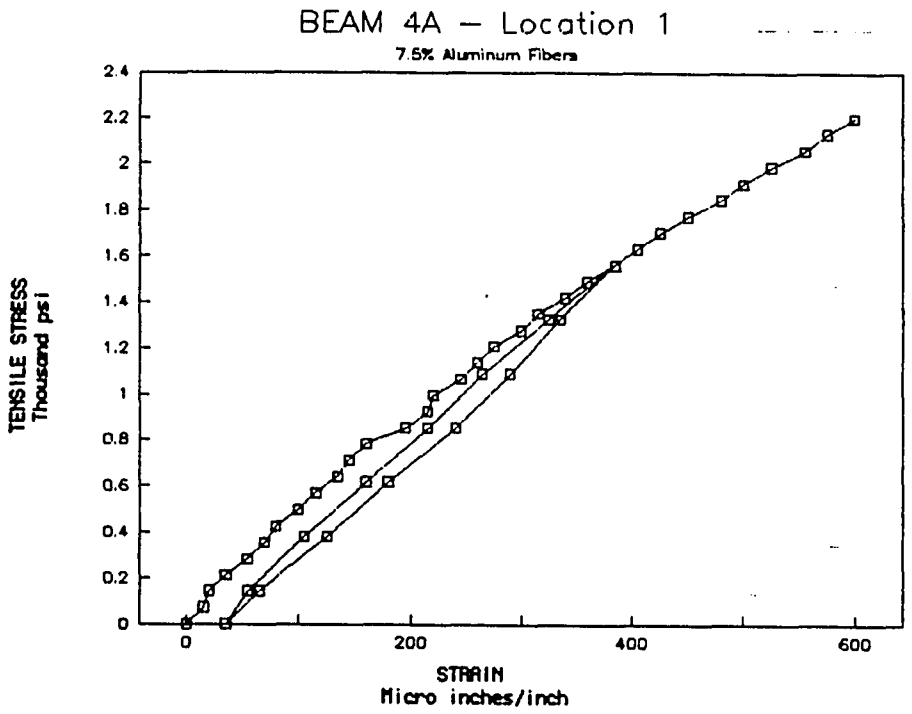
BEAM 4A – Location 1
7.5% Aluminum Fibers
TENSILE STRESS
Thousand psi
2.4
2.2
2
1.8
1.6
1.4
1.2
1
0.8
0.6
0.4
0.2
0
0
200
400
600
STRAIN
Micro inches/inch

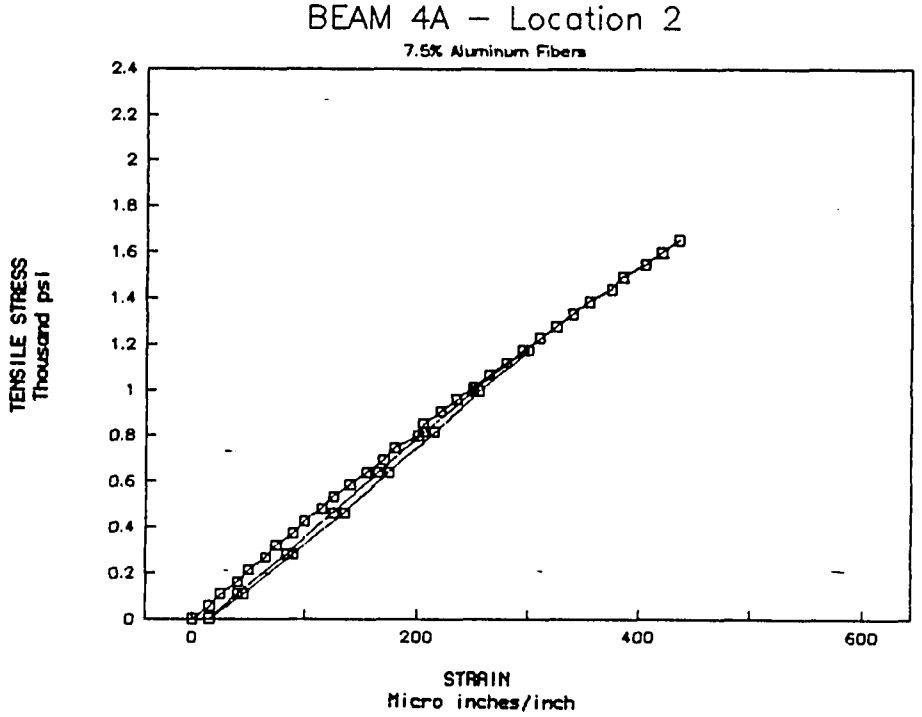
BEAM 4A – Location 2
7.5% Aluminum Fibers
TENSILE STRESS
Thousand psi
2.4
2.2
2
1.8
1.6
1.4
1.2
1
0.8
0.6
0.4
0.2
0
0
200
400
600
STRAIN
Micro inches/inch

(APPENDIX B)

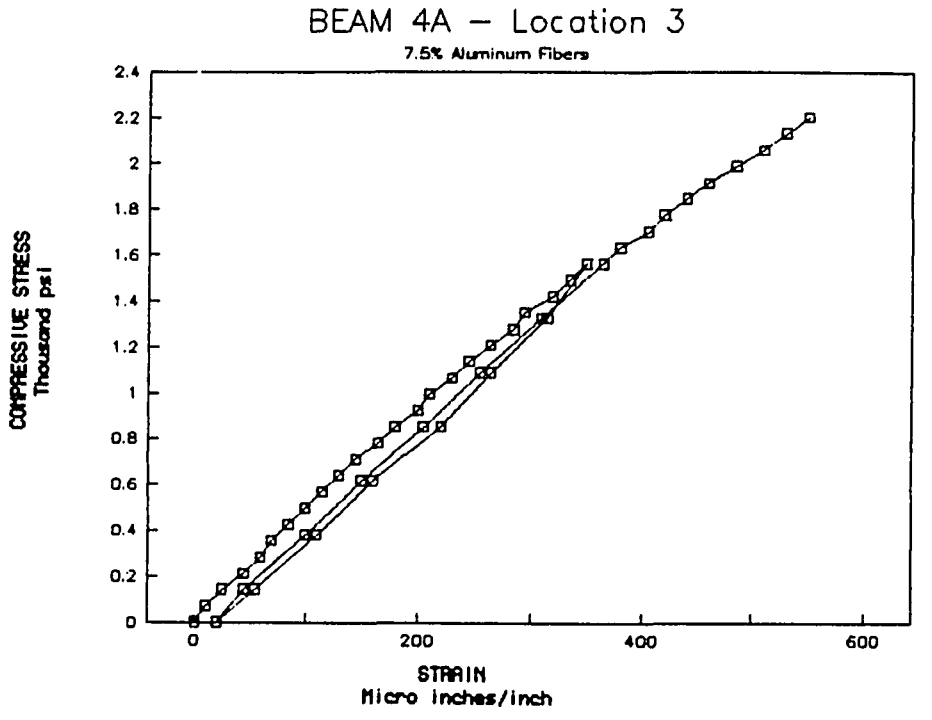
BEAM 4A – Location 3
7.5% Aluminum Fibers
COMPRESSIVE STRESS
Thousand psi
2.4
2.2
2
1.8
1.6
1.4
1.2
1
0.8
0.6
0.4
0.2
0
0
200
400
600
STRAIN
Micro inches/inch

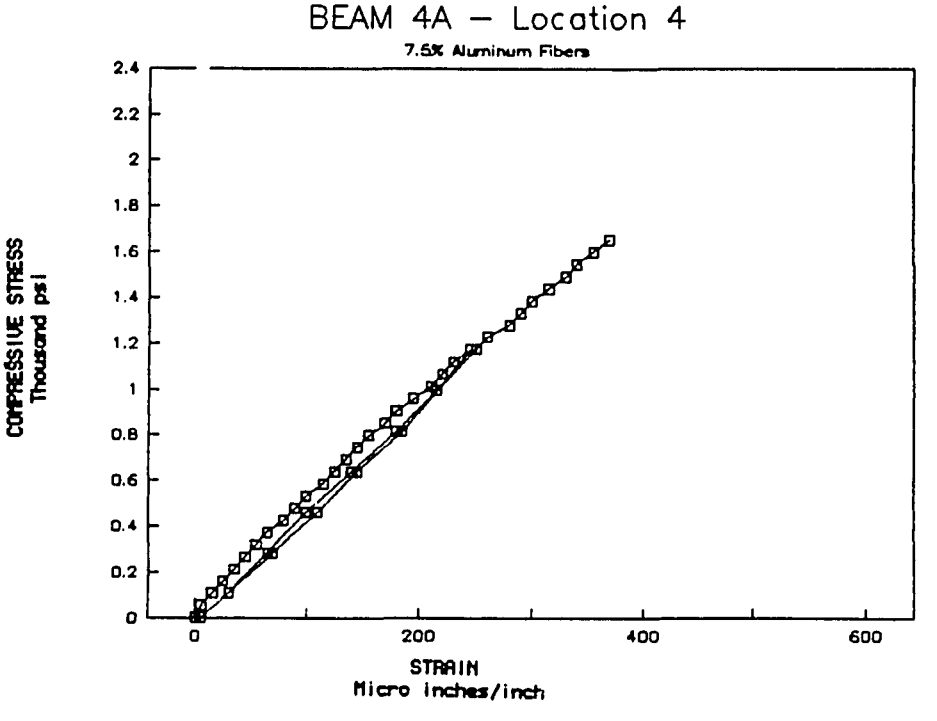
BEAM 4A – Location 4
7.5% Aluminum Fibers
COMPRESSIVE STRESS
Thousand psi
2.4
2.2
2
1.8
1.6
1.4
1.2
1
0.8
0.6
0.4
0.2
0
0
200
400
600
STRAIN
Micro inches/inch

(APPENDIX B)

BEAM 5A – Location 1

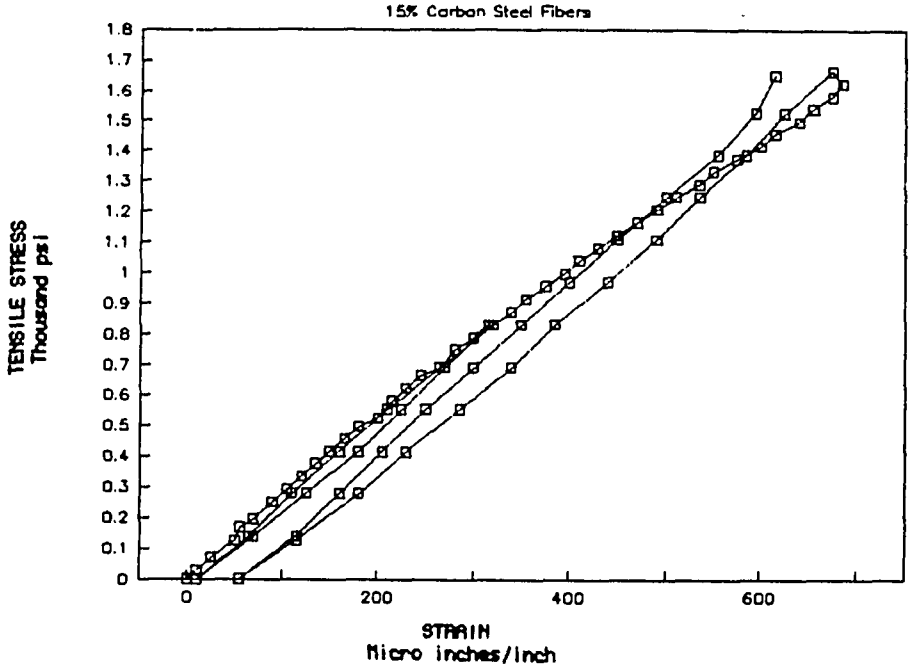


BEAM 5A – Location 2

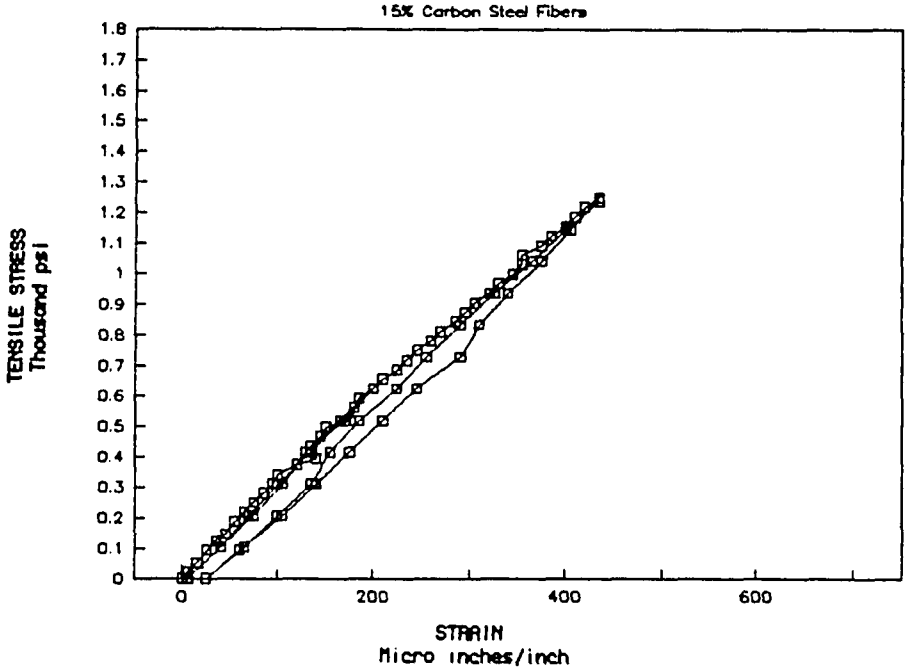

(APPENDIX B)

BEAM 5A – Location 3

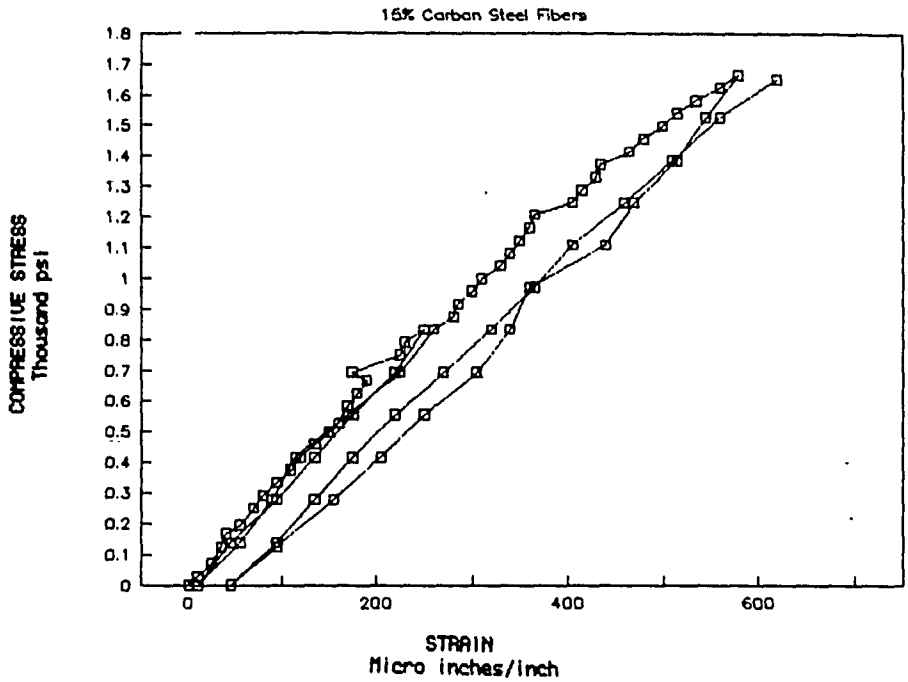


BEAM 5A – Location 4

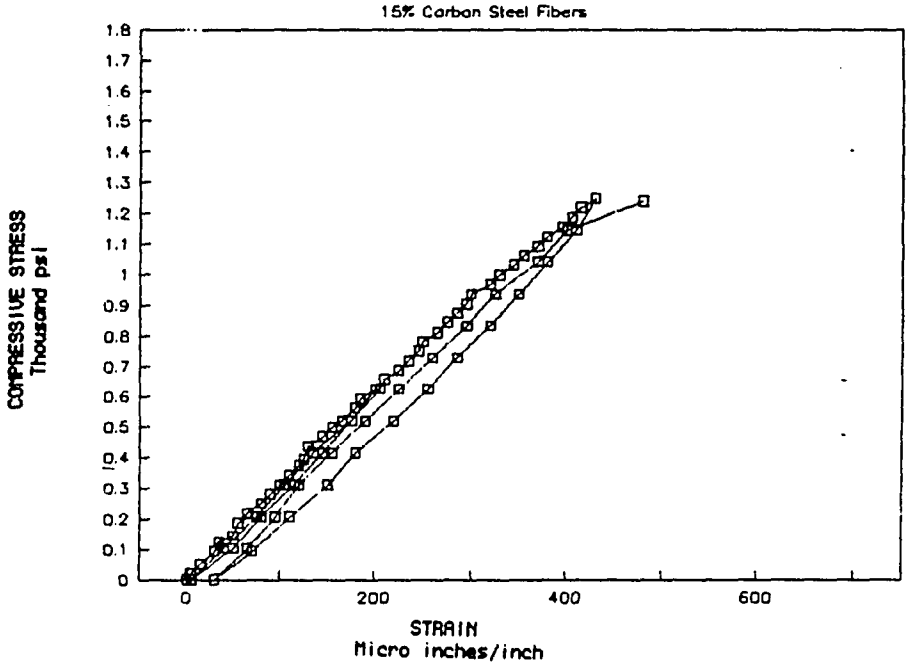

(APPENDIX B)

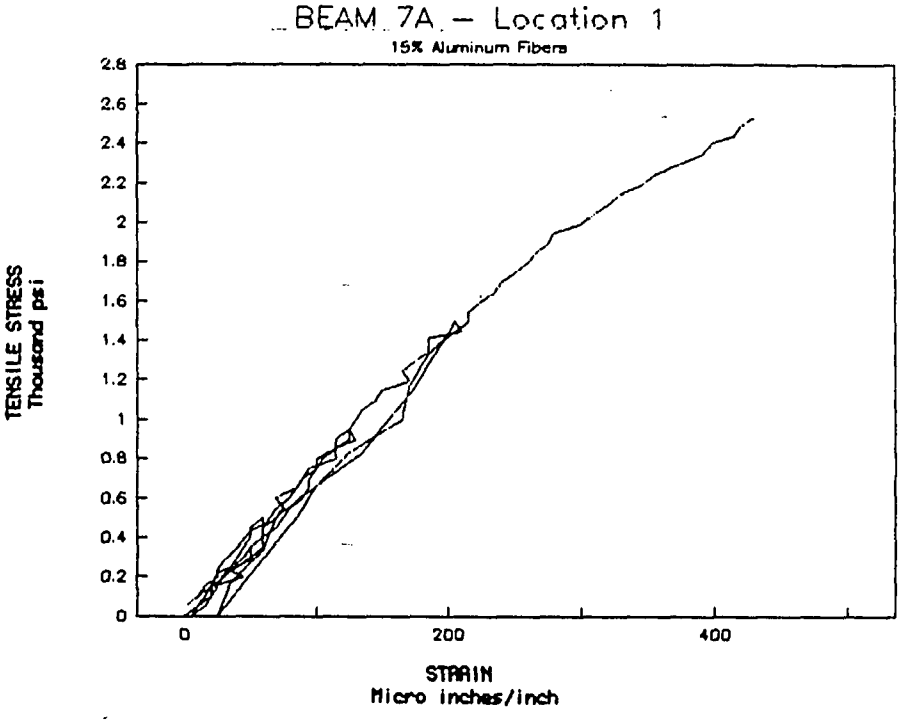
BEAM 7A – Location 1
15% Aluminum Fibers
TENSILE STRESS
Thousand psi
2.8
2.6
2.4
2.2
2
1.8
1.6
1.4
1.2
1
0.8
0.6
0.4
0.2
0
0
200
400
STRAIN
Micro inches/inch

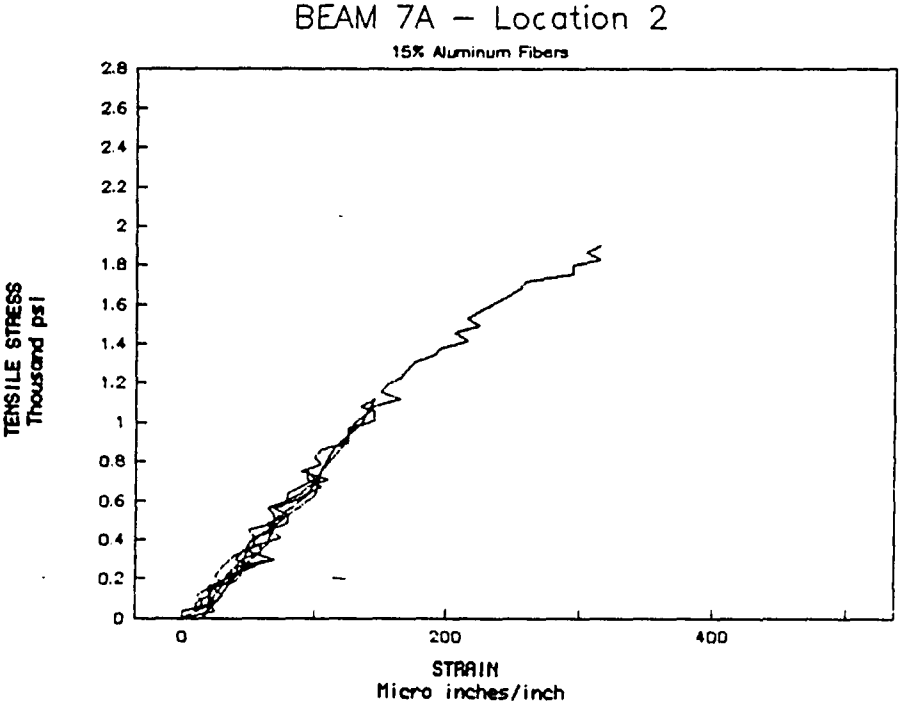
BEAM 7A – Location 2
15% Aluminum Fibers
TENSILE STRESS
Thousand psi
2.8
2.6
2.4
2.2
2
1.8
1.6
1.4
1.2
1
0.8
0.6
0.4
0.2
0
0
200
400
STRAIN
Micro inches/inch

(APPENDIX B)

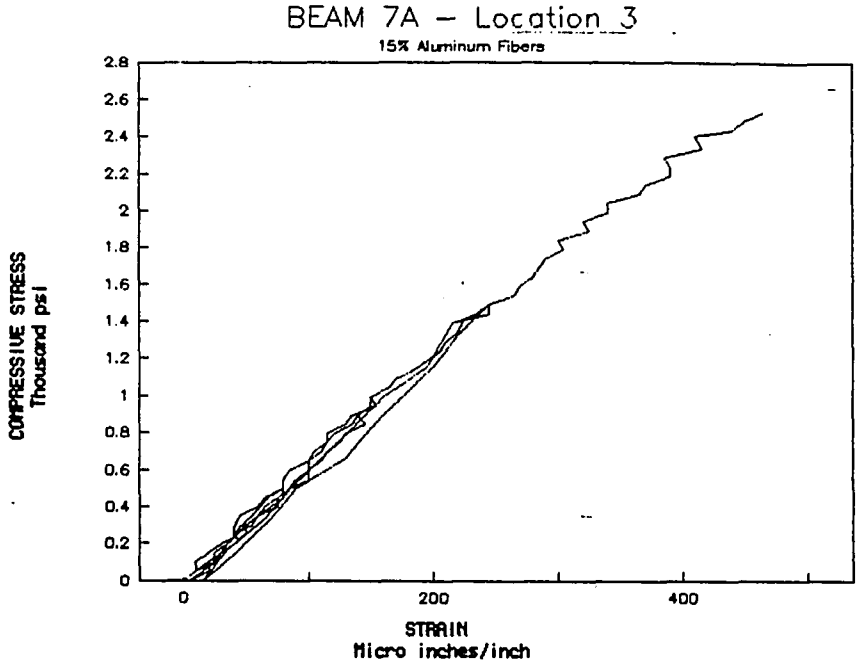
BEAM 7A – Location 3
15% Aluminum Fibers
COMPRESSIVE STRESS
Thousand psi
2.8
2.6
2.4
2.2
2
1.8
1.6
1.4
1.2
1
0.8
0.6
0.4
0.2
0
0
200
400
STRAIN
Micro inches/inch

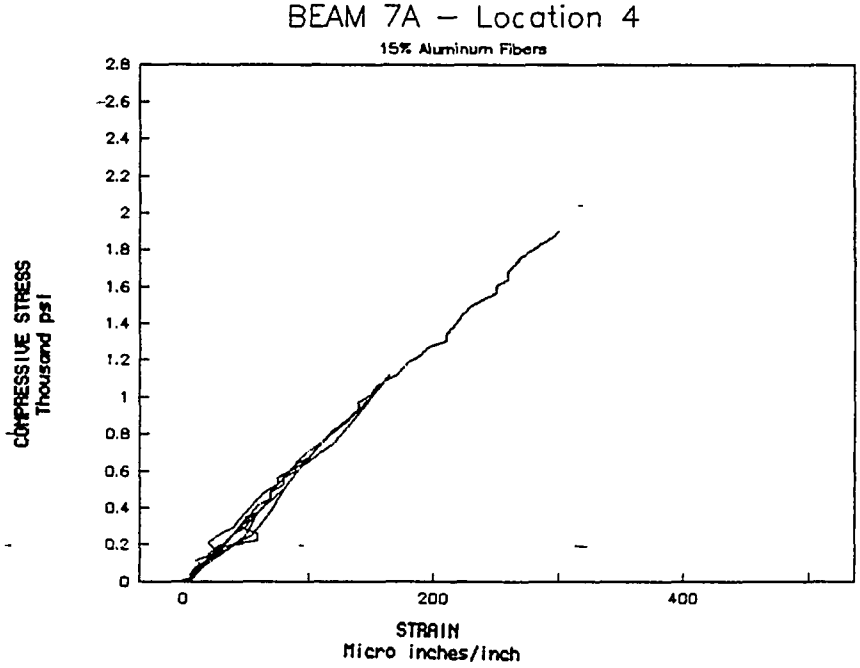
BEAM 7A – Location 4
15% Aluminum Fibers
COMPRESSIVE STRESS
Thousand psi
2.8
2.6
2.4
2.2
2
1.8
1.6
1.4
1.2
1
0.8
0.6
0.4
0.2
0
0
200
400
STRAIN
Micro inches/inch

(APPENDIX B)

BEAM 8B - Location 1

15% Stainless Steel Fibers

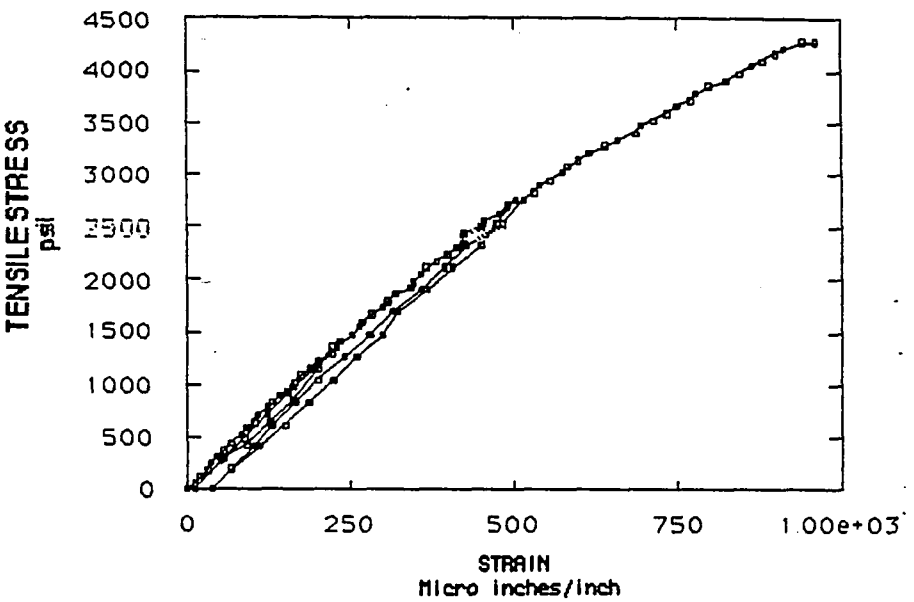


BEAM 8B - Location 2

15% Stainless Steel Fibers

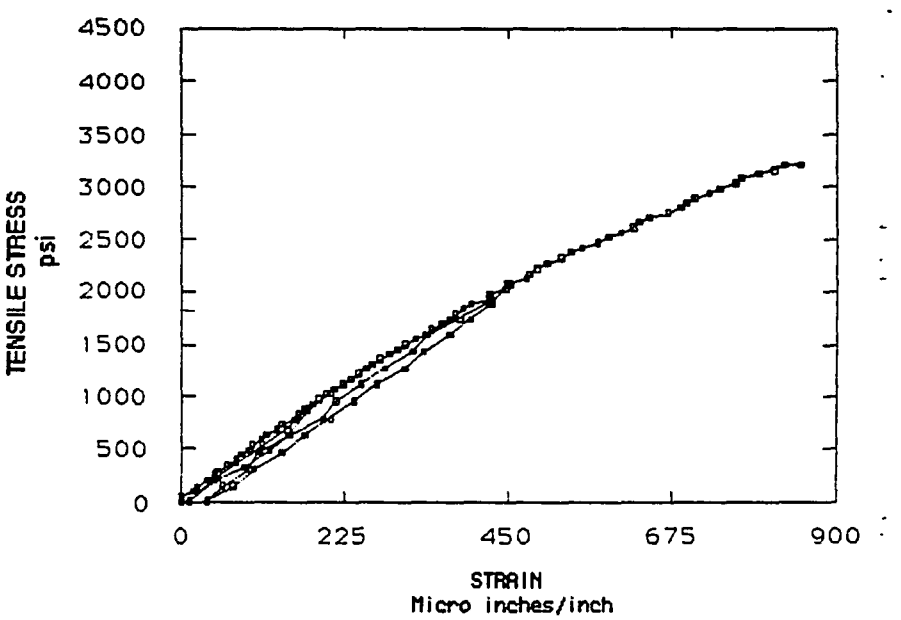

(APPENDIX B)

BEAM 8B - Location 3

15% Stainless Steel Fibers

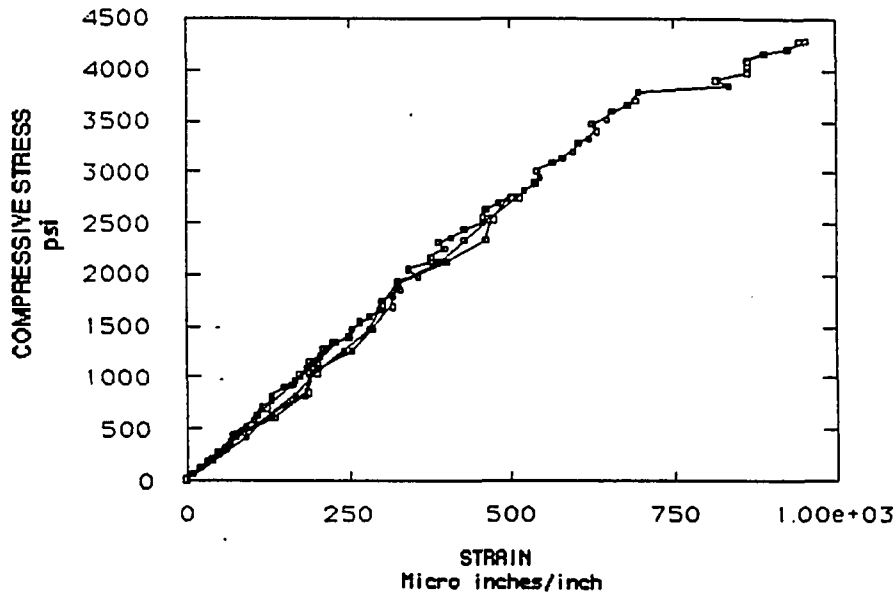


BEAM 8B - Location 4

15% Stainless Steel Fibers

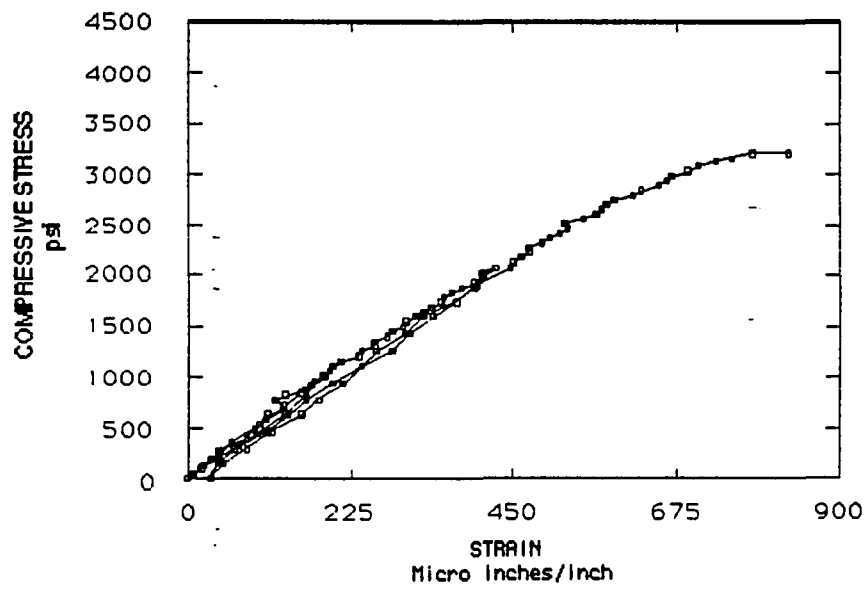

(APPENDIX B)

BEAM 11 – Location 1

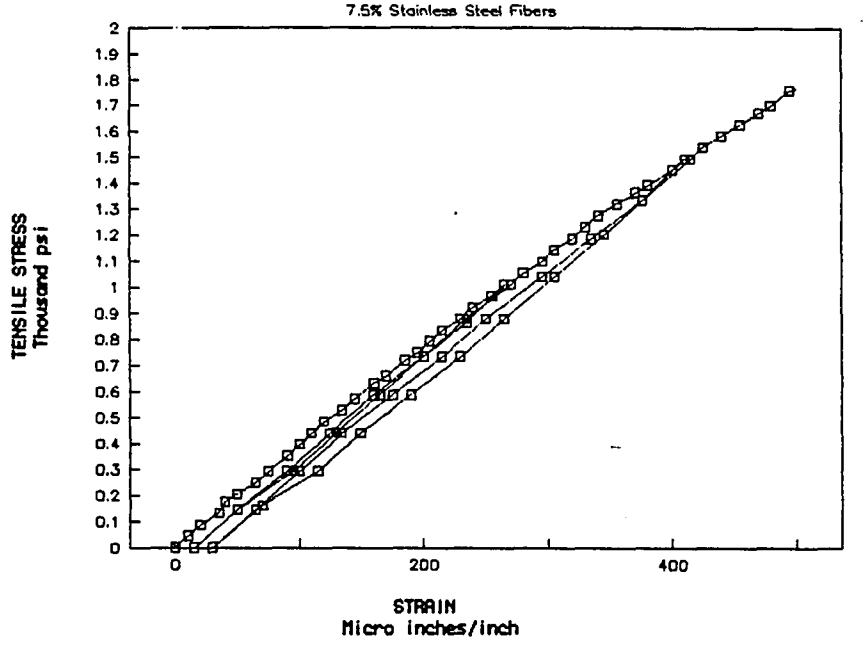


BEAM 11 – Location 2

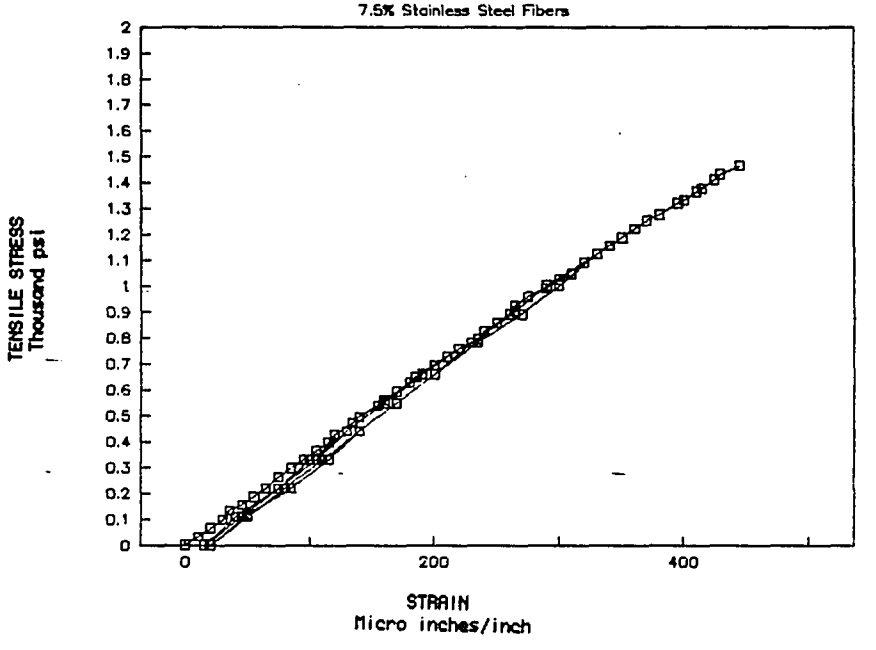

(APPENDIX B)

BEAM 11 – Location 3

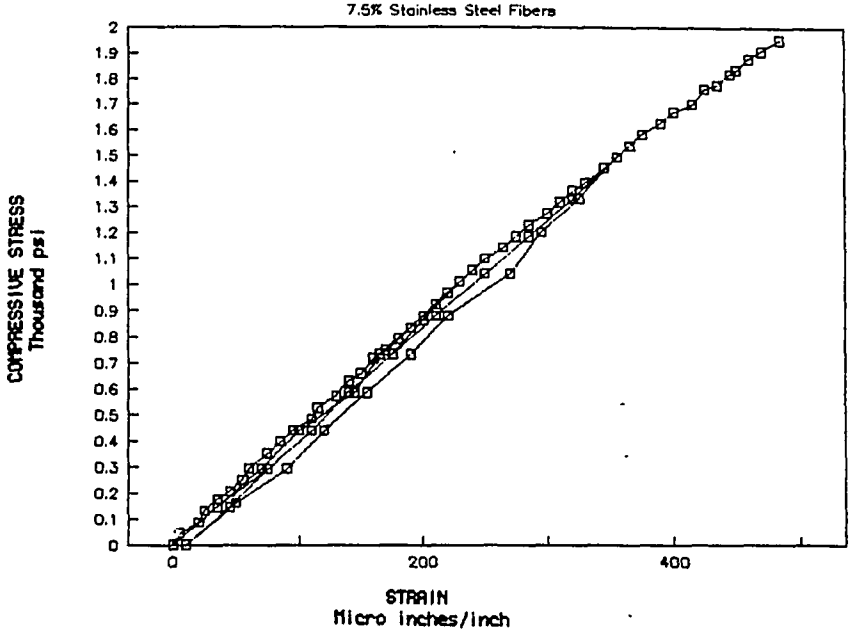


BEAM 11 – Location 4

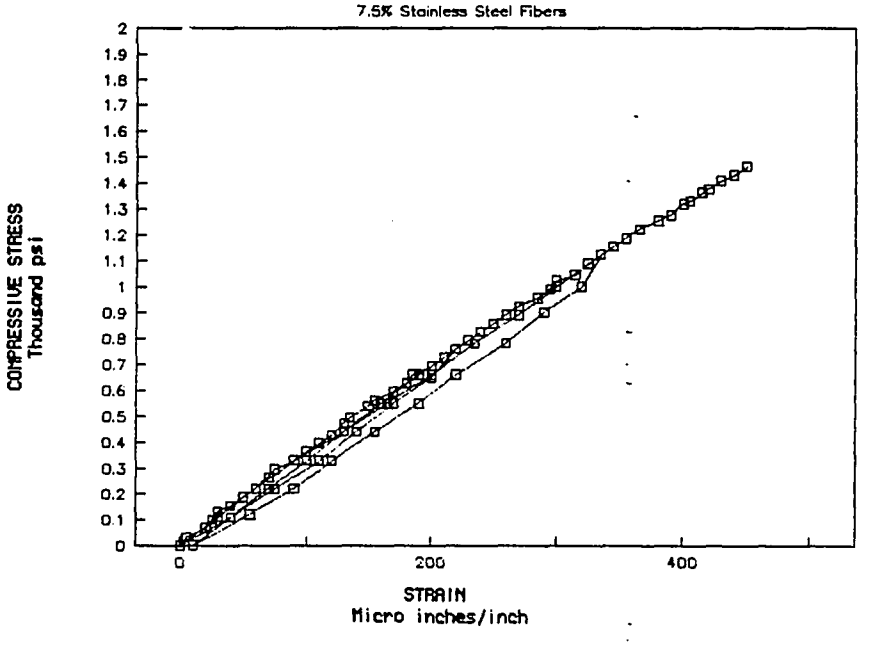

(APPENDIX B)

BEAM 12B – Location 1

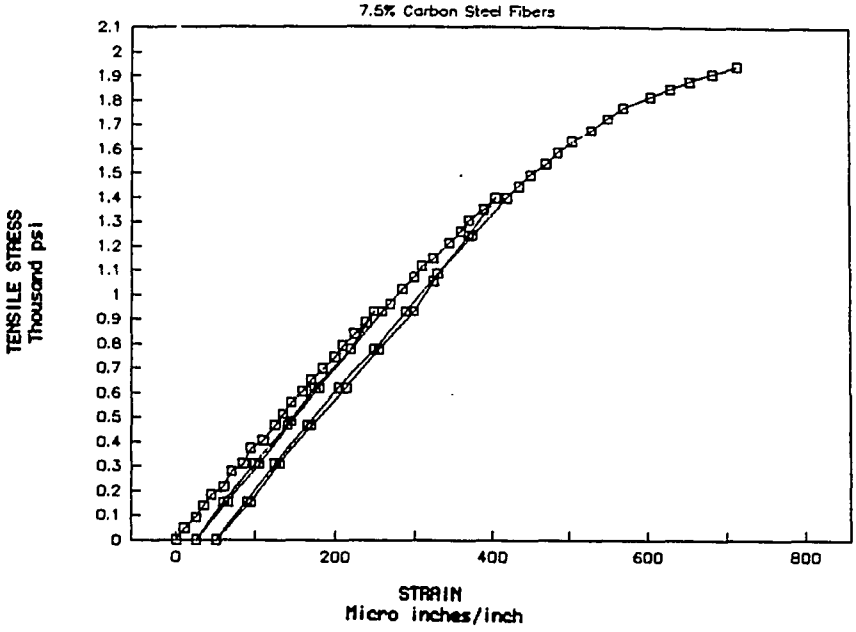


BEAM 12B – Location 2

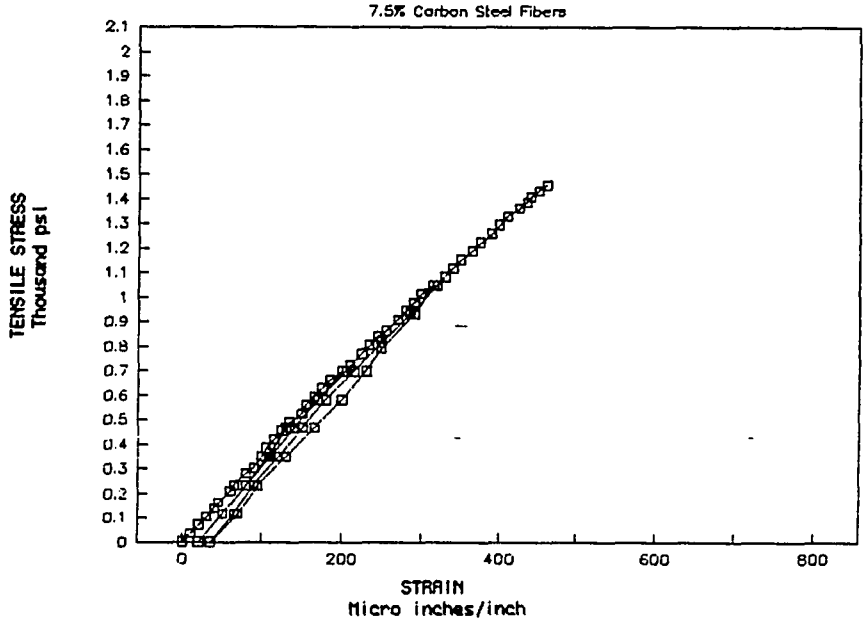

(APPENDIX B)

BEAM 12B – Location 3

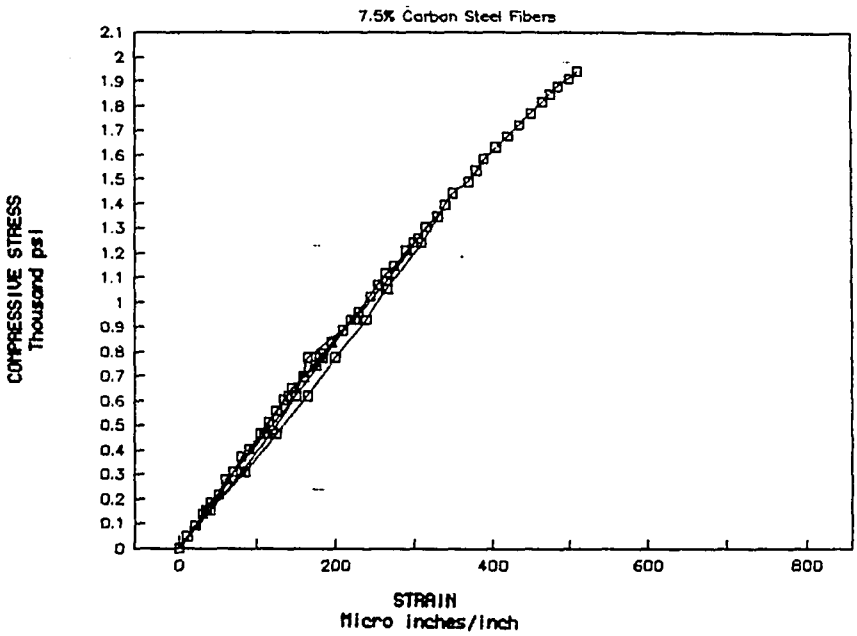


BEAM 12B – Location 4

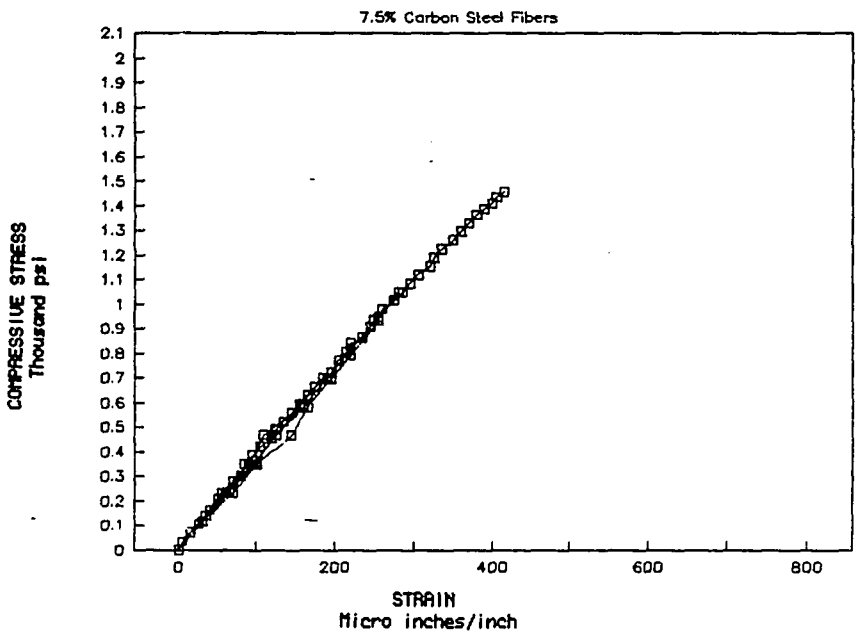

(APPENDIX B)

BEAM 18A – Location 1

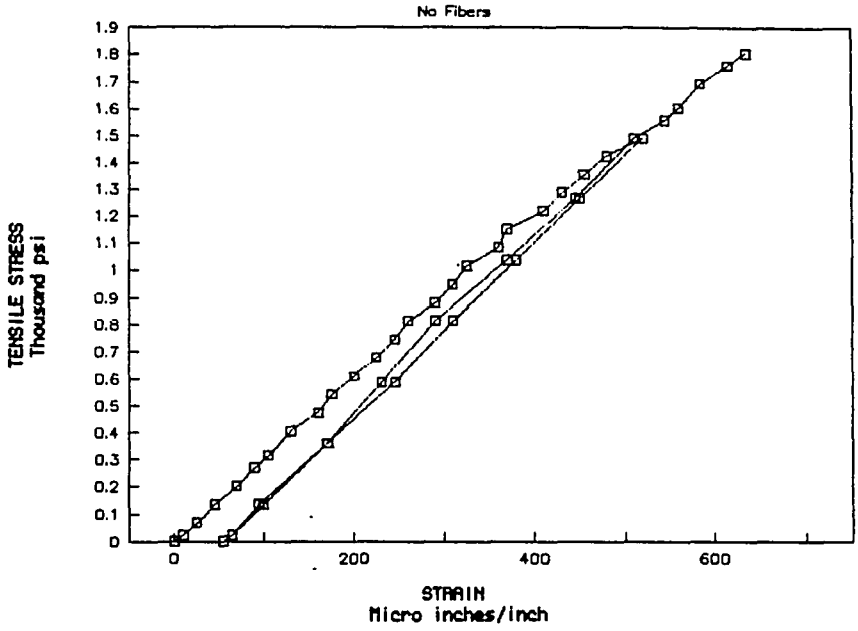


BEAM 18A – Location 2

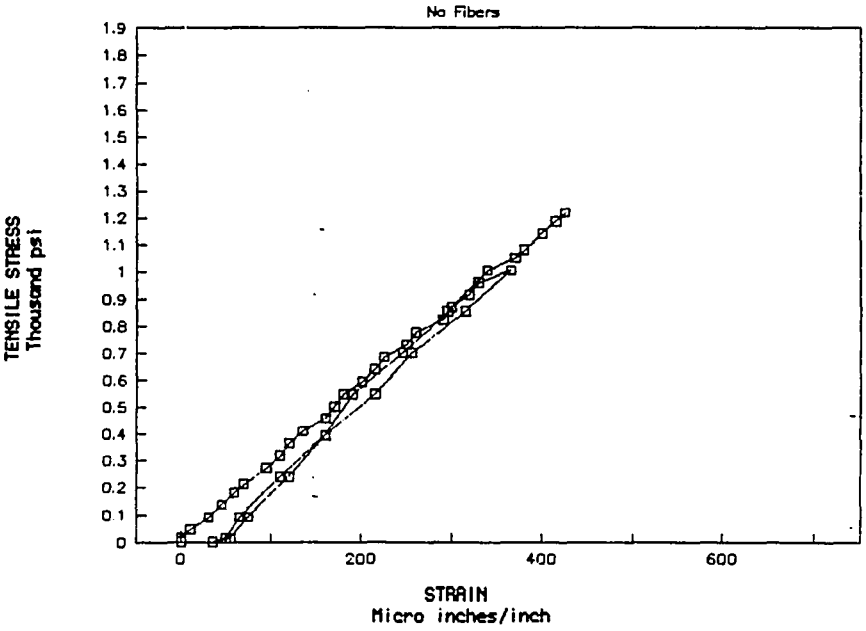

(APPENDIX B)

BEAM 18A – Location 3

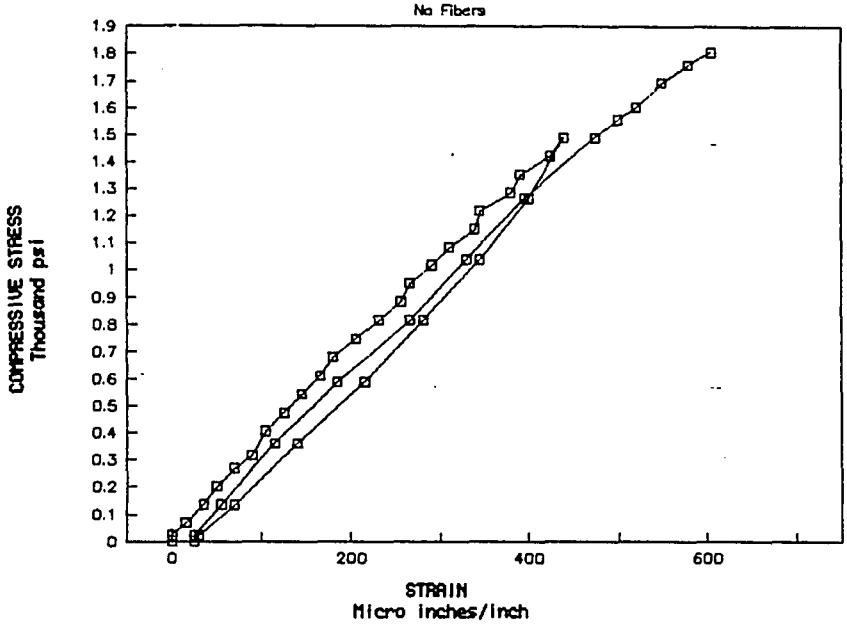


BEAM 18A – Location 4

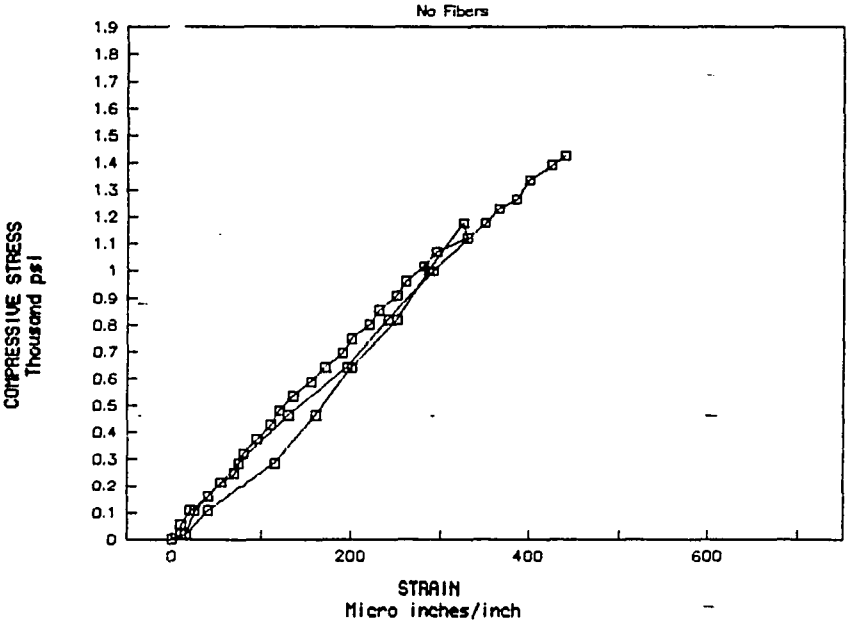

(APPENDIX B)

BEAM 18B – Location 1

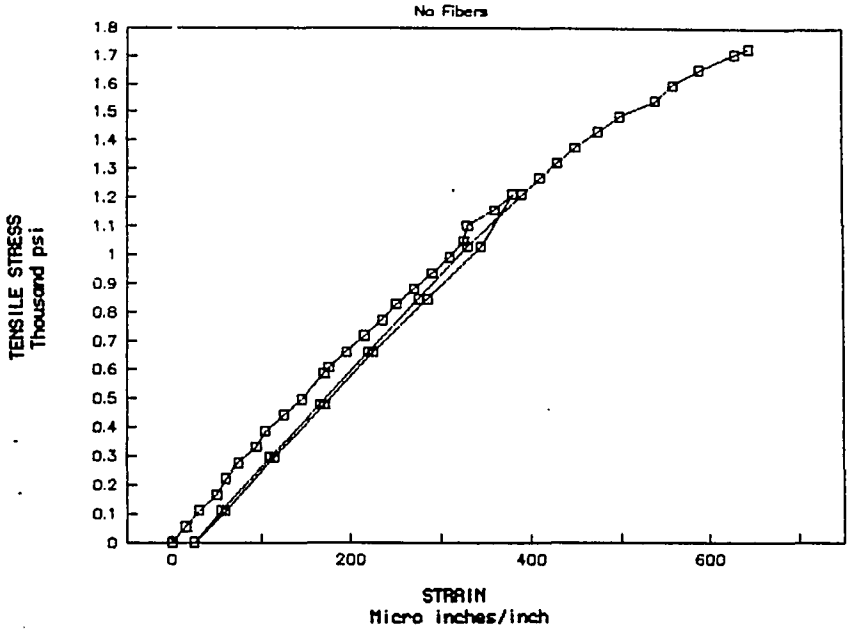


BEAM 18B – Location 2

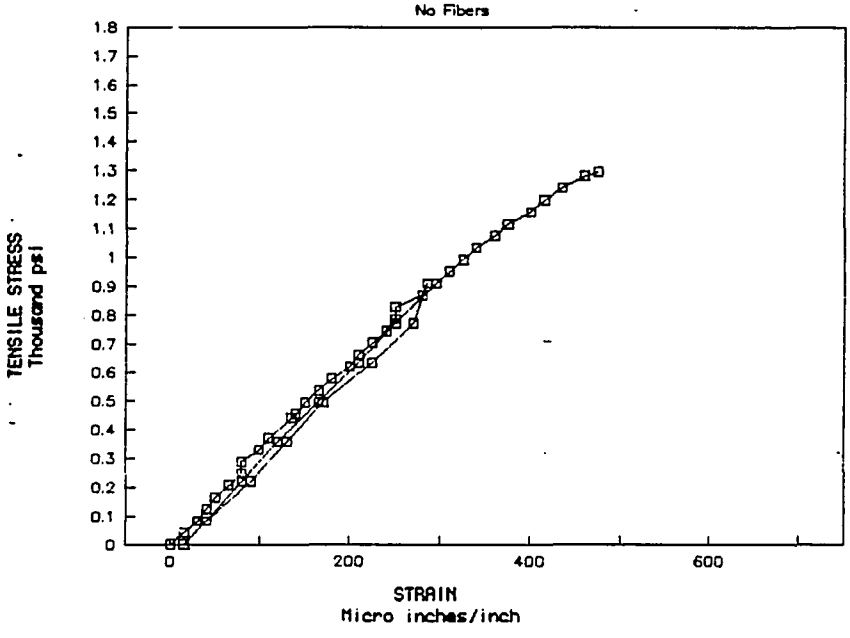

(APPENDIX B)

BEAM 18B – Location 3

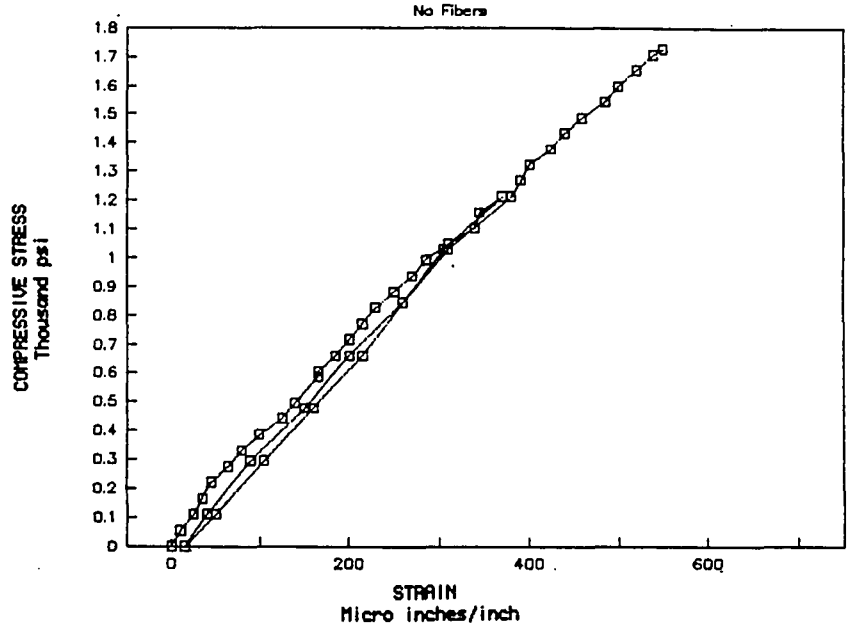


BEAM 18B – Location 4

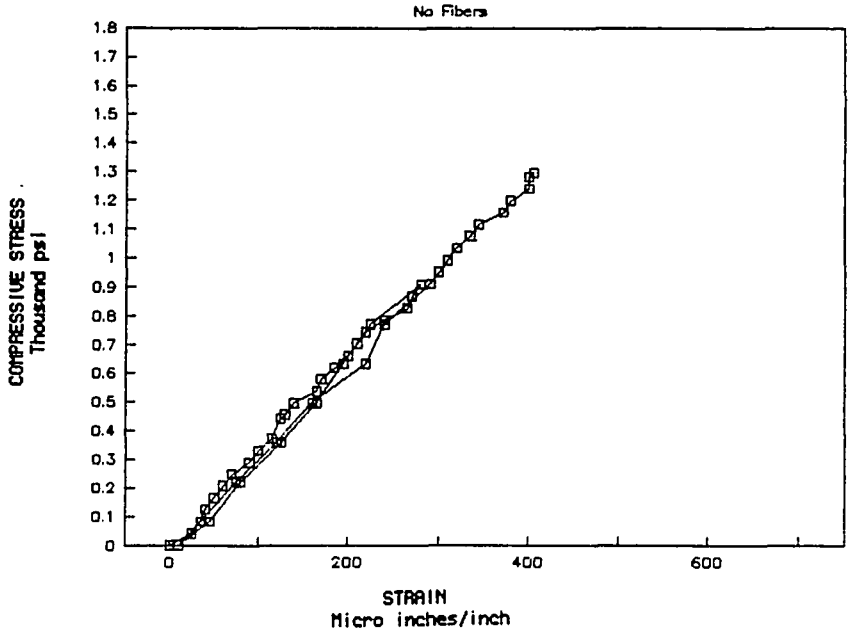

(APPENDIX B)

BEAM 4B – one–third point

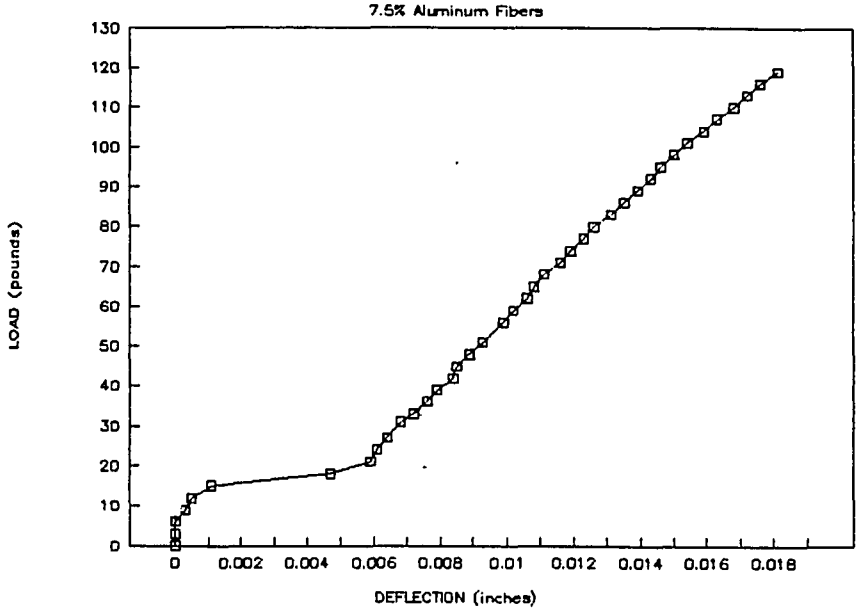


BEAM 1B – one–third point

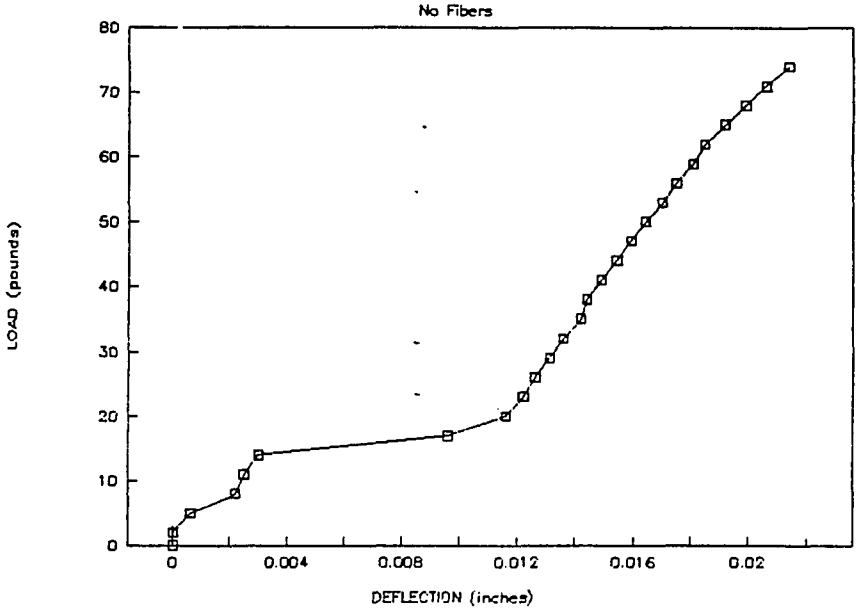

# (APPENDIX B)

## BEAM 4A – one–third point

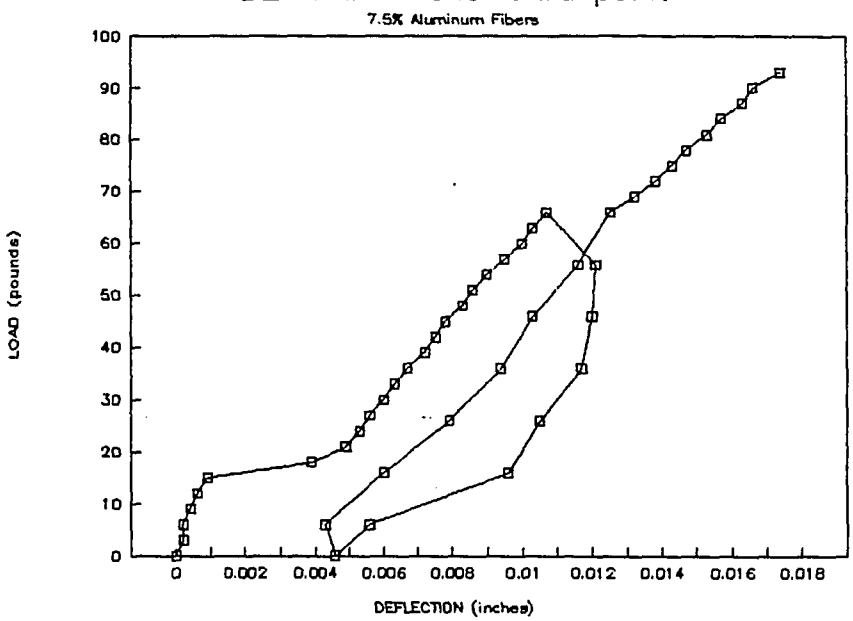


## BEAM 5A – one–third point

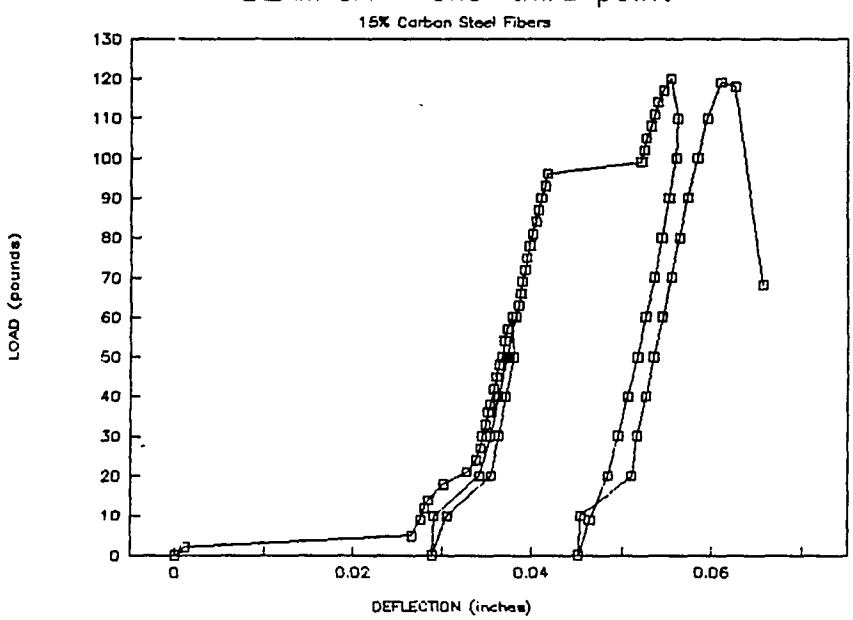

(APPENDIX B)

BEAM 7B – one–third point

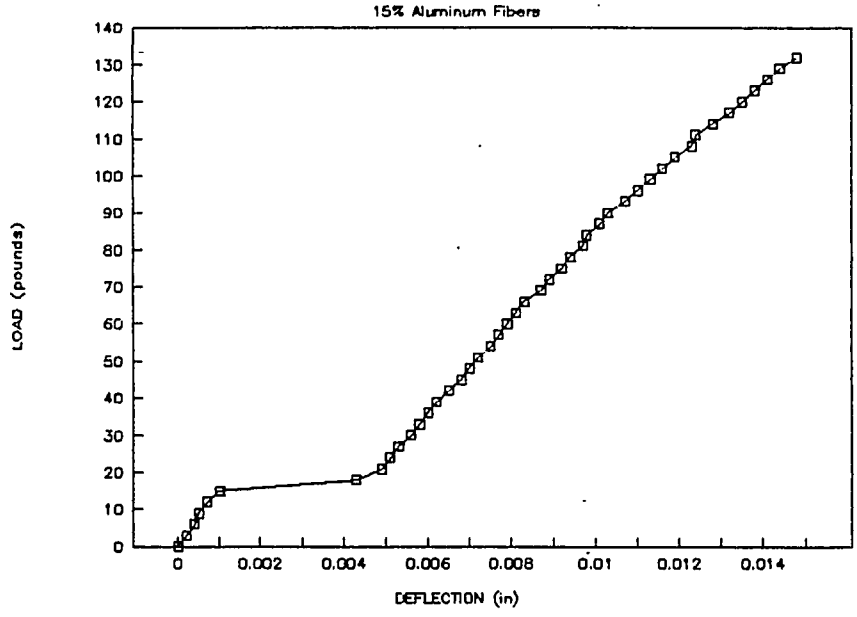


BEAM 8C – one–third point

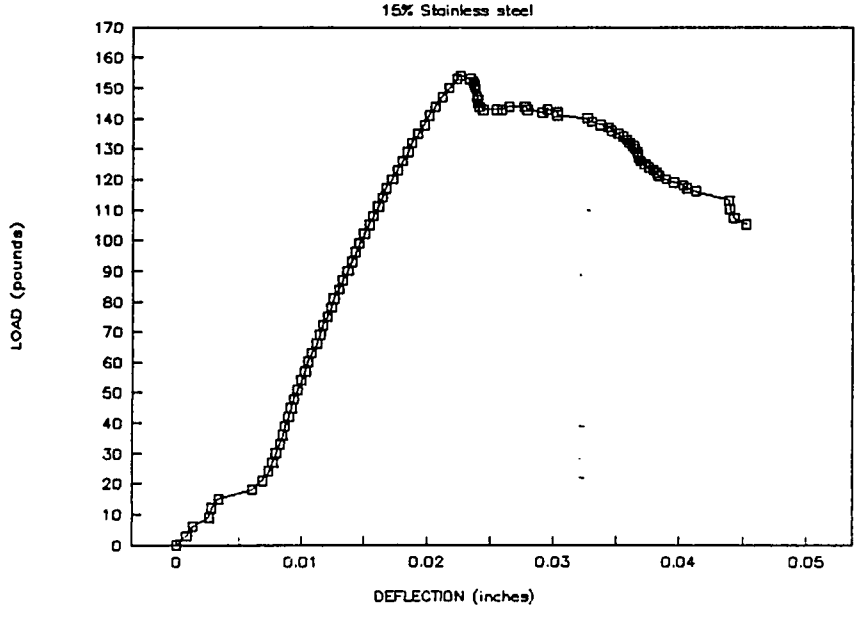

(APPENDIX B)

BEAM 8B - Center

15% Stainless Steel Fibers

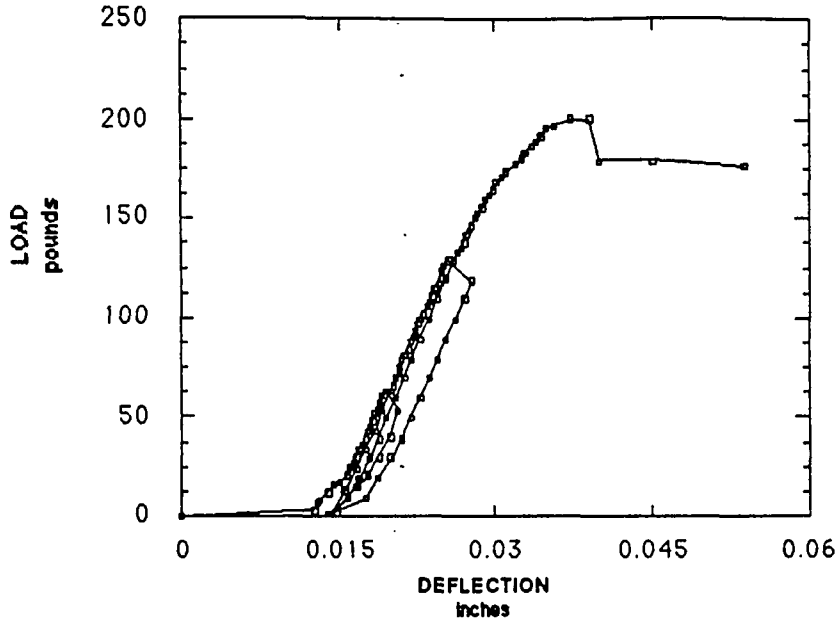


BEAM 9 — one—third point

No Fibers

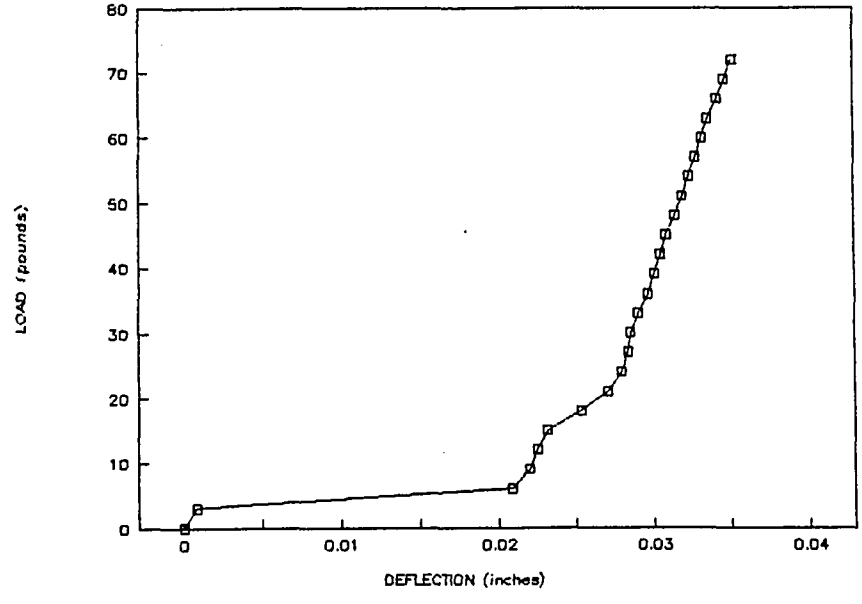

# (APPENDIX B)

## BEAM 12B – Center

7.5% Carbon Steel Fibers

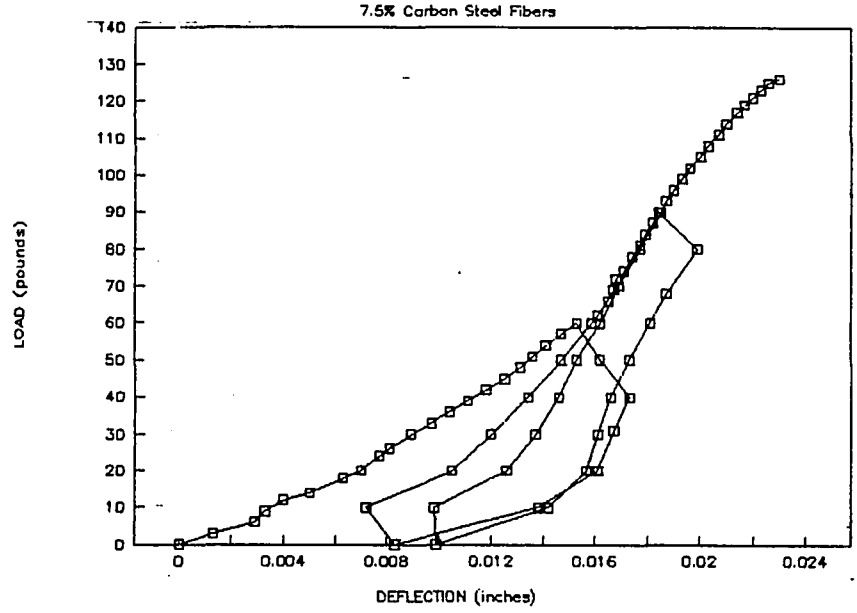


## BEAM 11 – center

7.5% Stainless Steel Fibers

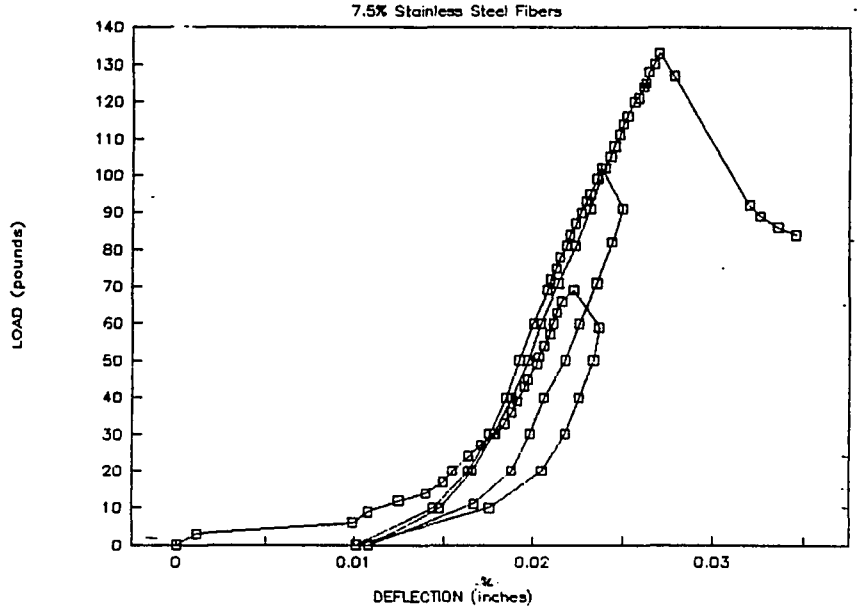

(APPENDIX B)

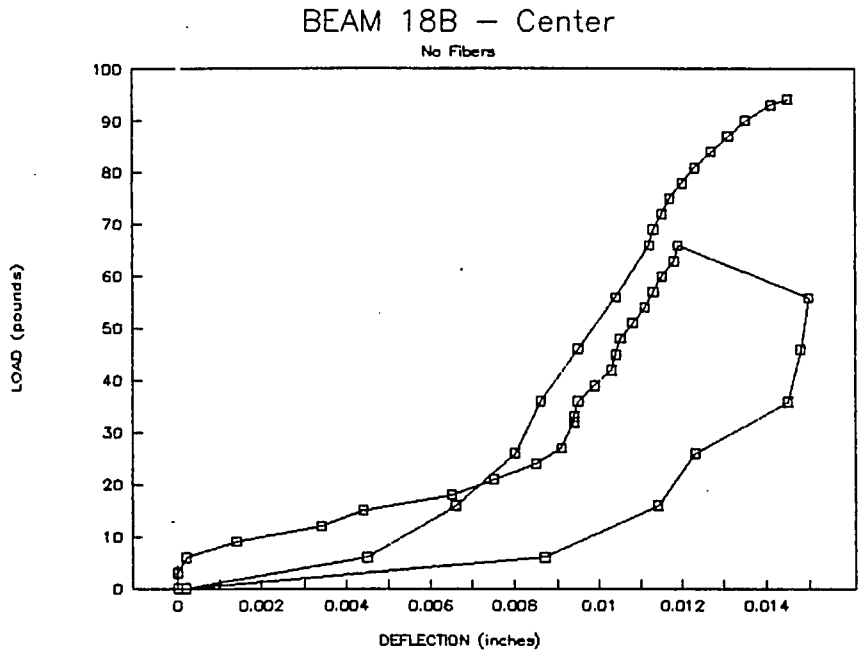
BEAM 18B – Center
No Fibers
LOAD (pounds)
DEFLECTION (inches)
0
10
20
30
40
50
60
70
80
90
100
0.002
0.004
0.006
0.008
0.01
0.012
0.014

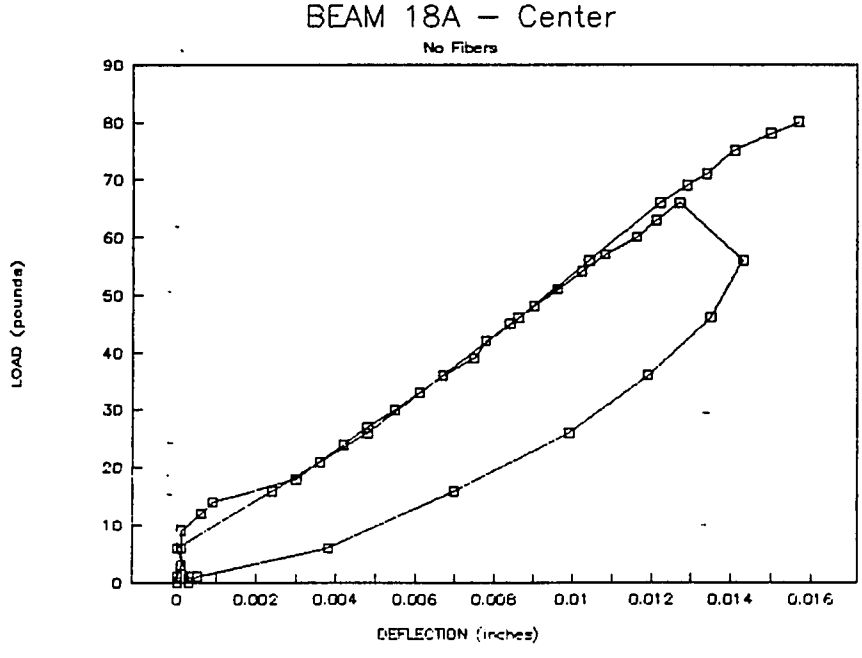
BEAM 18A – Center
No Fibers
LOAD (pounds)
DEFLECTION (inches)
0
10
20
30
40
50
60
70
80
90
0.002
0.004
0.006
0.008
0.01
0.012
0.014
0.016

# APPENDIX C

# COMPRESSION TEST RESULTS

(APPENDIX C)

**UNIAXIAL COMPRESSION TEST**

**SAMPLE 2 - 1**

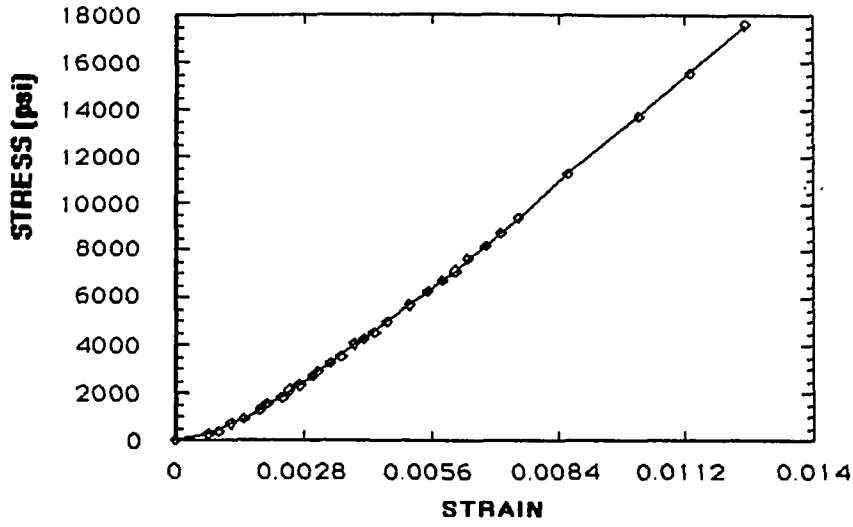


**UNIAXIAL COMPRESSION TEST**

**SAMPLE 2 - 2**

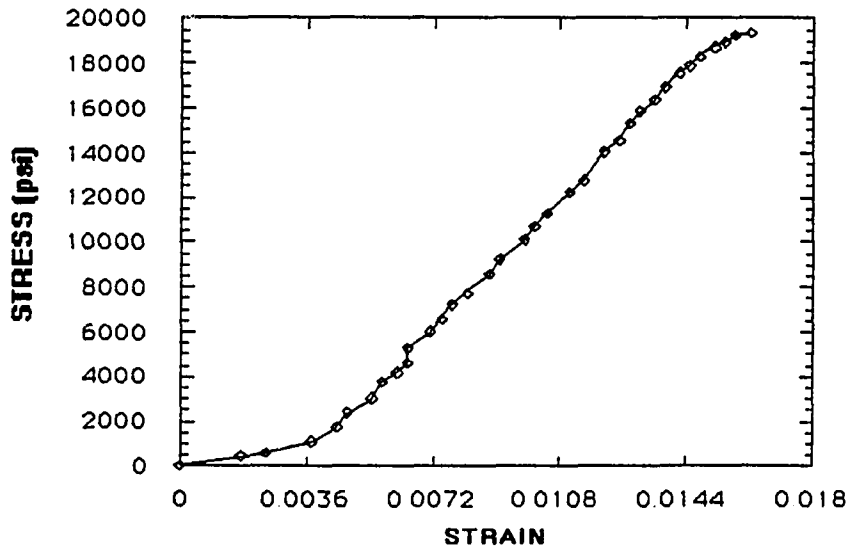

(APPENDIX C)

UNIAXIAL COMPRESSION TEST

SAMPLE 4A - 1

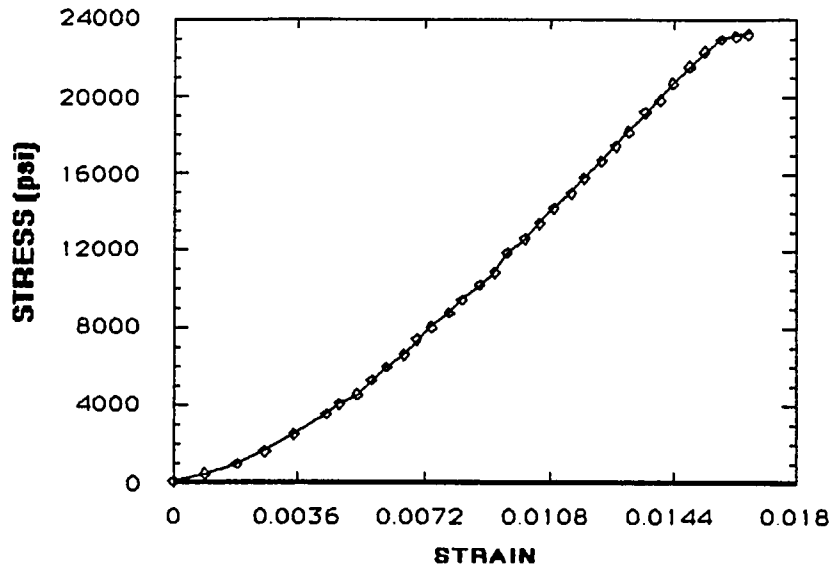


UNIAXIAL COMPRESSION TEST

SAMPLE 4A - 2

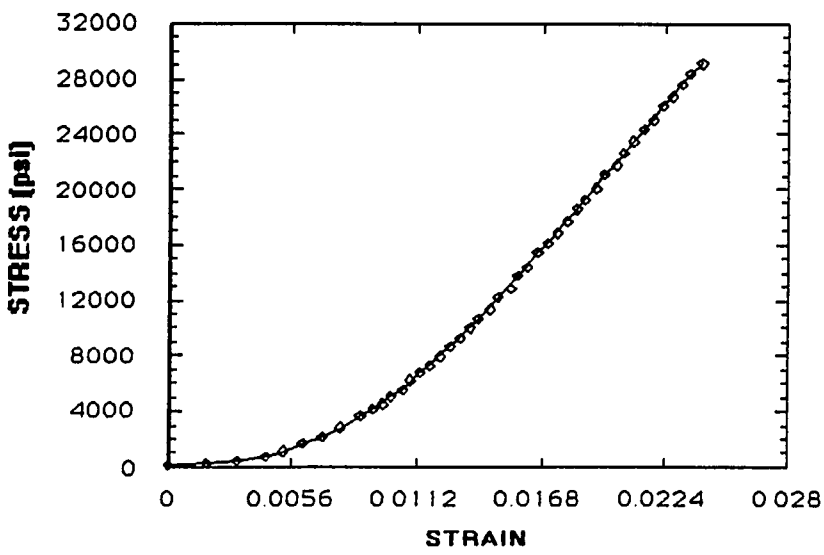

(APPENDIX C)

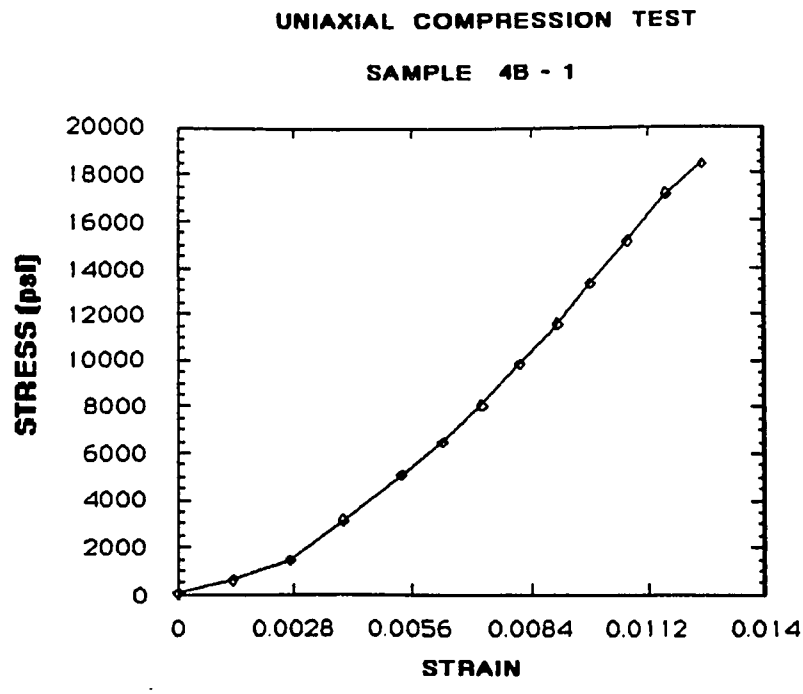
UNIAXIAL COMPRESSION TEST
SAMPLE 4B - 1
STRESS (psi)
20000
18000
16000
14000
12000
10000
8000
6000
4000
2000
0
0
0.0028
0.0056
0.0084
0.0112
0.014
STRAIN

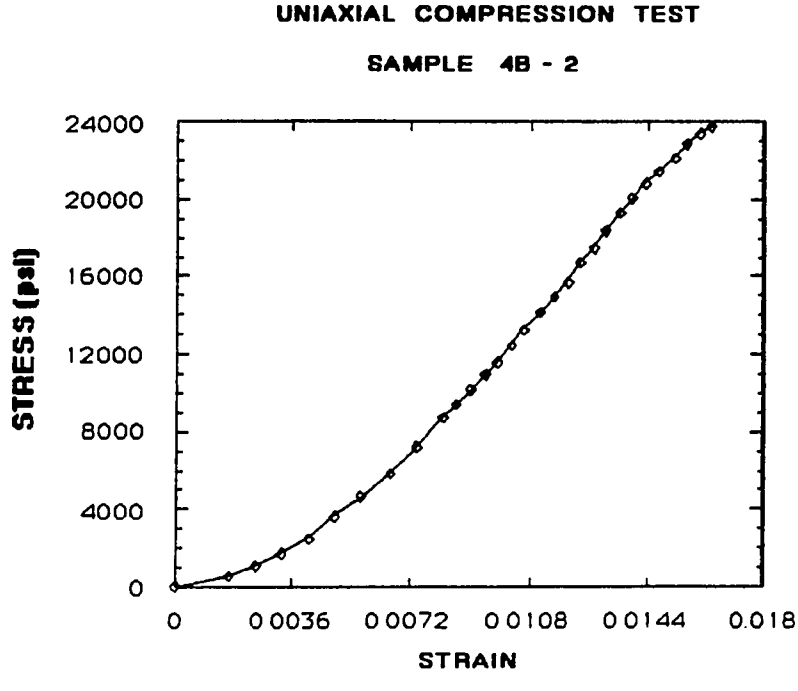
UNIAXIAL COMPRESSION TEST
SAMPLE 4B - 2
STRESS (psi)
24000
20000
16000
12000
8000
4000
0
0
0 0036
0 0072
0 0108
0 0144
0.018
STRAIN

(APPENDIX C)

UNIAXIAL COMPRESSION TEST

SAMPLE 4B - 3

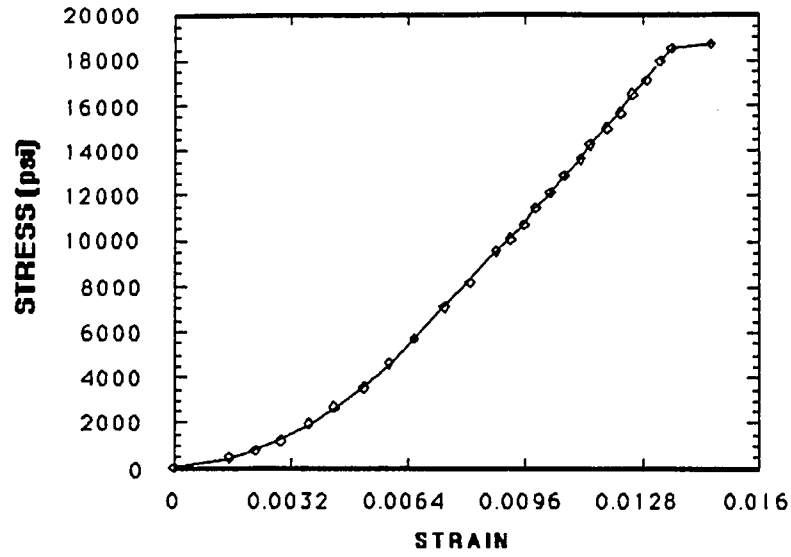


UNIAXIAL COMPRESSION TEST

SAMPLE 7B - 1

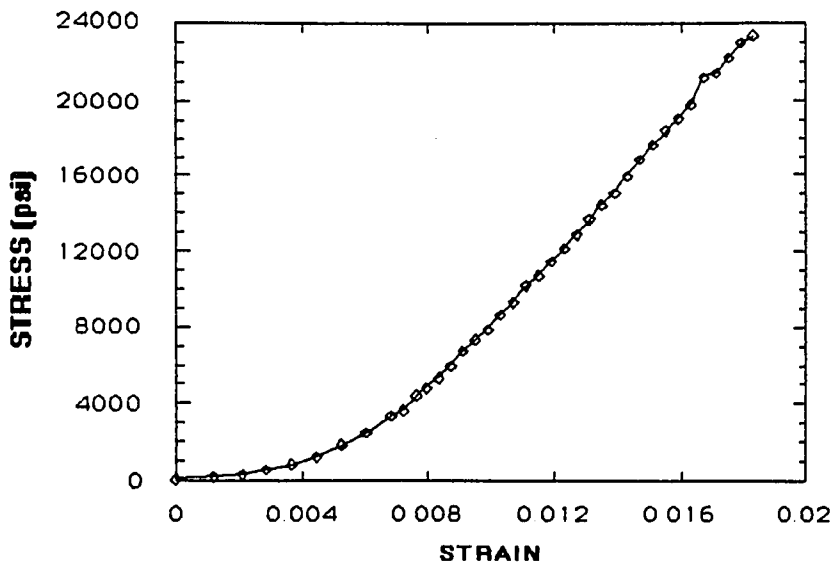

(APPENDIX C)

UNIAXIAL COMPRESSION TEST

SAMPLE 7B - 2

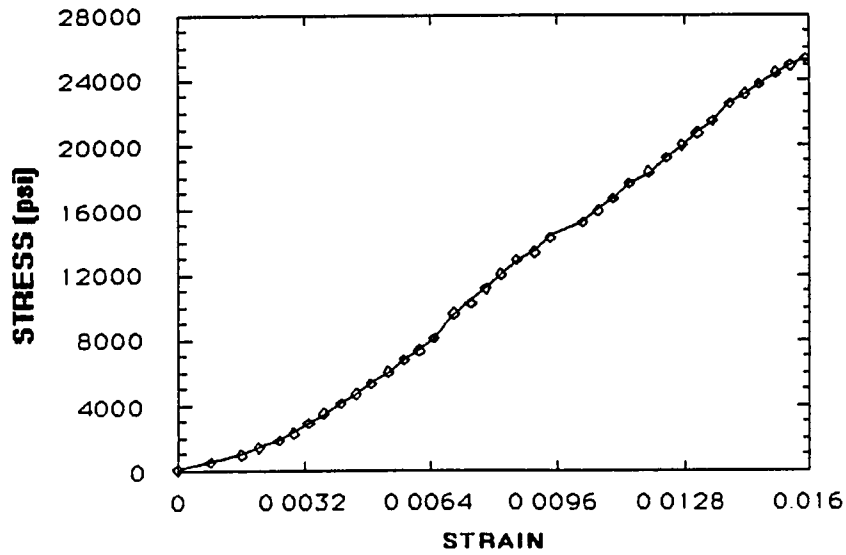


UNIAXIAL COMPRESSION TEST

SAMPLE 8C -1

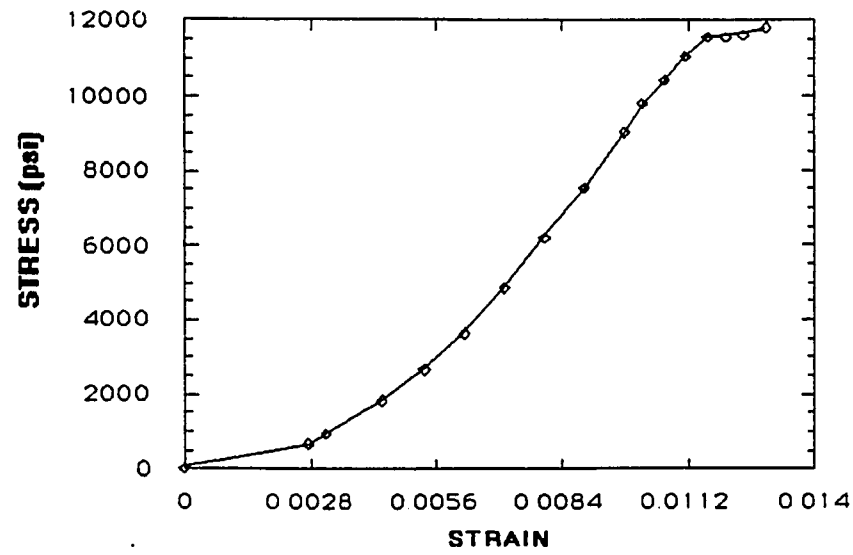

(APPENDIX C)

UNIAXIAL COMPRESSION TEST

SAMPLE 8C - 2

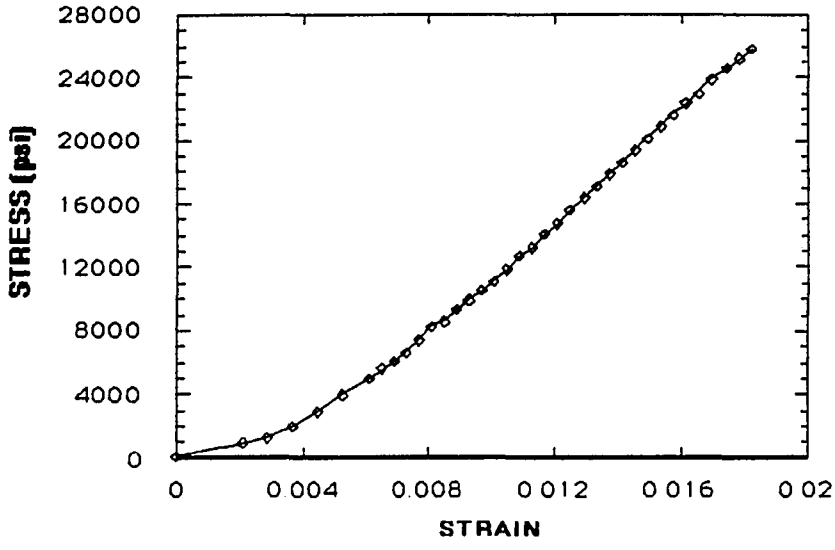


UNIAXIAL COMPRESSION TEST

SAMPLE 8C - 3

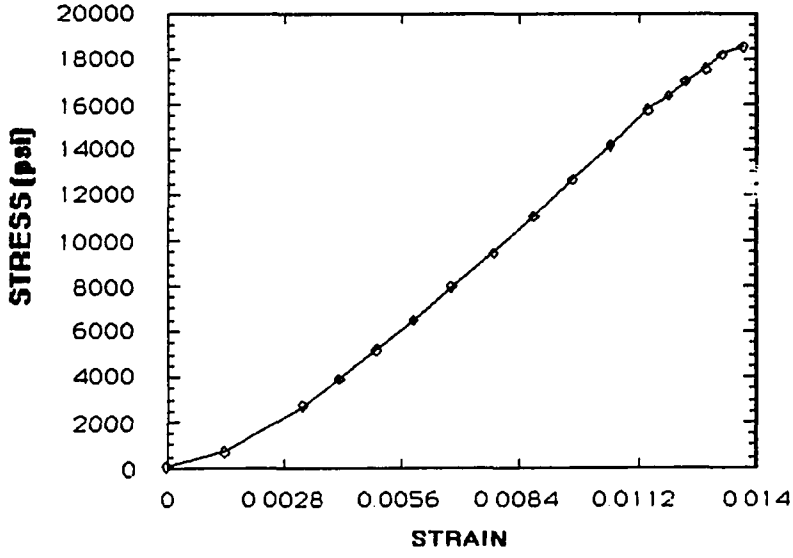

(APPENDIX C)

UNIAXIAL COMPRESSIVE STRENGTH

SAMPLE 5A - 1

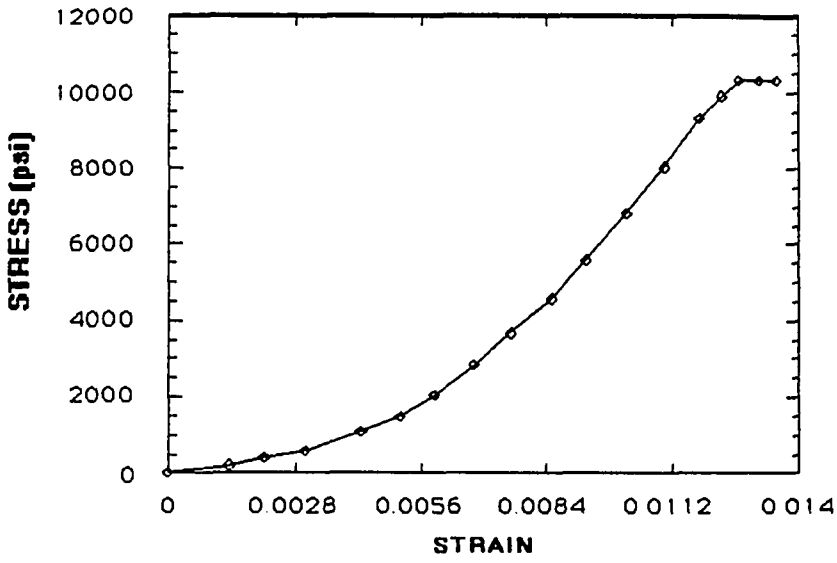


UNIAXIAL COMPRESSIVE STRENGTH

SAMPLE 5A - 2

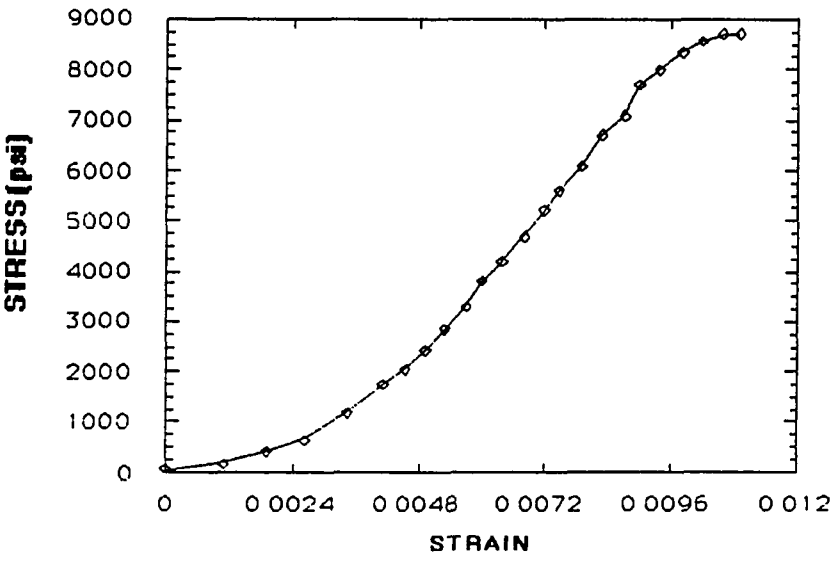

(APPENDIX C)

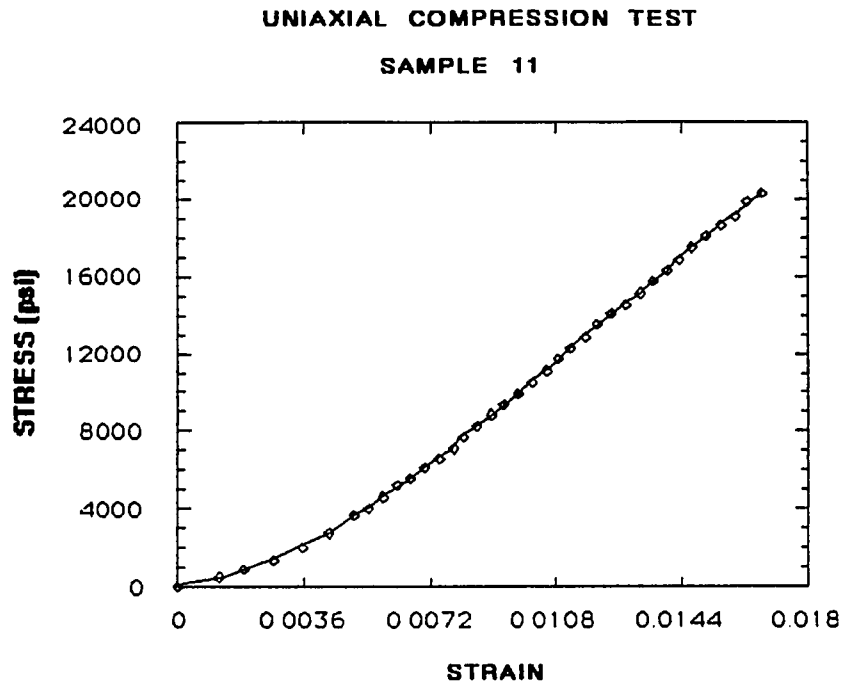
UNIAXIAL COMPRESSION TEST
SAMPLE 11
STRESS [psi]
24000
20000
16000
12000
8000
4000
0
0
0 0036
0 0072
0 0108
0.0144
0.018
STRAIN

(APPENDIX C)

UNIAXIAL COMPRESSION TEST

SAMPLE 18B - 1

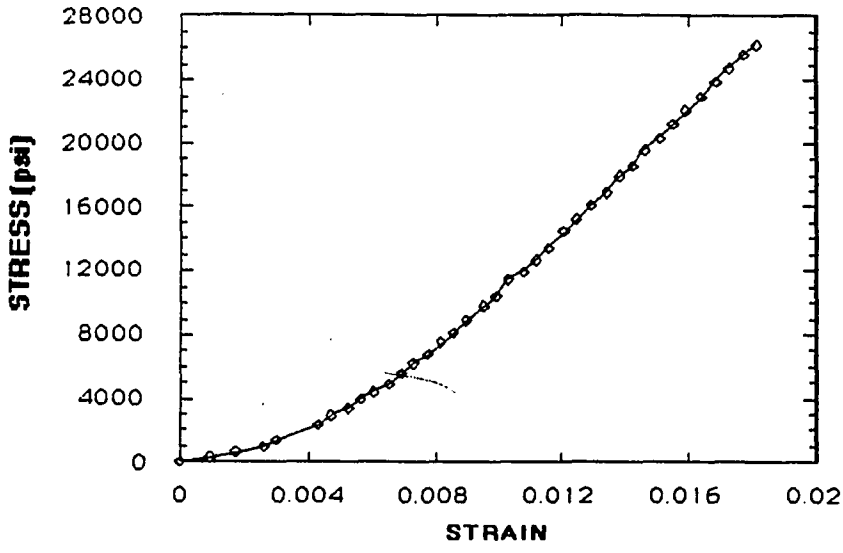


UNIAXIAL COMPRESSION TEST

SAMPLE 18B - 2

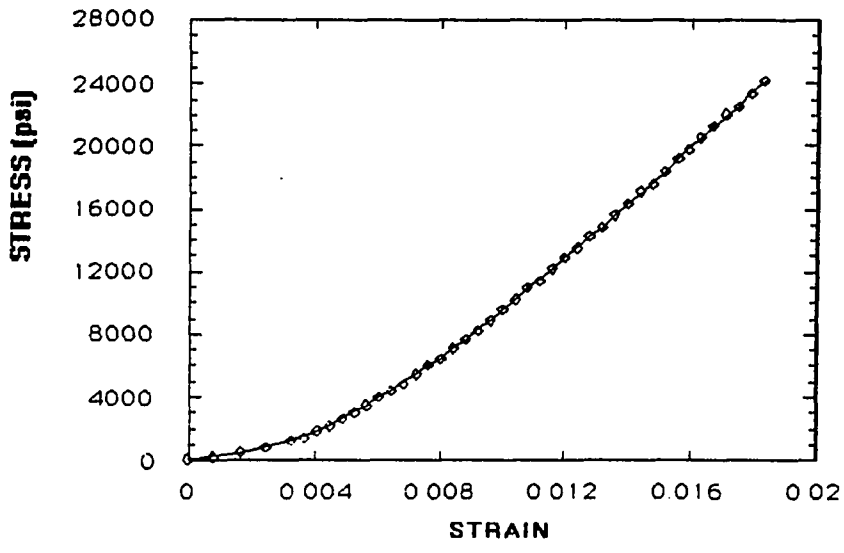

## LIST OF REFERENCES

Allen, T. L., "Effect of Low Vacuum On Density and Stress-Strain-Strength Behavior of Lunar Soil Simulant", M.S. Thesis, 1990

Binder, A. B., et al, "Lunar Derived Construction Materials: Cast Basalt", Engineering, Construction and Operations in Space II, S. W. Johnson and J. P. Wetzel, eds., ASCE, NY, 1990.

Capps, S. and Wise, T., "Lunar Basalt Construction Materials", Engineering, Construction and Operations in Space II, S. W. Johnson and J. P. Wetzel, eds., ASCE, NY, 1990.

Dalton, C. and Hohmann, E., eds., Design of A Lunar Colony, NASA Manned Spacecraft Center, Houston, TX.

Desai, C. S., personal communication, 1990.

Desai, C. S., Sadaatmanesh, H. and Allen, T., "Behavior of Compacted Lunar Simulants Using New Vacuum Triaxial Device", ASCE Journal of Aerospace Engineering, Accepted 1991.

Fuenkajorn, K., and Daemen, J, "Experimental Assesment of Borehole Wall Drilling Damage in Basaltic Rocks", NUREG/CR-4641.

Goldsworthy, W. B., "Composites, Fibers and Matrices from Lunar Regolith", Space Manufacturing 5, AIAA and SSI, 1985.

Guerra, Lisa, "A Commonality Assessment of Lunar surface Habitiation", Engineering, Construction and Operations in Space, S. W. Johnson and J. P. Wetzel, eds., ASCE, NY, 1988.

Ho, D and Sobon, L., "Extraterrestrial Fiberglass Production Using Solar Energy", Space Resources and Space Settlements, NASA SP 428, Houston, 1979.

Kopecky, L., and Voldan, J., "The Cast Basalt Industry", Annals of the NY Academy of Sciences, Vol123, 1965.

Meek, T. T., et al, "Sintering Lunar Simulants Using 2.4 GHz Radiation", Engineering, Construction and Operations in Space, S. W. Johnson and J. P. Wetzel, eds., ASCE, NY, 1988.

Schmitt, H., "Contstraints on Lunar Base Constuction", Engineering, Construction and Operations in Space, S. W. Johnson and J. P. Wetzel, eds., ASCE, NY, 1988.

Simonds, C. H., "Hot Pressing of Lunar Soil and Qualification for Manned Applications", Engineering, Construction and Operations in Space, S. W. Johnson and J. P. Wetzel, eds., ASCE, NY, 1988.

Subramanian, R. V. et al, "Reinforcement of Polymers by Basalt Fibers", SAMPE Quarterly, July 1977.

Weiblein, P. and Gordon, K., "Characteristics of a Simulant for Lunar Surface Materials", Lunar Bases and space Activities in the 21st Century, NASA 1988.

ASTM C78-84, "Standard Test Method for Flexural Strength of Concrete", Vol 04.02 Concrete and Aggregates, 1990 Annual Book of ASTM Standards, ASTM, Philadelphia, PA.

ASTM C116-89, "Standard Test Method for Compressive Strength of Concrete Using Portions of Beams Broken in Flexure" Vol 04.02 Concrete and Aggregates, 1990 Annual Book of ASTM Standards, ASTM, Philadelphia, PA.